Inflammatory-Based Therapies Driven by Intervertebral Disc Injury Responses

Hagar Mohamed Kenawy

Submitted in partial fulfillment of the
requirements for the degree of
Doctor of Philosophy
under the Executive Committee
of the Graduate School of Arts and Sciences

COLUMBIA UNIVERSITY

2024

Abstract

Inflammatory-Based Therapies Driven by Intervertebral Disc Injury Responses

Hagar Mohamed Kenawy

Intervertebral disc (IVD) degeneration is a major cause of low back pain (LBP) worldwide which is expected to affect 80% of the world's population. IVD degeneration (IDD) is a key player in the degenerative cascade associated with LBP. Pro-inflammatory cytokines and mediators, such as nitric oxide, have been shown to be triggers and mediators of IDD. Due to the avascular nature of the adult IVD, the disc is unable to heal or regenerate when damaged. The multi-components of the IVD, namely glycosaminoglycan (GAG)-rich nucleus pulposus (NP), a concentric collagen dense annulus fibrosis (AF), and cartilage endplates (CEPs), further complicate possible regenerative solutions. Cell therapies show promise. This is supported by studies that demonstrate the use of mesenchymal stem cells (MSCs) in animal models showing potential in mitigating inflammatory signaling as well as recovering proteoglycan content. Despite these promising findings, several gaps in knowledge remain.

While the biochemical and mechanical properties of an injured disc (via physical or chemical stimulation) have been characterized, the resulting inflammatory signaling cascades

remain undefined. A growing body of evidence suggests that TLR4 is involved in the pathogenesis of the IVD. However, it is unknown how TLR4 mediates injury responses of the IVD. Second, it is unknown how mechanical loading of IVDs can influence the transcriptome or secretome of the IVD. The IVD is normally exposed to multimodal loading (e.g., compression, tension, shear, hydrostatic pressure, and osmotic pressure). Both frequency and magnitude regulate whether loading is beneficial or detrimental to disc integrity, which will be explored. Furthermore, the secretome of the IVD, especially during loading, may be essential to creating therapies targeted for regeneration of the IVD. There may be key, distinct paracrine factors that are released in IVD conditioned loading media which can influence the regenerative and anti-inflammatory capabilities of cell-based therapies.

To address these gaps, this thesis describes a series of experiments employing novel *ex vivo* organ culture model to study the response of the IVD to various injury modalities (inflammatory stimulation, puncture injury, compressive loading), and resulting changes in inflammatory, biomechanical, and biochemical responses. Through methods such as RNA sequencing and proteomics, we now have expanded the characterization to beyond candidate genes or proteins, and are more informed on (1) the IVD response to injury, (2) the role of TLR4 signaling in this *ex vivo* organ culture model, in addition to (3) the downstream effects of loading and how paracrine factors can be used to improve and develop potential cell and molecular therapies. Sex-based differences, in male and female rat caudal IVDs, were also identified and are analyzed in the context of response to injury.

Table of Contents

List of Figures

Acknowledgments

I would first like to thank Dr. Nadeen Chahine and Dr. Clark Hung. I would not be where I am today in my scientific training without either of them. I would not be here today if Clark never offered me a position in his lab in March 2018 after I had met him on a Skype call (yes, not Zoom) since he was not available to meet during interview weekend. I would also like to thank Drs. Andrea Tan, Robert Stefani, Eben Estell, and Krista Durney for talking to me that weekend and convincing me to choose Columbia if I was accepted. However, most importantly, I would like to thank Nadeen for taking a chance on me and welcoming me into her lab despite never meeting me. You have taught me so much about the scientific process, which avenues one should pursue, how to manage one's time, navigate professional networks, and even how to balance the PI life as a mother. I will forever be grateful for this opportunity to not only be at Columbia to pursue my PhD but also to be mentored by two PIs who are experts in their respective careers: Clark, an established male PI, and Nadeen, a female PI who had recently joined the Columbia community as faculty, when I joined the CEL and Chahine labs in the Fall of 2018. I would like to thank them both for sharing their knowledge, life experiences, and advice with me and for being patient as I slowly picked up what the orthopedic research field had to offer. Thank you, Clark and Nadeen, for making me feel at home while I was away from home. Thank you for your never-ending support and encouragement through all the scientific and personal ventures I have undertaken over the years.

Next, I would like to thank my extended lab family PIs: Dr. Stavros Thomopoulos and Dr. Gerard Ateshian. Attending journal clubs and career development sessions with both of your labs has given me some of the best highlights of my PhD journey. From the 9 am bagels to scientific banter, I have learned so much about the orthopedic community, its history, how close-knit it can

be despite how large it is, and how it all comes back to Columbia. I appreciate your advice throughout the years at all the meetings, holiday parties, and even via email.

I would also like to thank the other members of my thesis committee, Dr. Helen Lu and Dr. Treena Arinzeh, for their guidance and assistance during this process. Thank you, Helen, for always being a warm presence in the BME hallways, during my thesis proposal, or even when I first interviewed with you uptown (in Nadeen's office, ironically) in February 2018. Thank you, Treena, for being willing to serve on my thesis committee despite your busy schedule. I would also like to thank Dr. Gordana Vunjak-Novakovic for serving on my qualifying examination during that busy week in January 2020.

I'd like to thank the rest of the Carroll labs, including Dr. Alice Huang, who joined the lab space almost two years ago now and who has also provided me with countless scientific and life advice, and Thomas Gardner, whom I have bothered more times than I can count, yet was always willing to help me (I will never forget drilling through the building walls and installing the x-ray coat rack in the animal surgery room). Special thanks to previous Carroll lab members Silvio Betancur and Linda Effiong for your constant support and encouragement. Additionally, special thanks to administrative staff who have helped me get reimbursements, grants submitted, and a good laugh in the day: Chloe (Libing) Huang, Catherine Konradt, Anca Meret, Karen Evans, Michelle Cintron, Aidan Hogan, Helen Cen, Alexis Newman, Zachary Corter, Scott Kelly, and James Ihn. Special thanks to Arthur Autz and Joe Viola for introducing me to the machine shop and assisting me with my random lab needs.

Now this is going to be a long page or two, but I would like to thank all the present and past lab members whom I have had the honor and pleasure to work with over the years. First, I would like to thank Dr. Eben Estell, Dr. Robert Stefani, Dr. Samantha Marshall, Dr. Timothy

Jacobsen, and Dr. Quynhhoa Nguyen for being the senior lab members when I first joined the CEL and the Chahine Lab and for teaching me so much about lab etiquette, protocols, and showing me the ropes. Thank you, Tim, for showing me the ropes of AFM and answering my frantic texts despite having graduated from Columbia for at least a year. Thank you, Sam, for teaching me PCR, mechanical testing uptown, and responding to my texts even now. I would also like to give a special thanks to Dr. Lee Song, who has helped me with so many random things in the lab (from dry ice to replacing carbon dioxide tanks, ordering research supplies, giving me research advice, and even ordering coffee) and for most importantly, always smiling. I would also like to thank Dr. Dan Viola for introducing me to surgical techniques on rodents and being a positive presence in the lab. Although not a part of the Carroll labs, I would like to thank Michael Kissner for explaining science so clearly, introducing me to flow cytometry and working with my hectic schedule.

Next, I would like to thank my lab mates who have seen me go through it all, and I have learned so much from these past few years. Dr. Kevin Burt, thank you for always helping me navigate science and encouraging me through the roughest days and the endless memes. Lauren Lisiewski, thank you for your constant support and help throughout the years. It feels like we have learned and discovered so much science together during this PhD journey, from improving PCR methods and dissecting rat IVDs to where the best place to get a coffee in Washington Heights is or how to get posters made and delivered. Special thanks to Dr. Mark Kim, who has been a significant source of help, knowledge, and support for the past two years. Thank you, Mark, for always being available, and when you are not, offering your help when you are free. Thank you, Gigi Bond, for being the younger sister I never had. Your constant support and presence have been essential to getting me to the finish line, and for that, I am incredibly grateful. I would also like to thank present Chahine Lab members: Nicholas Toosi, Leonardo Campos, Maho Koga, and Elyse

Fleck for expanding the lab and giving it some fresh energy that I did not realize I was missing, as well as previous Chahine Lab undergraduate members: Erik Emsbo, Aala Nasir, and Archana Murali.

Thank you, Dr. Andy Lee, for helping me start this thesis project back when we were cutting IVD motion segments with a scalpel blade and a wooden hammer. Lance Murphy, thank you for being so welcoming when I first started in CEL and for always encouraging a positive community and bringing people together. Thank you, Lianna Gangi, for being my desk buddy, helping me with classes, and being there throughout all the ups and downs of the fundamental PhD research years (never forget bubbly gels). Thank you, Matthew Pellicore, for educating the lab on molecular methods, fantasy football, as well as how to make the best chocolate chip banana muffins and bread. Thank you, Jack Rogot, for helping me publish my first paper, keeping the lab organized, fueling my EDM music addiction, and for always being down. Neeraj Sakhrani, to this day, it feels like you started the PhD journey in 2019, so thank you for deciding to stay as a PhD student in CEL, as your endless support and encouragement have been essential over the past few years and months. Thank you for always being down to explore all the Columbia/NYC has to offer. Howard Nicholson, thank you for introducing me to a whole new side of research, for your willingness to help whenever you can, and for always making sure that no one gets left out. Thank you for becoming a dog dad as well. Thank you, Andy García, for your enthusiasm for biotech ventures, refined wardrobe, and taste in music when it comes to Spanish or Arabic genres.

I would also like to thank the various undergraduates who have taught me the ropes around CEL: Saiti Halder, Sofía Barbosa, Rika Ichinose, and the undergraduates that I have had the pleasure of mentoring and working alongside: María Nuñez, Athena Pagon, Ratna Sharma, and

Xóchitl Morales. I would also like to thank the current undergraduates: Spencer Robbins, Caroline Schleif, Inioluwa Ojediran, and Claire Pinnie.

Thank you to visiting undergraduate students, Aamna Siddiqui and Steven Robles, for having such a positive presence during those lab summers. Thank you, Tsunagu Ichikawa, Joshua Ou, Sid Guha, and Victoria Bahena, for working in the lab during challenging times.

Thank you to everyone in the Thomopoulos and Huang labs for being a positive presence during my PhD and for helping me navigate lab life. Thank you, Dr. Fei Fang, Dr. Mikhail Golman, Dr. Brittany Marshall (will never forget all the rats we sacrificed together), Dr. Iden Kurtaliaj (for being my late-night work buddy and NYC café explorer), Kenzie Sup (fellow tea and coffee connoisseur), Giulia Crosio (thank you for life advice and food recommendations), Angela Montero, Emily King (for doing some random NYRR runs with me), Dr. Beth Ashinsky (for your scientific and life perspectives), Dr. Varun Arvind, Astia Innis, Jennifer Kunes, Jennifer Kim, Dr. Lynn-Ann Forester, Dr. Xavier Ferrer, and Dr. Andrew Luzzi.

When it comes to MBL, thank you, Dr. Courtney Petersen, Dr. Jay Shim, Dr. Brandon Zimmerman, C.V. Sise, Katie Spack, Kim Kroupa, Shivam Sonar, and Ashritha Eadara. Thank you, Courtney, for always being a positive presence in lab and conferences. Thank you, C.V. and Katie, for being some of the most supportive friends in our cohort. I still remember meeting up to do TE homework that first fall and wondering how everything would be in 5 years. Little did we know. Thank you, Kim, for being the best president EGSC has seen, for reminiscing with me on our separate but similar Madrid memories, and for always being down to explore new cities. Thank you to the rest of my PhD cohort for your continuous support and advice: Dr. Naveed Tavakol, Dr. Vira Behnam, Hannah Childs, Carolyn Kim, Mary-Kate Dwyer, Michael Chan, Jad El Harake, and John Durel.

I would like to give special thanks to my former roommates and lab mates: Lianna Gangi and Kenzie Sup. Thank you for being there for me, especially during the first few years of this PhD journey. Some of the best times of my life were when I got home to apartment 46, and you guys were there to hang out, watch TV (I'll never forget the Stranger Things or La Casa de Papel binges), or even de-stress from BME classes and qualifying exams, and throw the best graduate Halloween party there ever was. Thank you for being my confidants and giving me the opportunity to grow surrounded by other BME graduate students. Despite COVID happening and shutting down everything, you guys made living in New York enjoyable, and for those memories, I am extremely grateful. I would also like to thank Claire Lee (my SIPA roommate who introduced to me to a whole other side of Columbia), Reina Rivenska Dissa, and Lydia Agustina Marida.

I would also like to thank the Virginia Tech PREP program, specifically Dr. Ed Smith and Dr. Luke Achene, for believing in me and providing me the opportunity to conduct research as a NIH post-baccalaureate scholar at Virginia Tech with Dr. Aaron Goldstein. That year, I learned so much about what research entails, if the PhD is right for me, and which doors can open if I take a chance. Thank you to my PREP sisters, Dr. Dominique Munson and Tasmine Clement, for your continuous support, and thank you, Dr. Aaron Goldstein for pulling my name out of a pile and giving me the opportunity to conduct tissue engineering research for the first time in my life in the summer of 2016.

I would like to thank my high school friends, Elizabeth Wroblewski, Rebecca Emonds, Sabrina Thomas, Karina Tavarez, Sasha Abdalla, and Amani Mansour, for still being there for me despite all the time that has passed. I would also like to thank my college friends, Zainab Hussein, Noureen Abdelrahman, Jaimie Sheppard, Samantha Buczek, Aaliyah Shodeinde, Gabrielle Minassian, Jenny Ghosh, and many more for providing me with company and laughs during this

journey. Additionally, thank you to my lifelong sister and cousin, Sara Khalil, for being there for me during these formative years. I could not imagine my life without you.

Most importantly, I would like to thank my family for their continuous support for my whole life. Thank you to my parents for immigrating to the United States in the late 90s and leaving their college accounting degrees, families, and lives behind to secure a better life for my siblings and me. Thank you for walking the streets of Brooklyn in the early 2000s, learning English, and surviving in a city completely different from what you knew growing up. Thank you, Mom, for taking us to the New York City schools, to the libraries, and the parks, and making sure we got an "American" childhood. Thank you for checking up on me daily since I moved away for college and always being down to talk. Thank you, Dad, for working odd late-night jobs in the 2000s and making sure we were able to go on a beach vacation at least once every summer. Thank you for taking the time to really get to know me and for always supporting my dreams and wishes, even if it meant being at least 6 hours away from you. Thank you for driving me (and my laptop charger) when you were able to go to New York these PhD years, despite the traffic, and for giving me life advice during those car rides. Thank you, Aly, for your unconditional support, for introducing me to Birria LES Tacos, and for the times you randomly showed up in New York. Thank you, Omar, for letting me call you at random times just to chat and for advising me on how to write a thesis. I would be nowhere without your continuous support throughout these years, and I am so grateful that you guys are my family. To many more random summer and winter vacations together.

Last but not least, thank you to the following grants for funding the studies described in this thesis: NIH R01AR069668, R01AR077760, and NIH R21AR080516.

Dedication

To my loving family: my parents, Mohamed and Nihal, and my brothers, Aly and Omar.

To my extended family who have been supportive of me despite only seeing me every so often.

To my late grandmother, Ragah, an art teacher and primary school principal, who instilled a love in me for education at an early age and who always encouraged me to keep trying no matter what.

To my late great-aunt Laila who was so welcoming and always reminded me of home whenever I visited her place during the last 10 years.

To my late uncle Bayoumi (Mohamed Mansour) who was my emergency contact growing up in Easton, PA, and who was always there.

Chapter 1: Introduction

1.1 Motivation

Intervertebral disc degeneration (IDD) is a major cause of low back pain (LBP) worldwide. In 2017, it was estimated that, globally, 577 million people experienced LBP at least once in their lifetime [1]. Furthermore, healthcare costs attributed to LBP have soared to at least $100 billion in annual worldwide spending [2]. No effective treatment currently exists. Conventional treatments, such as spinal fusion or disc replacement with implants, appear to be inadequate at decreasing pain and reconstituting the native IVD biomechanical and biological environment [3]. However, it is known the IVD is a critical player in the degenerative cascade, and that pro-inflammatory cytokines and mediators have been implicated as triggers and mediators of IDD.

First, the innate immune response of the IVD subjected to injury is still unclear. While the biochemical and mechanical properties of injured discs (via physical or chemical stimulation) have been characterized, the resulting inflammatory signaling cascades remain unfamiliar. A growing body of evidence suggests that toll-like receptor 4 (TLR4) participates in the pathogenesis of the IVD [4-6]. TLR4 expression in the IVD increases with degeneration severity and mediates catabolic and inflammatory processes [4, 5, 7, 8]. Furthermore, damage associated molecular patterns (DAMPS), such as high mobility group box-1 (HMGB1) or fibronectin fragments, can signal through TLRs leading to degenerative effects on disc cells including increased expression of inflammatory cytokines and matrix degrading enzymes [9-11]. Additionally, HMGB1 can serve as an agonist of TLR4 and lead to downstream nuclear factor kappa-light-chain-enhancer of activated B cells (NF-κβ) activation [12]. However, it is unknown how injured IVD responses are mediated through TLR4.

Second, it also needs to be clarified how different mechanical loading profiles can influence the transcriptome or secretome of the IVD. The IVD is normally exposed to multimodal loading (e.g., compression, tension, shear, torsion, hydrostatic pressure, and osmotic pressure) [13-18]. It is estimated that human lumbar motion discs experience 4.4–6.7% axial strain [19, 20] and intradiscal pressures ranging from 0.03–0.7 MPa [21] under physiologic conditions. However, both frequency and magnitude regulate whether loading is beneficial or detrimental to disc integrity [22-25]. Static loading associated with sedentary posture or dynamic activities that involve high-frequency loading (e.g. motor vehicle drivers or aircraft operators) has a higher incidence of LBP [26-33]. Furthermore, the secretome of the IVD during loading may inform the creation of therapies targeted for regeneration of the IVD. There may be key, distinct paracrine factors that are released in conditioned loading media (CLM) from loaded IVDs, which can influence the regenerative and anti-inflammatory capabilities of cells such as mesenchymal stem cells (MSCs).

The use of an organ culture model can have many advantages, including the ability to have precise control of the disc microenvironment with regard to physical, chemical, and mechanical stimuli. While organ culture models do not reproduce the full complexity of the *in vivo* microenvironment, including inflammatory responses, they allow for more localized injury responses that more explicitly represent the response of the IVD tissue rather than the crosstalk between the IVD and *in vivo* immune system (e.g., systemic circulation).

1.2 Specific Aims

To address the aforementioned gaps in knowledge, the inflammatory response of the IVD subjected to injury is investigated. Chemical stimulation using (lipopolysaccharide) LPS and a physical puncture are employed to understand the resultant IVD response to injury using outcomes

such as biochemical assays, mechanical testing, and histological analysis. Additionally, inhibition of TLR4, in tandem with the application of the various injury modalities, is examined to gain a better understanding of the role of TLR4 signaling in injured discs. Furthermore, the innate immune response (including the role of TLR4) of the IVD subjected to loading is also clarified by assessing various loading profiles and analyzing the resultant IVD response via cytokine assays, gene expression, and histological analysis.

Following the characterization of the innate immune response of the injured and loaded IVD, analysis of the loaded disc secretome is performed with the goal of defining how loading magnitudes and frequencies can influence resultant paracrine factor release and thus, inform potential therapeutics. Furthermore, MSC priming using the loaded IVD secretome is assessed for immunomodulation and regenerative capability post-injury. Thus, the specific aims outlining this work are as follows.

Specific Aim 1: *Characterize the innate immune response of IVD motion segments to injury, namely through HMGB1 and TLR4 signaling.* Changes in the IVD motion segment response to injury are investigated through the use of chemical and physical injury using various *ex vivo* models. Chemical injury is employed using exogenous LPS, while the physical injuries are executed using the traditional puncture model. It is **hypothesized** that puncture injury will produce a greater innate immune response, characterized by elevated release of HMGB1, compared to LPS stimulation. Furthermore, contributions of TLR4 signaling in response to injury will be investigated for potential anti-inflammatory effects. Specifically, blocking TLR4 signaling may be protective of inflammatory signaling in response to LPS and puncture stimulation.

Specific Aim 2: *Investigate differential inflammatory responses of the IVD subjected to static and dynamic loading ex vivo.* Injurious loading profiles of static and dynamic loading will

induce a greater pro-inflammatory signaling environment through TLR4 signaling compared to unloaded motion segments. It is **hypothesized** that injurious high dynamic loading will induce greater pro-inflammatory signaling and morphological disruptions in the IVD compared to unloaded conditions and that this signaling may be mitigated through TLR4 inhibition.

Specific Aim 3: *Assess how key, distinct paracrine factors that are released in CLM of static and dynamic loaded IVD organ cultures can influence the regenerative and anti-inflammatory capabilities of MSCs.* The secretome of loaded IVD motion segments subjected to static and dynamic loading profiles is identified in order to better elucidate paracrine signaling of the IVD milieu. Proteins, including cytokines, released during loading will be characterized using multiplex assays as well as a proteomics LC-MS/MS analysis. It is **hypothesized** that the IVD motion segment secretome is dependent on the loading profile with varying applied frequency and compression magnitude. It is also **hypothesized** that the paracrine factors in CLM will have a pro-to-anti-inflammatory contribution on naïve MSCs that will be frequency-dependent (static or dynamic). Furthermore, by uncovering the transcriptome of CLM-primed MSCs (CLM-MSCs), it is **hypothesized that** injurious CLM-MSCs will be more immunomodulatory due to increased regenerative and anti-inflammatory priming potential than naïve MSCs. This will be additionally confirmed via standardized assays measuring T-cell proliferation and indoleamine 2, 3-dioxygenase (IDO1) activity. Additionally, it is **hypothesized** that injection of CLM-primed MSCs will improve the regional response of NP and AF post-puncture injury, compared to naïve MSCs, by mitigating the resultant IVD inflammatory response and ECM loss post-puncture.

1.3 Organization

The following chapters will begin by discussing common injury models such as LPS stimulation and puncture injury *ex vivo* and elucidate the unique regional inflammatory and

biochemical response of the IVD. Furthermore, the role of TLR4/HMGB1 signaling will be discussed using the LPS and puncture injury modalities. Next, the role of physiological and detrimental mechanical loading on the IVD in regard to its inflammatory response will be uncovered using various loading profiles on the IVD motion segment *ex vivo*. In addition, the role of TLR4 signaling in mediating the response to loading will be studied via TLR4 inhibition. The following chapter will then delve into characterizing the secretome of a loaded IVD using the aforementioned mechanical loading profiles and investigate the potential of using the secreted CLM to prime MSCs for use as a form of cell therapy. Finally, the last chapter will characterize the CLM-MSCs' therapeutic potential using immunomodulatory assays and functionally by injection in the previously described *ex vivo* puncture model.

Chapter 2: Background & Significance

2.1 Background

2.1.1 Intervertebral Disc (IVD) Structure & Composition

The IVD is the largest avascular structure in the human body. The viscoelastic tissue also separates the vertebrae, allowing for compression and tension of the spine. It is composed of the nucleus pulposus (NP), the annulus fibrosis (AF), and the cartilaginous endplates (CEPs). The NP comprises randomly oriented type II collagen fibrils embedded in a proteoglycan-rich matrix [34-37]. Aggrecan is a major glycosaminoglycan (GAG) constituent in the IVD, comprising 70% of the NP and 25% of the AF. It is responsible for the osmotic properties that allow the NP to act as a resilient "jelly" donut to resist compression [34-38]. Since aggrecan carries a net negative and fixed charge density, the NP is subject to high interstitial swelling and osmotic pressures during joint loading since it retains water inside the matrix. The AF is a collagen-rich structure made of concentric, aligned fibrils enclosed by sheaths of elastic fibers. The AF is composed of two parts: the inner AF and the outer AF. The inner AF is considered the transition area between the NP and the AF, which also helps support compressive loads. It is composed of more collagen type II fibrils and has a higher proteoglycan content than the outer AF [34-37]. The collagen fibril bundles that run obliquely between the lamellae of the annulus in alternating directions in the outer AF are abundant in type I collagen, allowing for the resistance of tensile loads [38]. The CEP lines the superior and inferior surfaces of the IVD. The CEP not only provides additional support to resist compression, but it is also the source of nutrients for the disc [34-37]. The IVD's nutrition comes from the subchondral bone vessels adjacent to the hyaline cartilage of the end plate. Hence, small molecules, such as glucose and oxygen, are transported via a passive diffusion process from the CEP into the IVD [38].

2.1.2 TLR4/HMGB1 signaling in the IVD

A growing body of evidence suggests that TLR4 is involved in the pathogenesis of the IVD [4-6]. IVD expression of TLR4 increases with increasing degeneration severity and mediates catabolic and inflammatory processes [4, 5, 7, 8]. Thus, a growing body of evidence suggests that TLR4 engages in the pathogenesis of the IVD [4-6]. Furthermore, DAMPS, such as HMGB1 or fibronectin fragments, have been shown to have degenerative effects on disc cells including increased expression of inflammatory cytokines and matrix degrading enzymes by signaling through TLRs [9-11]. HMGB1 can serve as an agonist of TLR4 and lead to downstream NF-κβ activation [12].

TLRs are a superfamily of pattern recognition receptors that, when activated, lead to cytokine production. TLR2/TLR4 signaling pathways ultimately activate transcription factors, such as NF-κB, which trigger the production of inflammatory cytokines. Activation occurs when adaptor molecules, such as MyD88, are recruited by TLR2/TLR4 and initiate the signaling pathways and the intracellular cascade [39-41]. TLR signaling has been shown to be upregulated when chondrocytes are mechanically loaded and, in return, experience hydrostatic stress, tensile strain, and fluid flow [42]. OA cartilage and matrix fragments are also known to upregulate TLR signaling, thus leading to cytokine release and an inflammatory response. Thus, TLR signaling may be why various inflammatory markers like interleukin (IL) -1β (IL-1β), IL-6, IL-8, and tumor necrosis factor alpha (TNFα) are produced as seen in loading and cytokine stimulated injury models in the literature [43-46]. However, it is unknown how injured IVD responses are mediated through TLR4.

2.1.3 IVD Chemical Injury Models

LPS is a known chemical stimulant that has been shown to induce a pro-inflammatory cascade in IVD cells with subsequent loss of IVD matrix integrity [7]. It functions by binding to the TLR receptor and has been used widely in preclinical models of inflammation [47, 48]. Many studies have examined the effect of LPS stimulation on NP cells and found that NP cells are indeed responsive to LPS stimulation, leading to suppressed cell proliferation [49], an increase of various pro-inflammatory genes such as *Nos2*, *Il1b*, *Il6*, and *Tnfa*, and an increase in proteoglycan catabolism [45, 50-52]. One study investigated the use of sesamin, a bioactive component extracted from sesame, on LPS-stimulated cells and saw the recovery of NP proteoglycan content in addition to a dose-dependent response attenuating pro-inflammatory gene expression levels [45]. Rat lumbar IVDs were treated with LPS for one week which led to the increase of catabolic enzymes such as metalloproteinase (MMP)-1, MMP-3, MMP-13, a disintegrin and metalloproteinase with thrombospondin motifs (ADAMTS)-4, and ADAMTS-5, and increase in inflammatory cytokine release of TNFα, nitric oxide (NO), prostaglandin-endoperoxide synthase 2 (COX-2), and Prostaglandin E2 (PGE2). LPS treatment also led to the depletion of proteoglycan content in the NP. However, sesamin was able to preserve and protect ECM loss in the NP and inhibit inflammatory signaling, specifically through *Il1b* and *Tnfa* gene expression. However, sesamin was unable to significantly attenuate activated *Tlr4* gene expression [45].

Another study investigated the use of cordycepin, which has been shown to have anti-inflammatory effects on an IVD organ culture system treated with LPS for 7 days in rats. Results showed a protective effect of cordycepin against LPS-induced matrix degradation through NP GAG content, in addition to attenuating activation of the NF-κB pathway specifically through inhibiting phosphorylation of IκBα and p65 [53]. Additionally, one study examined the effect of

microRNA-16 on LPS treated rat NP cells and saw inhibitory effects on the resulting inflammatory response through decreased *Ptges2*, *Ptgs2,* and *Nos2* gene expression levels [52]. Previous papers from our lab have shown that TLR4 can be activated by chemical stimulation using LPS on bovine NP cells, can lead to significant increases in TNFα, IL-1β, IL-6, and NO levels and significant inhibition in aggrecan (ACAN) and collagen-2 (COL2A1) [7] but can be mitigated with the use of the Resatorvid drug, or TAK-242, a small molecule TLR4 inhibitor [7, 54]. Our lab has previously shown how effective TAK-242 is in mitigating inflammation due to chemical injury models such as LPS treated bovine NP cells [54] or through exogenous HMGB1 supplementation in the cell culture media of human NP cells [11].

Existing literature on LPS stimulation of AF cells shows that LPS-treatment increased HMGB1 release from rabbit AF stem cells and increased cell senescence. Furthermore, the following inflammatory genes, IL-1β, IL-6, COX-2, and TNF, were upregulated in LPS treated AF cells, yet the drug metformin was able to attenuate HMGB1 translocation and cell senescence [55]. In a 3D culture model of rat AF cells in a type I collagen gel, LPS treatment led to contraction of the collagen matrix and a decrease in construct mechanical properties, specifically reducing elastic modulus and strength [56]. However, existing literature on the long-term effects of LPS stimulation on a whole *ex vivo* motion segment remains limited.

2.1.4 Traditional IVD Physical Injury Models

IVD puncture injuries are considered traditional models of disc degeneration. However, it is unknown how a puncture injury can affect the innate immune response. A study by Sobajima *et al.* punctured the AF of rabbit discs *in vivo* and saw upregulation of inflammatory markers IL-1β, MMP-3, and NOS2 over 24 weeks using a 16G hypodermic needle [57]. However, a goat study using a 22G sham saline injection in lumbar IVDs did not result in or exacerbate disc degeneration

[58]. Another beagle study using an annular puncture with a 25G needle did not see significant disc degeneration [59]. A needle diameter to disc height ratio of 40% is what is required, according to the literature, to cause a change in the mechanics of the lumbar disc; at the same time, a much larger defect is necessary for the alteration of rat caudal disc mechanics [60-62].

Zhang *et al.* attempted to develop a more consistent and less invasive method of the puncture model by testing two needle gauges. Male Sprague-Dawley rats were punctured using either an 18G or a 21G needle, and outcomes were magnetic resonance (MR) imaging, histological analysis, and immunohistochemical staining of bone morphogenetic protein receptor type 2 (BMPRII) at 4- and 12-weeks post puncture. Starting at 4 weeks, both needle gauges led to decreases in MR T2 density and NP area via histological analysis. BMPRII immunohistochemical expression also increased in both the NP and AF regions of the disc at 12 weeks post puncture, suggestive of increased receptor sites to serve as anchors for the delivery of BMP as a potential therapeutic [63].

Another study examined punctured rats *in vivo* and analyzed magnetic resonance imaging (MRI) scores and histological changes at 4-, 8-, and 12-weeks post puncture. It appeared that puncture injury increased MRI and histology scores at 8 weeks compared to sham [64]. Furthermore, one *in vivo* puncture model attempted to mitigate IVDD development post-injury by injecting the substance, procyanidin B3, and outcome measures included hematoxylin and eosin (H&E), Safranin O staining, and MRI to determine efficacy. Results showed that procyanidin B3 may delay IVDD development in rats, and it may be related to targeting MD-2 (the co-receptor of TLR4) [65].

HMGB1, or fibronectin fragments, may also have a significant role in puncture injuries since they are DAMPs and can be released when significant tissue damage occurs in the IVD.

HMGB1 signaling increases the expression of TLR4, suggesting a possible potentiation of signaling or feedback through TLRs [12]. Yet, the role of TLR4 or HMGB1 in puncture injury remains understudied. Thus, examining HMGB1 release due to puncture injury may provide insight into whether this DAMP is leading to a feedback loop effect in the inflammatory cascade of IDD.

2.1.5 Mechanical Loading of the IVD

Generally, when a disc is loaded as part of its physiological function, NP cells experience hydrostatic and shear stress, while cells within the AF experience tensile strain [66-68]. Intensive mechanical loading of the disc can cause intense shear and compressive forces, leading to tears in the AF rings and bulging of the NP, further propagating ECM degradation and causing a degenerative inflammatory cascade [46]. It is also well known that mechanical loading influences biological responses of the IVD [22, 23, 69, 70].

Dynamic loading has been shown to promote disc degeneration by modulating various pro- and anti-inflammatory cytokines, with secretory profiles varying with loading magnitude and frequency [71]. Certain low-impact physiological stresses, like standing or slow running, have been shown to have beneficial effects on the IVD [72, 73]. Under physiological stresses, human lumbar motion disc segments will experience an average of 4.4 – 6.7% axial strain [19, 20] and intradiscal pressure ranging from 0.03 – 0.7 MPa [21]. For example, upright standing intradiscal pressures can range from 215-747 kPa in healthy individuals aged 22-29[74]. However, the frequency of dynamic loading regulates whether loading pressures are beneficial or detrimental to disc integrity [22-25]. Dynamic loading with pressures ranging from 0.2-0.8 MPa with a frequency of 0.1 – 1 Hz for 8 hours/day [75] has been shown to promote an anabolic response, namely maintaining matrix. Loaded bovine caudal AF and NP cells in alginate at 0.1, 1, or 3 Hz with a

daily compressive strain from 2-12% exhibited extracellular matrix (ECM) degradation when dynamic loading was set at frequencies higher than 1 Hz [76]. Additional studies have shown that static loading caused more detrimental effects on the IVD than dynamic loading, as evidenced by greater ECM degradation and inflammatory cytokine production [23, 77].

It is well established that loading profiles regulate the response of IVD cells in a magnitude- and frequency-dependent manner, where prolonged static loading or dynamic loading above 0.5 Hz promotes matrix degradation *in vivo* while loading at or below 0.5 Hz shows anabolic effects on the disc [22, 23, 69, 70]. Yet, while the anabolic effects of mechanical loading on the IVD have been extensively studied *in vitro* and in organ culture models of the disc, the inflammatory cascades in response to loading have not been as well characterized, though studies suggest that they are also influenced by the loading profile [23, 76, 77]. For example, IL-1β and TNFα were released when NP cells were subjected to compressive loading in addition to the upregulation of matrix components such as COL2A1, ACAN, and MMP3 [23, 76, 77]. Furthermore, Lang *et al.* injected TNFα into the NP as an inflammatory trigger before dynamically loading bovine caudal discs at 5 Hz for 2 hours/day for 11 days and observed an upregulation of IL-1β, IL-6, and IL-8 gene expression as well as increased NO release in TNFα-containing degenerative loading versus no-TNFα physiological loading groups [69]. Nevertheless, changes in inflammatory cytokine profiles to whole bone-disc-bone motion segments in response to loading remain understudied.

2.1.6 Secretome of the IVD

The secretome of the IVD, healthy or degenerated, is extremely understudied. It is known that healthy discs secrete cytokines such as TNFα, IL-1α, and IL-1β, and ECM such as proteoglycans, and that secretion of these pro-inflammatory cytokines and ECM loss are elevated during IDD compared to healthy disc levels [78]. There have been few studies identifying

important biomarkers of IDD[79, 80]; however, the knowledge is limited. Interestingly, in one study, RNA levels of IL-10 were higher in patients with painless neuropathy than in patients with painful neuropathy pain and healthy control subjects, while IL-4 protein levels were the highest in patients with painful neuropathy compared to healthy control subjects. [79, 80]. Another study saw the increase in IL-6 and IL-1β levels not only correlated with number of osteopathic lesions, but IL-6 also correlated with LBP severity in patients with lumbar radicular pain [81].

Few studies have examined the effect of the secretome on resident cells. One study used candidate factor approaches to examine the use of the inflammatory cytokine IL-1β on human NP, AF, and endplate cells [82]. Results showed an upregulation of pro-inflammatory *Nos2* and anti-inflammatory and anabolic tumor necrosis factor inducible gene 6 protein (TNFAIP6). Additionally, presence of IL-1 receptor antagonist (IL-1Ra) (at gene and protein levels), trophic insulin-like growth factor 1 (IGF1), and monocyte chemoattractant protein 1 (MCP-1) were observed in all cell types (NP, AF and CEPs). While this is one study that elucidates the secretome of inflamed IVD cells, there is a lack of knowledge in the literature of how loading can influence the IVD secretome. While it is known that proteins are released, it is unclear how magnitude and frequency of load can affect the level and type of paracrine factors emitted into the IVD milieu.

One study investigated by Navone *et al.* analyzed the secretome of bovine caudal IVDs that were subjected to high-frequency loading in an *ex vivo* bioreactor and saw increased levels of IL-8, nerve growth factor (NGF), interferon-γ (IFNγ), and IL-17 release into CLM compared to unloaded conditioned media. When the conditioned media was co-incubated with microglia for 48 hours, an upregulation of IL-1β, IL-6, TNFα, NOS2, ionized calcium-binding adapter molecule 1 (IBA1), and vascular endothelial growth factor (VEGF) was observed in the gene expression of microglia [83]. Another study by Pattappa *et al.* was novel in their investigation of the secretome

of loaded bovine caudal discs and focused on chemoattractants released by degenerated IVDs that would recruit MSCs. The study cultured bovine caudal discs and loaded them for 7 days using physiological (low-glucose and low frequency, 0.2 Hz, 0.6±0.2 MPa) or degenerative (puncture and high-frequency, 10 Hz) conditions. After 4-6 days of loading, the media was replaced with PBS for two days. Proteomics was conducted, and it led to the identification of 104 proteins in either physiological or degenerative media. Specifically, they saw increased levels of CCL5 or RANTES, a key chemoattractant necessary for immune cell infiltration from degenerative loading conditions [84]. They also saw increased levels of IL-1β and TNFα, which correlated with CCL5 concentration for each secretome sample [84].

Literature has also characterized the secretome of NP tissue homogenate in non-chondrodystrophic (NCD) and chondrodystrophic (CD) canine IVDs. It is hypothesized that the CD canine resembles human etiology/pathology compared to all animal models, where degeneration of the AF always occurs after NP degeneration [85, 86]. Thus, proteomic analysis of the NP protein homogenate in CD canine IVD would inform an NP secretome that would be translatable to humans. Using mass spectrometry along with isobaric tagging for relative and absolute quantification (iTRAQ), immunohistochemistry, western blotting, and proteoglycan extraction techniques, 377 identified proteins were present in both NCD and CD models [87]. Additionally, 13 proteins (decorin, fibronectin, cartilage oligomeric matrix protein, cartilage intermediate layer protein, HAPLN1, biglycan, isoform B of proteoglycan 4, fibromodulin, and aggrecan core protein) were upregulated in the CD NP compared to the NCD NP [87].

The same research group then characterized the secretome of notochordal cells in the NP. It was hypothesized that the secretome of notochordal cells in the NP would lead to identification of key proteins that would delay the onset of DDD. It was found that transforming growth factor

beta-1 (TGFβ1) and connective tissue growth factor (CTGF) were identified as major hubs, and so they conducted *in vitro* treatment to investigate the effects of these paracrine factors on degenerated human NP cells. Accordingly, female Wistar rats were punctured using a 26 g needle throughout the entire full thickness of the AF on both sides of the disc. Intradiscal injection of either serum-free notochordal cell-derived conditioned medium (NCCM)/CTGF or TGFβ1 occurred 4 weeks post-injury. Results exhibited an increase in healthy ECM protein production, increased cell proliferation, and decreased cell death in degenerated human NP cells post *in vitro* treatment of TGFβ1 and CTGF [88].

However, historically, simply injecting growth factors, such as BMP2, during anterior lumbar interbody fusion surgeries [89] has not always been effective at improving disc outcomes [88, 89]. BMP2, for example, may be limited by its osteo-inductive characteristics despite showing promise for treatment as an effective bone graft substitute [90]. Injection of anti-inflammatory agents such as IL-1Ra [91] and TNF/NFkB inhibitors [92] also have limited efficacy in improving the anabolic response of the disc due to their short half-life [88]. Based on these studies, more research is needed to understand and optimize the secretome of the loaded or degenerated disc to elucidate the paracrine factors at play during IDD.

2.1.7 Cell Therapy for IVD Disease

Although studies that inject soluble factors alone to improve degenerated IVD phenotype are promising [88], it can be difficult to translate such techniques using an *in vivo* model due to low retention and short half-lives of molecules [93]. Thus, cell therapy has gained traction in recent years. In recent years, MSCs have gained interest in the field of tissue engineering due to their anti-inflammatory function and ability to modulate tissue repair and regeneration [94-97]. They are attractive for IVD repair because they can differentiate into NP- and AF-like cells [98-102],

promote recovery of disc height, increase proteoglycan and collagen content, and are easy to isolate [98, 101-108]. However, identifying the suitable cell population for cell therapy is one obstacle that the research field has yet to determine to treat IDD. The heterogeneous tissue components of the IVD, consisting of the gelatinous NP, concentric collagen-rich AF, and cartilaginous CEPs, further complicate regenerative solutions.

To begin, a healthy IVD is an immune-privileged tissue due to its avascular nature, making it a suitable option for allogeneic cell transplantation. While IVD cells are the optimal choice for transplantation, they can be difficult to acquire without damaging a native IVD. Literature has identified a stem-like population, or NP progenitor cells, in the IVD NP from 8–12-month-old non-chondrodystrophic canine IVDs [109]. While these cells can express "stemness" genes such as Sox2 and Oct3/4r, this population of cells is reported to only represent 1% of the IVD NP (albeit debatable [110]), making it difficult to isolate for cell therapy purposes [109]. In a recent single-cell RNA sequencing study, stromal cells were abundant in human NP and AF, suggesting that MSCs are native to the IVD environment, maintaining IVD homeostasis [111]. Risbud *et al.* also demonstrated the presence of resident MSCs in the degenerate human disc, suggesting they may need stimulation to attempt repair; yet, it is unclear what stimulation is necessary for regeneration [112].

Nevertheless, MSCs are the most popular graft cells for cell-based therapies as they are easy to obtain and can differentiate into chondrogenic and IVD-cell lineages [84, 96, 110, 113, 114]. Exogenous MSC injections show promise as studies have shown improved MSC homing cell migration towards the site of injury [84, 115, 116], especially since MSCs exhibit the following key chemokine receptors (CCR-) CCR1, CCR7, CCR9, CXCR4, CXCR5 and CXCR6 [117]. These injections' success is attributed to increased chemokine/chemoattractant signals provided

by the injury site, potentially through the presence of growth factors such as platelet-derived growth factor (PDGF)-BB, PDGF-AB, epidermal growth factor (EGF), Heparin-binding EGF-like growth factor (HB-EGF), transforming growth factor (TGFα), insulin growth factor (IGF-I), hepatocyte growth factor (HGF), fibroblast growth factor (FGF-2), and thrombin [115, 116, 118].

One study examined the transplantation of human MSCs into IVDs using a xenogeneic porcine model where the injury was induced by the aspiration of the NP. Results showed reduced MRI T2 intensity with cells compared to injury alone. Additionally, MSCs survived for at least 6 months and expressed typical chondrogenic gene expression markers, like COL2A1, COL2A2, versican, COL1A1, ACAN, and SOX9, suggesting differentiation toward chondrocyte-like disc cells [119]. While this study was promising for MSCs as an injectable therapy, it did not quantify the number of surviving cells that differentiated toward chondrocyte-like cells. Additionally, it did not factor in a more native injury model where NP, AF, and endplates of the disc were degenerated [119].

Despite successful differentiation towards disc-like cells, improved proteoglycan content, and reduced T2 intensities with injection of MSCs in an IDD model, challenges in MSC therapy via injections include low survival rates of MSCs, due to cells dying or undergoing apoptosis [119-121], when transplanted into a degenerated IVD [110]. Sivan *et al.* investigated MSC cell viability post injection via encapsulation of human BMSCs in alginate microspheres into an injured rat model post-nucleotomy and observed long-lasting viability of MSCs for at least 8 weeks post implantation based on H&E staining. However, NP recovery was not evaluated post the nucleotomy [122].

Nevertheless, while clinical success with animal models is promising, no evidence exists yet to support human MSC use [123-125]. One study conducted with autologous adipose MSCS

for treatment of LBP saw a 68% reduction in Visual Analogue Scale (VAS) at 6 months [123]; however, no other outcomes were reported. Mochida *et al.* were able to slow further degeneration of discs using NP cells that were "activated" via culture with autologous bone marrow-derived MSCs prior to transplantation [124]. Results showed that Japanese Orthopaedic Association (JOA) scores doubled, representing decreased LBP post 3 years of cell injection. However, no difference in disc hydration was reported [124]. Thus, research is still needed on MSC usage in clinical models of IDD.

MSC secretome is another component of cell therapy that has promise to mitigate IDD. MSC secretome has been seen to decrease the inflammatory response of AF organ cultures [126] and decrease NP cell metabolism while improving ECM gene expression *in vitro* [127]. One paper examined the effect of extracellular vesicles (EVs) and soluble fractions (SFs) versus the entire conditioned medium (CM) of adipose tissue-derived human MSCs on TNFα-treated human NP and AF cells and concluded that the presence of whole CM modulated pro-inflammatory and catabolic factors is at a greater level than EVs or SFs alone [128]. Thus, while EVs are an interesting direction for cell therapy, one drawback is scale-up and the limitation on the biological factor subset that is present in EVs.

Another study examined how an IL-1β preconditioned MSC secretome modulates inflammatory response and aggrecan deposition in IVD. By preconditioning human MSCS with IL-1β and low oxygen conditions, MSCs produced a secretome (MSCsec) with elevated levels of IL-6, IL-8, and MCP-1. The generated MSCsec was then placed in a co-culture with a degenerated, IL-1β treated *ex vivo* bovine IVD for up to 2 weeks. Downregulation of IVD gene expression of IL-8 and IL-6 was observed in addition to increased aggrecan deposition after 14 days of co-culture. Additionally, when analyzing the protein content of the MSCsec-IVD supernatant, there

was an increase of the following proteins, CXCL1, MCP-1, IL-6, IL-8, and a decrease of IFNγ, IL-10, IL-4, IL-5 and TNFα (associated with T-cell receptor signaling) was reported [129].

Nevertheless, cell therapy has shown promise through the encapsulation of MSCs into delivery systems, such as gelatin or human Wharton's jelly, as cell encapsulation can improve on the localization of MSCs upon delivery and regulate the controlled release of growth factors. This method not only uses MSCs as a therapeutic but also uses carriers to improve outcomes. One study looked at improved MSC differentiation into NP-like calls by not only having a hydrogel material that was similar to NP, but also by also loading the construct with TGFβ3 nanoparticles to establish a co-delivery system with the dextran/gelatin hydrogel [130]. Their results showed improved biochemical content post 28 days with the construct as the TGFβ3+PLGANP group led to the greatest GAG and collagen production compared to the controls or the TGFβ3 only or PLGANPs only groups. This suggests that these constructs could be used for the discogenesis of MSCs *in situ*. However, the limitation of this study was that it was conducted *in vitro*, and it does not consider if this delivery system will function *in vivo* due to bodily circulation [130]. A similar study looked at the efficacy of Wharton's Jelly-derived MSC (WJ-MSC) transplantation in an animal model of IVD degeneration using percutaneous annular puncture and NP aspiration and found improvement in T2-weighted MRI and histological analysis 12 weeks after transplantation [131]. While these studies were preclinical models and showed improvement in biochemical and water content independently, none have examined the anti-inflammatory effects of MSCs in an injured disc model.

Remarkably, one study has examined the potential use of nasal chondrocytes as a source of cell therapy for a degenerated disc. Under acidic, inflamed (treated with TNFα, IL-1β, and IL-6) conditions, Gay *et al.* showed how nasal chondrocytes can serve as a cell therapy source for

IVD repair in a manner that is better than MSCs or articular chondrocytes through improved GAG and collagen type II synthesis and downregulated inflammatory cytokine receptor gene expression (mainly TNFαR and IL1R1)[132]. While this study adds to the literature that nasal chondrocytes may be better than MSCs at surviving in the harsh, acidic, degenerated IVD environment [133, 134], such technology has not yet been tested *in vivo*. This delayed progress keeps MSCs as the gold standard for IDD cell therapy despite their drawbacks of failing to adapt and limited survival in the IVD environment. Cell therapy may be the solution to improving degenerated IVD phenotype and function[135], yet the exact mechanism of MSC therapy on degenerated discs remains unclear. Thus, without further investigation, one cannot yet conclude that MSCs can serve as a regenerative and anti-inflammatory source of cells to treat IDD.

2.1.8 MSC Priming as Cell Therapy

One major function of MSCs in tissue repair is their anti-inflammatory abilities in modulating disease microenvironments. Prior studies have shown that priming human MSCs with IFNγ or poly I:C-leads to a pro- or anti-inflammatory effect, respectively [136]. Studies have also emphasized the importance of the MSC secretome and the benefits of immunomodulation from MSC conditioned medium (CM) [96, 137, 138], where primed MSC secretome led to immunomodulatory effects on IL-1β-stimulated chondrocytes [139] and in many other instances covered in Section 2.1.7. However, few studies have examined how a tissue's secretome, such as the IVD, can influence MSC phenotype and immunomodulation. One study analyzed conditioned media derived from healthy, traumatic, and degenerated human IVDs and used the IVD secretome to analyze its effect on MSC secretion, proliferation, viability, and metabolic activity [138]. The IVD secretome exhibited distinct profiles among human sources of IVD CM, and the primed MSCs appeared to respond differentially to the sources of CM [138]. Upregulated proteins

identified in the secretome of MSCs cultured with healthy, traumatic, or degenerative IVD CM were chondroadherin (CHAD), decorin (DCN), cartilage oligomeric matrix protein (COMP), and TGFβ1. Proteins identified in healthy IVD CM only included EGF-containing fibulin-like extracellular matrix protein 1 (EFEMP1), olfactomedin-like 3 (OLFML3), and alpha-2-Macroglobulin (A2M). Proteins identified in degenerative IVD CM included galectin-7 (LGALS7) and keratin-16 (KRT16), while IL-1β treated MSCs released IL-6 and myosin heavy chain beta (MYH7) [138]. Thus, given these distinct paracrine factors being released from IVD-CM cultured MSCs, it suggests that priming mechanisms take place by subjecting MSCs to various versions of IVD medium stimuli within 24 hours.

Studies have emphasized the importance of the IVD secretome, its potential for MSC stimulation/priming, and the benefits of immunomodulation from MSC CM [96, 137, 138], where primed MSC secretome leads to immunomodulatory effects on IL-1β-stimulated chondrocytes [139]. Pattappa *et al.*, previously mentioned in Section 2.1.6, not only characterized the secretome of loaded bovine caudal discs but also cultured human MSCS in a Boyden chamber with the native or chemokine depleted media. These primed MSCs significantly increased CCR1 and CCR4 gene expression compared to naïve MSCs. Additionally, both CCL5/RANTES receptor expression post priming increased with the CLM from physiological and degenerative conditioned PBS media [84].

Another study has reported that MSCs are able to secrete anti-inflammatory mediators IL-1Ra, IL-10, IL-13, and tumor necrosis factor-inducible gene 6 protein (TSG-6), anti-catabolic factors (TIMPs), and growth factors (TGF-β, GDF-5) when cultured in IDD-like conditions (potentially through TNFα or IL-Lβ stimulation), thus exerting an immunomodulatory effect on surrounding cells [96, 135]. In a recent study, Teixeira *et al.* evaluated the biological responses of

human BM-MSCs using an *ex vivo* bovine model of IDD (needle puncture with IL-1β supplementation) [140]. Although unable to improve ECM production of bovine NP, BM-MSCs showed an increased production of the following cytokines IL-6, IL-8, PGE2, and MCP-1, and downregulation of the expression of IL-6, IL-8, and TNFα on bovine IVD cells [140].

According to the literature, there are 4 main priming approaches to improve MSC therapeutic efficacy. They are 1) priming with cytokines or growth factors, 2) using pharmacological or chemical agents, 3) hypoxic conditions, and 4) 3D culture conditions [141]. As previously mentioned, cytokines such as IFNγ, TNFα, and IL-1β can be used as additive effects to increase IDO transcription factors or IL-6 or TGFβ soluble factor release. Such priming is immunomodulatory and regenerative. Meanwhile, chemical agents such as LPS can also be used to increase IL-6 and TNFα release from MSCs, and this also has a regenerative, immunosuppressive, and angiogenic effect on the MSCs. Hypoxia promotes an undifferentiated stem cell state as it may allow cells to escape oxidative stress and possible DNA damage [142], having an anti-apoptotic effect while upregulating NOTCH signaling. 3-D culture can lead to an increase in IL-1, IL-6, and IL-8 release from the MSCs, which is suggested to be immunomodulatory while increasing stemness [141].

However, literature suggests that cytokine priming of MSCs may be more influential than priming through loading. Goncalves *et al*. looked at IL-1β precondition human AF cells versus applying the secretome from MSCs subjected to a physiological cyclic tensile strain (CTS) for 72 hours and found that the MSC secretome from the cyclic tensile strain stimulation upregulated collagen type 1 on the AF cells, but the IL-1β MSC secretome led to increased IL-6, IL-8, MMP-1, and MMP-3 gene expression and as well as prostaglandin E2 production on the AF cells. The combination of CTS + IL-1β had a similar outcome as IL-1β alone, thus suggesting that the

paracrine factors from an IL-1β stimulation of MSCs are more potent than a physiological load on MSCs [137]. Nevertheless, there is still a gap in knowledge on the effect of the paracrine factors released during IVD loading and if that is enough to prime MSCs and alter their function.

IDO activity has been used as a tool to explain MSC stemness and immunosuppressive ability [143-145]. IDO1 is an inducible heme-containing enzyme whose upregulation has been seen as essential for immunoregulatory abilities [146]. IDO1 leads to the degradation of L-Trp (or L-tryptophan), a common essential amino acid [146]. This decrease in L-Trp then activates a kinase, general control nonrepressible 2 (GCN2) [147] which can shut down genes, including IL-6. The kinase activation leads to immunomodulatory effects, such as blocking the conversion of Treg cells to pro-inflammatory T helper type 17 [146]. Additionally, IDO1 leads to the production of L-Kyn (L-kynurenine), which is an endogenous agonist that can lead to the differentiation of effector T cells into Treg cells as well as reprogramming dendritic cells (DCs) towards long-term immunoregulatory phenotype. Furthermore, IFNγ is considered to be the main IDO1 inducer across many cell types (**Fig. 2.1**). Other cytokines, such as TNFα, IL-6, and IL-10, may synergize with each other to increase IDO1 expression [148]. Thus, when an MSC is exposed to a degenerative environment, there is high potential that IDO is upregulated, leading to an increase in immunosuppression and regenerative effects (**Fig. 2.1**).

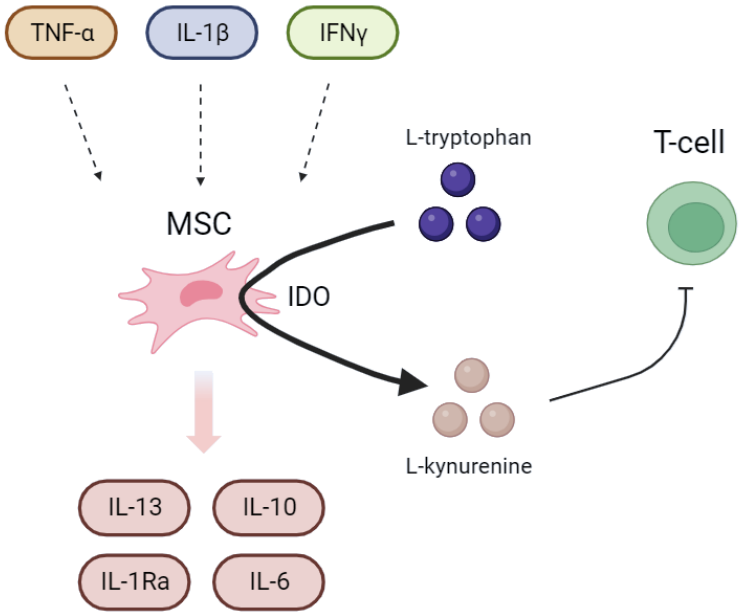

Figure 2.1: MSC priming in a degenerated environment

Pro-inflammatory cytokines, such as TNFα, IL-1β, or IFNγ, can lead to restoration of a healthy cell phenotype through potentially mediated by IDO and the release of certain inflammatory cytokines. Created with Biorender.com

2.2 Significance

The work in this thesis is the first to characterize inflammatory and biochemical differences in the response of the IVD motion segment to injury. Additionally, this is the first study to separate the injury response by IVD region (NP vs AF) as well as by donor sex, which has been observed to be a significant contributor to degeneration and pain. This work is also novel in characterizing the inflammatory response of the IVD motion segment to various loading profiles deemed physiological and detrimental by literature. Last but not least, this work is one of the first to fully characterize the secretome of a loaded IVD motion segment and then use the secretome to prime MSCs. Additionally, this work examines the functional aspect of primed MSCs through an International Society for Cellular Therapy (ISCT)-approved T-cell proliferation assay and IDO1 protein levels. An *ex vivo* puncture injury model was conducted, and then the functional aspect of injected primed MSCs was assessed through regional IVD gene expression differences.

Chapter 3: Characterizing the innate immune response of IVD motion segments to injury, namely through HMGB1 and TLR4 signaling

3.1 Introduction

Sexual dimorphism, or sex-based differences, appear to exist in levels of LBP as there is greater prevalence and severity of musculoskeletal pain in women compared to men. According to the Global Burden of Disease Studies in 2019, the prevalence of LBP globally was 7.64% worldwide; however, when stratified by sex, 8.83% of women experienced LBP compared to 6.42% of men [149]. Additionally, in Spain, women reported greater prevalence (17.8%) of LBP than men (11.3%) [150]. There are cultural and gender differences (ex. manual labor jobs or one's likelihood to go to a doctor) that can influence the data on the onset and severity of LBP. Pregnancy may also be a factor for women, leading to a 50% incidence rate of LBP and exacerbating the development of degenerative spinal spondylolisthesis [151, 152]. Sex hormones, such as estrogen, may also contribute to the onset of LBP and IDD [151, 153, 154]. Interestingly, postmenopausal women above the age of 50 are more susceptible to lumbar IDD than age-matched males [155]. However, men are more susceptible to IDD in their youth, most likely due to increased mechanical stress and physical injury from an increased likelihood of participating in high-impact physical activities [156-158]. IDD typically becomes apparent for males in the second decade of life, 10 years earlier than in women. Nevertheless, Wang *et al.* showed that elderly women had more severe IDD than elderly men at all lumbar levels [158].

Despite this clinical evidence, it is unknown if there are differences in IVD composition between sexes. Biomechanics analysis of the human spine has shown that female specimens

demonstrate a greater overall range of motion in all planes compared to males, regardless of severity of degeneration [151, 159]; however, this may be due to many factors, including differences in spinal anatomy, vertebral anatomy, or tissue laxity. Meanwhile, T1ρ values for the nucleus pulposus (NP) taken from MRIs of lumbar discs suggest that males may have higher proteoglycan content than females [160]. Studying sex-based differences among human subjects can be difficult due to cultural and gender biases. Research animals, however, live in a controlled environment, allowing for the study of sexual dimorphism while minimizing societal influences.

Few studies to date have evaluated the effect of sex on IVD response to injury. In a set of studies by Mosely *et al*., disc degeneration was simulated *in vivo* using an IVD annular puncture injury, with findings indicating that rats exhibit sexual dimorphism in injury responses. While both sexes had decreased cellularity and increased fibronectin at injury sites, females had an increased degeneration grade in the outer annulus fibrosus (AF) compared to males. Meanwhile, male IVDs had greater mechanical properties, while females had reduced second-harmonic generation (SHG) intensity, suggestive of a decrease in collagen (COL) density [161], compared to males post-puncture injury, signifying improved healing in male punctured IVDs than their female counterparts. A follow-up study on pain behavior found that male rats showed increased allodynia compared to females after IVD puncture injury [162]. In mice, a study showed that a high advanced glycation end products (AGE) diet increased compressive stiffness and torque range for females than males [163]. In SPARC-null mice, while similar inflammatory responses between sexes in degenerated IVDs were reported, increased voluntary running was observed to reduce inflammatory mediator release (CXCL1 and CXCL5) *ex vivo* only in female mice [164]. To our knowledge, not many studies have investigated sex differences in animal models *ex vivo*, and of those that did, their results were consistent with *in vivo* findings [165, 166]. One advantage of

using an *ex vivo* approach is that by removing tissues and cells from the complex interactions with other cells, hormones, neurotransmitters, nutrients, and environmental exposures *in vivo*, which themselves vary in living organisms by sex, we are able to isolate sex-based differences in an organ of interest: the IVD. Therefore, investigating the effect of donor sex *ex vivo* can help define IVD specific differences that are not dependent on regional or systemic responses to injury.

The goals of this study were to evaluate the response of both male and female IVD motion segments to puncture injury or inflammatory stimulation with LPS *ex vivo* and to investigate the contributions of TLR4 signaling to injury responses. A growing body of evidence suggests that TLR4 is involved in the pathogenesis of the IVD [4-6]. TLR4 expression in the IVD increases with degeneration severity and mediates catabolic and inflammatory processes [4, 5, 7, 8]. Furthermore DAMPS, such as HMGB1 or fibronectin fragments, have been shown to have degenerative effects on disc cells, including increased expression of inflammatory cytokines and matrix degrading enzymes by signaling through TLRs [9-11]. HMGB1 can serve as an agonist of TLR4 and lead to downstream NF-κβ activation [12]. However, it is unknown if IVD puncture injury responses are mediated through TLR4. To evaluate this, we assessed sex-based differences in response to injury with the presence of a small molecule TLR4 inhibitor, TAK-242. We hypothesized that donor sex would be a significant contributor to the inflammatory response, as well as biomechanical, biochemical, and histological properties of the IVD motion segment when subjected to chemical or physical injury. Subsequently, we expected that TAK-242 would modulate the inflammatory response and improve biomechanical, biochemical, and histological outcomes post-injury through inhibition of the TLR4 pathway.

3.2 Material and Methods

3.2.1 Study design

This chapter uses an *ex vivo* organ culture model to investigate the IVD response to injury using LPS as a chemical stimulation and puncture as the physical injury model. The inflammatory, biomechanical, biochemical, and histological responses of the IVD, as a whole and through regional differences, were examined in both male and female rats. The results would determine whether to focus on one sex at a time or combine data from both sexes for future chapters in this thesis.

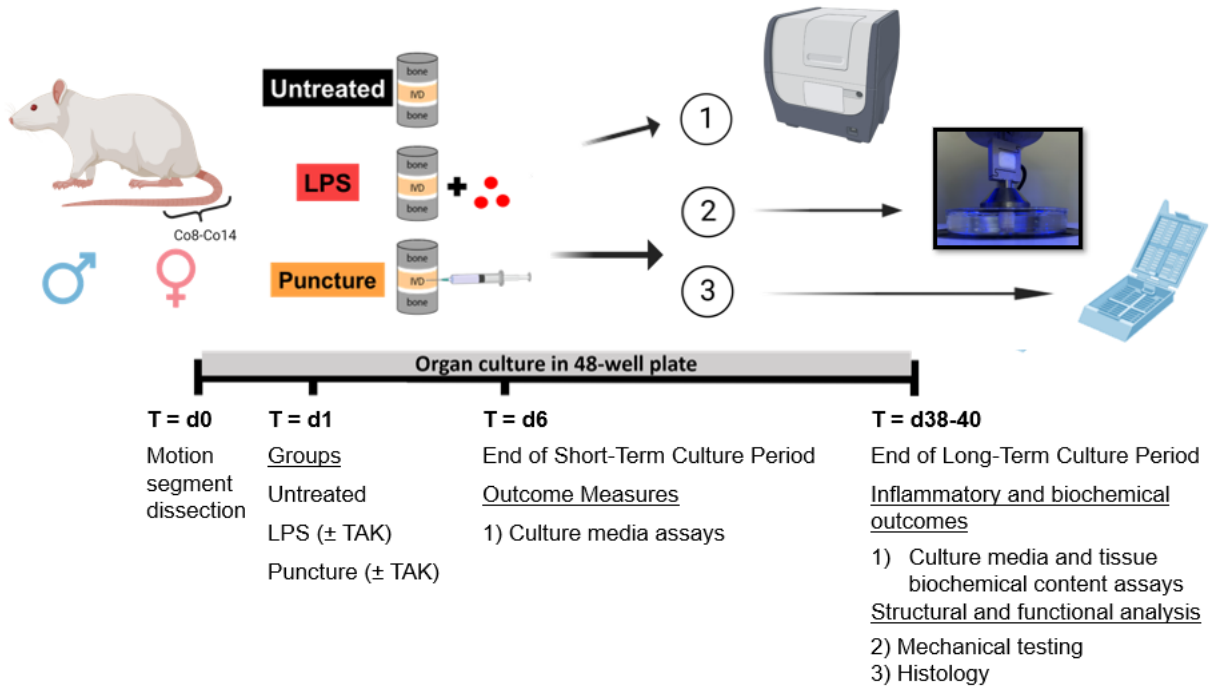

Figure 3.1 Experimental plan of Chapter 3.

Created with Biorender.com

.

3.2.2 Sample isolation and tissue culture of discs for LPS and puncture model

The use of animals in this work was approved by the Institutional Animal Care and Use Committee (IACUC) at Columbia University. Caudal (Coccygeal/Co) bone-disc-bone motion segments (4 to 6 per animal) were isolated from multiple spinal levels (Co8 to Co14) of eight male and eight female Sprague-Dawley rats (200 – 350 g, 3-month-old). Cuts were made mid vertebral body to separate levels, and samples were washed in 1x PBS with 1% antibiotic-antimycotic (AA) and then briefly submerged in Dulbecco's Modified Eagle Medium (DMEM), 10% FBS, 1% AA (naïve media). Motion segments were then cultured in chemically-defined media (CM: phenol-free DMEM without L-glutamine, 100 µg/mL sodium pyruvate, 50 µg/mL L-proline, 1% AA, 1% ITS Premix, and a 4 mM concentration of 3:1 GlutaMax:Glutamine) for 24 hours [167]. After the 1-day equilibration period, samples were allocated into 1 of 3 injury groups: untreated (CM alone), LPS (1 µg/mL LPS in CM), or puncture (CM alone). Samples were cultured for either 6 days (short-term) or 38 days (long-term) to investigate changes in extracellular matrix (ECM) biomechanics, biochemistry, and histology. Motion segments were allocated consistently by spinal level for short-term and long-term studies (**Fig. 3.1**).

3.2.3 Chemical stimulation and puncture injury of discs

LPS (Sigma-Aldrich) was suspended in sterile deionized water by sonication (1 mg/mL) and diluted in CM to 1 µg/mL. Inflammatory stimulation was simulated by culturing motion segments with LPS (1 µg/mL in CM) throughout the duration of the study. For short-term culture, CM±LPS was replenished at days 2 and 4, while for long-term culture, CM±LPS was replenished at days 3, 6, 10, 13, 17, 20, 24, 27, 31, and 38. Physical injury was simulated with a one-time puncture injury, made using a 20-gauge (G) needle inserted 4 mm into the IVD and held in place for 15 seconds prior to start of the culture duration in CM.

3.2.4 TLR4 inhibition

A separate cohort of animals was used to determine the effect of TAK-242 on the response of IVD to injury. Five male and five female rats were used to isolate N=5 caudal motion segments per animal, as described above. The motion segments were exposed to puncture or LPS injury, as previously described. Samples were then cultured in CM±TAK-242 for up to 38 days in culture. TAK-242 (TLR4 inhibitor, EMD Millipore) was solubilized in DMF (Thermo Scientific) (25 mmol/L) and diluted to a working dose of 1 uM to block TLR4 signaling in the motion segments. The motion segments were allocated to the following groups: puncture (P), puncture+TAK (PT), LPS (LPS), or LPS+TAK (LPST). For long-term culture, CM ± TAK was replenished in these groups on days 3, 6, 10, 13, 17, 20, 24, 27, 31, and 38.

3.2.5 Disc supernatant analysis

Tissue culture media was collected every 2 days (short-term), or every 3 to 4 days (long-term), and stored for analysis. Media supernatant was analyzed for levels of NO using the Griess Reagent System (Promega), lactate dehydrogenase (LDH) with the Cytotoxicity Detection Kit (Roche), and GAG loss into the media with the 1,9-dimethylmethylene blue (DMMB) assay (Sigma-Aldrich) (Farndale et al., 1986). For the 6-day time point, levels of HMGB1 (Tecan) in the media were also measured. Supernatant levels were normalized to motion segment wet weight to reduce effects of segment variability**.**

3.2.6 Mechanical testing

Using digital fluoroscopy, disc height, and cross-sectional area were measured before discs were subjected to unconfined compression testing at the end of the long-term study (days 38-40) to normalize mechanical testing results. Radiographic analysis of IVDs was performed using a BenchTop Labscope (Glenbrook Technologies). Pre-loading images were acquired, and the radii

and disc heights of samples were analyzed using ImageJ [168]. For radius measurements, three equally-spaced measurements were taken across the width of each IVD and averaged. For height measurements, five equally-spaced measurements were taken across the length of each IVD and averaged. Preconditioning consisted of 20 cycles of 2 N applied at 0.1 Hz, followed by a creep load of 2N (equivalent to 1 rat body weight) until equilibration (20 mins). Dynamic and equilibrium moduli were calculated using a custom MATLAB code.

3.2.7 Biochemical content of IVDs

Post-mechanical testing, whole IVDs (encompassing the NP and AF regions) were dissected, and their wet weights were measured. Subsequently, the NP and AF regions were separated, and individual wet weights of each region were measured. Samples were then stored at -80°C until lyophilization. Samples were lyophilized for 48 hours using a benchtop freeze dryer (Labconco), and dry weights of separated NP and AF regions were measured. Tissue water content (%) was calculated based on the weights ((wet weight - dry weight)/wet weight). Samples were then digested in Papain (0.02% (v/v), P3125, Sigma-Aldrich) in a pH=6.0 digest buffer (sodium acetate anhydrous (S2889, Sigma-Aldrich), cysteine hydrochloric acid (HCl) (C9768, Sigma-Aldrich), ethylenediaminetetraacetic acid (EDTA) (E6758, Sigma-Aldrich) in a 60°C water bath for 24 hours. Quantification of DNA, GAG, and COL content from the tissue digests was measured using PicoGreen dsDNA Assay Kit (P11496, ThermoFisher), DMMB, and orthohydroxyproline (OHP) assay with a 1:7.64 OHP-to-collagen mass ratio [169], respectively. DNA content was measured to assess the cellular content of the treated groups versus controls. Furthermore, DNA content was used to normalize GAG and collagen content to inform differences observed with cellular density or activity.

3.2.8 Histology

To evaluate changes in IVD morphology, short- and long-term discs were fixed in 10% neutral buffered formalin phosphate overnight at 4°C post-mechanical testing. Motion segments were then decalcified in 14% EDTA for two weeks and cut longitudinally along the vertebral bodies. Decalcified discs were paraffin-embedded and sectioned (7 µm). Slides were stained with Safranin O with a Fast Green counterstain or Picrosirius Red, indicating GAG or COL content, respectively. Images were taken using a Zeiss Axio Observer Z1 and an Axiocam 503 color camera and graded for the histopathologic features using the recent ORS Spine Section initiative scale [170].

3.2.9 Statistical analysis

Data was assessed for normality using the Shapiro-Wilk Test. Two-way ANOVAs were performed for effect of injury (untreated, LPS, puncture), sex (male, female), and interaction between injury and sex. Group comparisons were performed with Holm-Šídák post hoc tests. When warranted by the result of the normality test, a non-parametric Kruskal-Wallis ANOVA with injury (untreated, LPS, puncture), sex (male, female), and their interactions was performed using Dunn's multiple comparisons test for group comparisons. Within each injury type, two-way ANOVAs were also performed to identify the effect of TAK-242 (with or without), sex (male, female), and interaction between TAK-242 and sex on injury response. Group comparisons were performed using Holm-Šídák post hoc tests. When warranted by the result of the normality test, a non-parametric Kruskal-Wallis ANOVA within each injury type was performed to determine the effect of TAK-242 (with or without), sex (male, female), and their interactions, with Dunn's multiple comparisons test used for group comparisons. In all tests, $p<0.05$ was considered statistically significant. The main effects p-values (injury or treatment, sex, interaction) are

presented above each subfigure in bold if any of the terms had $p<0.05$. Group comparisons are presented in the figures using symbols (*,†, a, or b). A significant interaction term indicates that the effect of injury (or treatment) depends on donor sex. Analyses were performed with GraphPad (9.5.0).

3.3 Results

3.3.1 Short-term inflammatory and long-term biomechanical and biochemical characterization of injured discs

Cumulative NO release into the media on day 6 had a significant effect on treatment (p=0.003) where LPS treated discs led to the greatest level of NO release into the media compared to control and punctured discs (**Fig. 3.2a**). HMGB1 levels in media were also dependent on treatment (p=0.0008). HMGB1 release from punctured discs (2.23 ng/g) was greater than untreated (0.242 ng/g, p=0.002) and LPS treated (0.187 ng/g, p=0.002) discs (**Fig. 3.2b**). LDH release into the media was not dependent on treatment (**Fig. 3.2c**).

Dynamic modulus results of 40-day cultured discs showed dependency on treatment where control discs had higher moduli than LPS (p<0.0001) or puncture treated discs (p<0.0001, **Fig. 3.2d**). After 40 days, equilibrium modulus exhibited dependency on treatment where punctured discs were significantly less stiff than control discs (p=0.0032, **Fig. 3.2e**).

There was no difference in NP DNA/DW (**Fig. 3.2f**) or NP COL/DW (**Fig. 3.2h**) content of injured discs versus untreated discs; however, puncture injury did decrease NP GAG/DW content (157.4 μg/mg) compared to untreated discs (344.7 μg/mg, p=0.033, **Fig. 3.2g**). There were no differences in normalized NP GAG/DNA content across all discs (**Fig. 3.2i**), however, there was an increase in NP COL/DNA (0.33 μg/ng) content in punctured discs versus untreated discs (0.0054 μg/ng, p=0.013, **Fig. 3.2j**).

In the AF, there was also no difference in DNA/DW (**Fig. 3.2k**) or COL/DW (**Fig. 3.2m**) content of injured discs versus untreated discs. However, puncture injury also decreased AF GAG/DW content (10.4 μg/mg) compared to untreated discs (19.4 μg/mg, p<0.0001, **Fig. 3.2l**).

There was no difference in normalized GAG/DNA (**Fig. 3.2n**) or COL/DNA content across all discs (**Fig. 3.2o**).

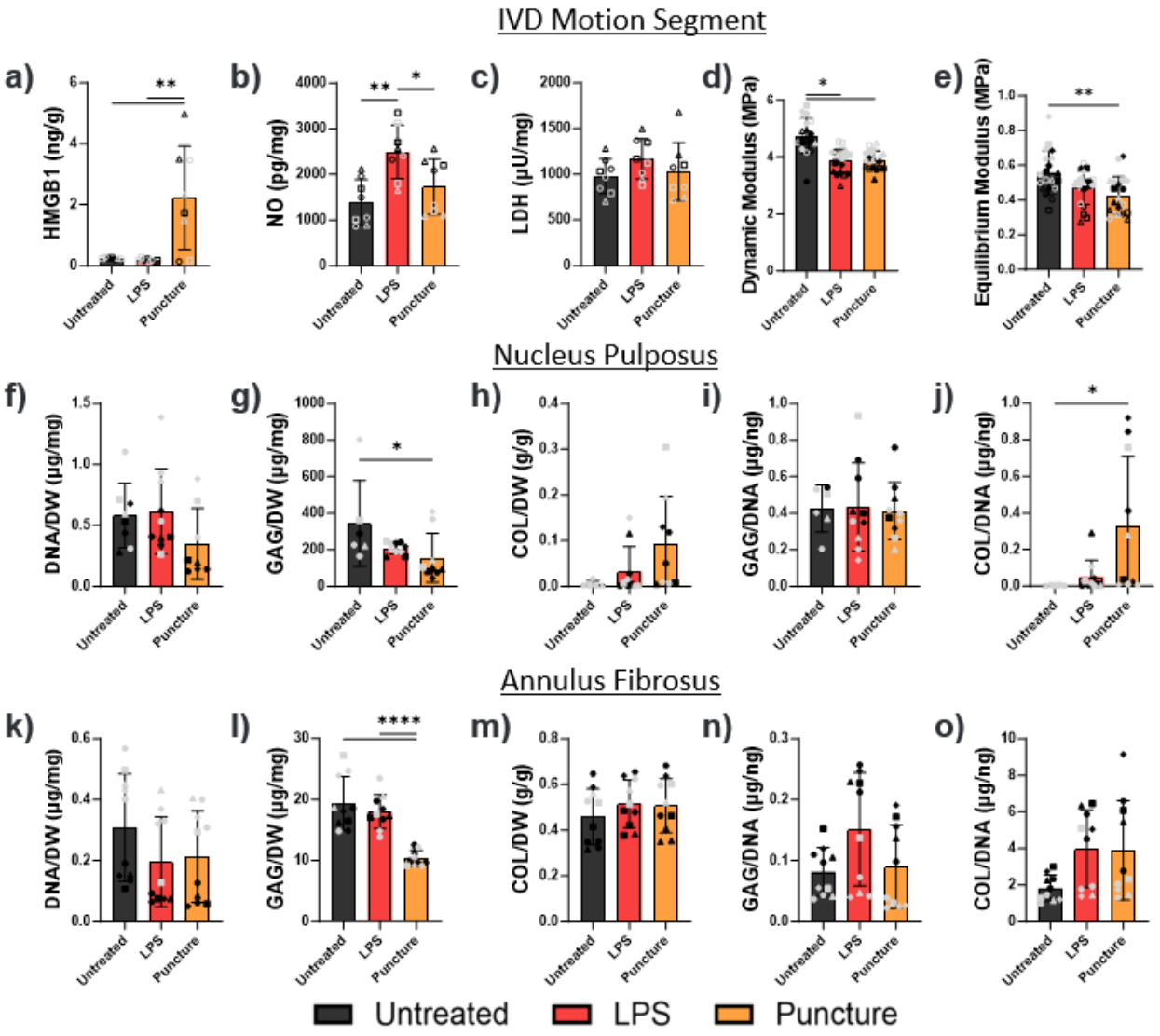

Figure 3.2: Short-term inflammatory and long-term biomechanical and biochemical characterization of injured discs

Short-term release of **(a)** HMGB1 (N=7-8) and long-term release of **(b)** NO (N=8) and **(c)** LDH (N=8) into the media. Mechanical properties of long-term untreated, LPS, and puncture treated motion segments (both sexes): **d)** dynamic modulus (N=20) and **e)** equilibrium modulus (N=20). Biochemical content of long-term cultured motion segments separated by NP **(f-j)** and AF **(k-o)** regions. Biochemical content of the NP region of the disc is displayed as **f)** DNA/DW, **g)** GAG/DW, **h)** COL/DW, **i)** GAG/DNA content, and **j)** COL/DNA content (N=4-5 for all except for COL/DW and COL/DNA graphs where samples for male untreated were lost or undetectable). Biochemical content of the AF region of the disc is displayed as **k)** DNA/DW, **l)** GAG/DW, **m)** COL/DW, **n)** GAG/DNA content, and **o)** COL/DNA content. For NP COL/DW and NP COL/DNA graphs, ANOVA was only conducted on LPS and puncture groups for both sexes due

to missing samples. Salvaged male untreated was used for DNA and GAG analysis. *p<0.05, **p<0.01, and ****p<0.0001 for post hoc between injury. Each symbol represents a different donor for each sex.

3.3.2 Sex-based differences in IVD motion segment size

Both motion segment levels allocated for the male LPS group (2.0 mm, $p<0.0001$) and the male puncture group had greater radii (1.94 mm, $p=0.013$) compared to the untreated caudal level (1.77 mm, **Fig. 3.3a**). Both motion segment levels allocated for the female LPS group (1.86 mm, $p=0.0007$) and the female puncture group had greater radii (1.77 mm, $p=0.037$) compared to the untreated caudal level (1.63 mm, **Fig. 3.3a**). All male motion segment levels had significantly greater radii than their female counterparts ($p<0.0001$, **Fig. 3.3a**).

Motion segment levels allocated for the male LPS group (1.73 mm) had greater height than the male puncture (1.55 mm, $p=0.0036$) group and the untreated caudal level (1.54 mm, $p=0.0032$, **Fig. 3.3b**). Motion segment levels allocated for the female LPS group (1.62 mm) had greater height than the female puncture (1.43 mm, $p=0.0017$) group and the untreated caudal level (1.41 mm, $p=0.0007$, **Fig. 3.3b**). All male motion segment levels had significantly greater height than their female counterparts ($p<0.05$, **Fig. 3.3b**).

Motion segment levels allocated for the male LPS group (22.9 mm^3) had greater volume than the male puncture (18.5 mm^3, $p=0.022$) group and the untreated caudal level (15.5 mm^3, $p=0.0002$, **Fig. 3.3c**). Motion segment levels allocated for the female LPS group (17.8 mm^3) had greater volume than the untreated caudal level (12.0 mm^3, $p=0.0040$, **Fig. 3.3c**). All male motion segment levels had significantly greater volume than their female counterparts ($p<0.05$, **Fig. 3.3c**).

Motion segment levels allocated for the male LPS group (423.9 mg) had greater mass than the untreated caudal level (291.9 mg, $p=0.0004$, **Fig. 3.3d**). All male motion segment levels had significantly greater mass than their female counterparts ($p<0.05$, **Fig. 3.3d**).

NP male LPS (0.23 mg) had greater mass than NP male puncture (0.085 mg, $p<0.0001$) and NP male untreated (0.072 mg, $p<0.0001$, **Fig. 3.3e**). NP female LPS (0.16 mg) had greater

mass than NP female puncture (0.037 mg, p=0.0005) and NP female untreated (0.041 mg, p=0.0005, **Fig. 3.3e**).

AF male LPS (11.6 mg) had greater mass than AF untreated (7.3 mg, p=0.0086, **Fig. 3.3f**). AF female LPS (9.5 mg, p<0.0001) and AF female puncture (6.9 mg, p=0.0068) had greater mass than AF female untreated (2.7 mg, p=0.0005, **Fig. 3.3f**). AF male untreated (7.3 mg) had significantly greater mass than their female counterparts (2.7 mg, p=0.0051, **Fig. 3.3f**).

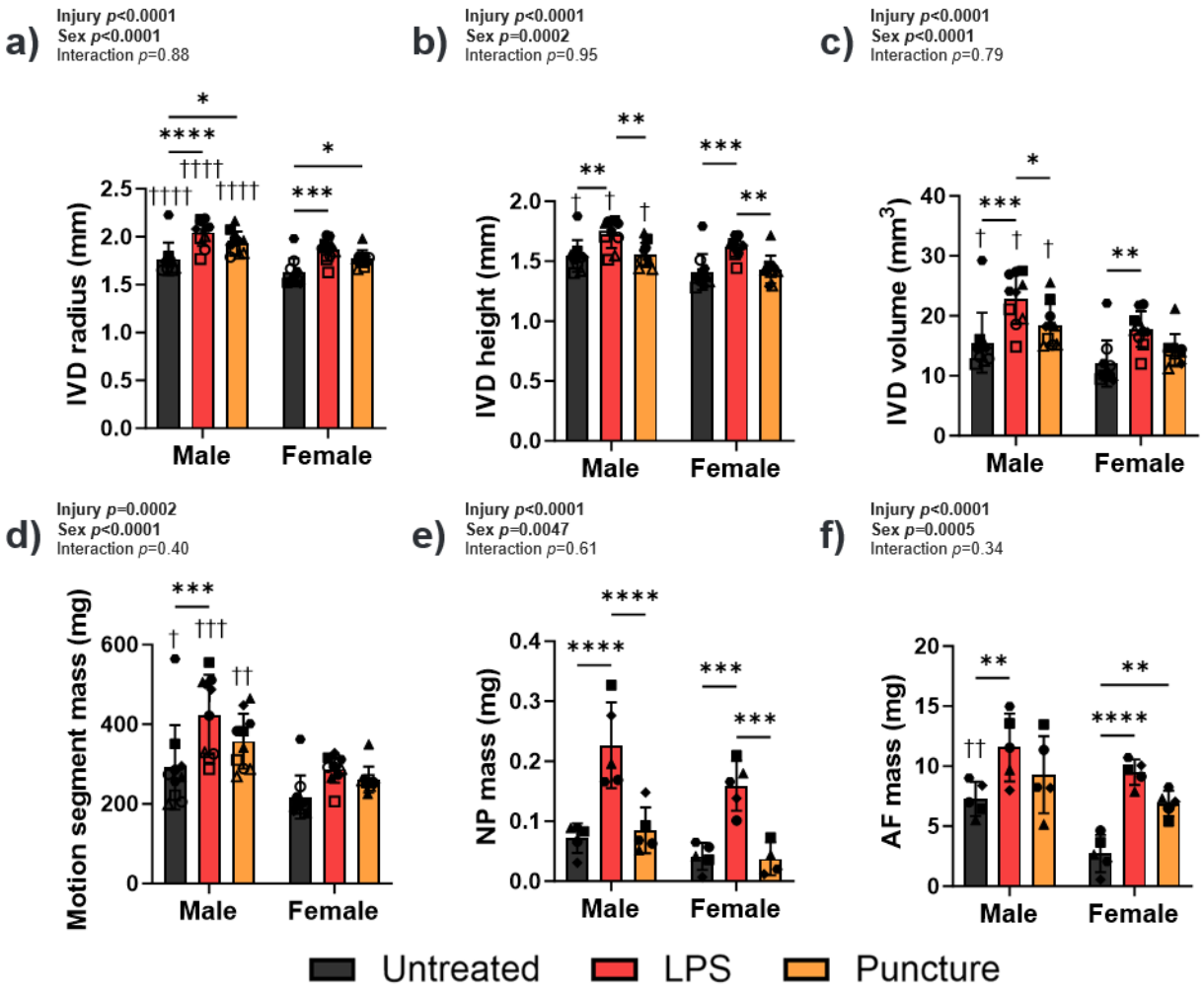

Figure 3.3: Long-term IVD size in radius, height, volume, and mass separated by sex.

Long-term IVD **(a)** radius, **(b)** height, **(c)** volume, and **(d)** motion segment mass in wet weight (N=10) as well as mass in dry weight of **(e)** NP and **(f)** AF alone. *p<0.05, **p<0.01, ***p<0.001, and ****p<0.0001 for post hoc between injury; $^{\dagger}p$<0.05, $^{\dagger\dagger}p$<0.01, $^{\dagger\dagger\dagger}p$<0.001, $^{\dagger\dagger\dagger\dagger}p$<0.0001 for post hoc between sex. Each symbol represents a different donor in each sex.

3.3.3 Sex-based differences in baseline and untreated IVD regions

There were no differences between sex in NP or AF DNA/DW, GAG/DW, COL/DW, GAG/DNA (N=3), and COL/DNA (**Fig. 3.4a-j**).

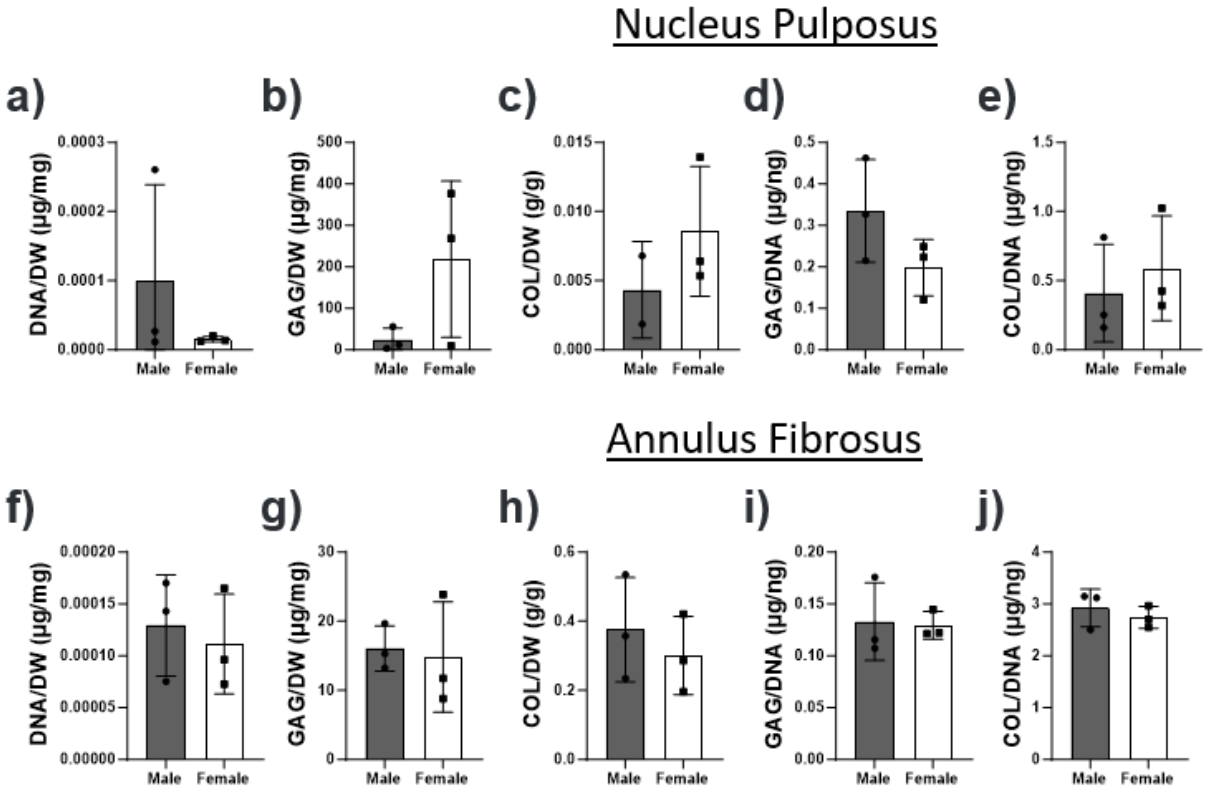

Figure 3.4: Biochemical content of day 0 motion segments separated by IVD region.

Biochemical content of day 0 motion segments separated by NP **(a-e)** and AF **(f-j)** regions. Biochemical content of the NP region of the disc is displayed as **a)** DNA/DW (N=3), **b)** GAG/DW (N=3), **c)** COL/DW (N=3), **d)** GAG/DNA (N=3), and **e)** COL/DNA (N=3). Biochemical content of the AF region of the disc is displayed as **f)** DNA/DW (N=3), **g)** GAG/DW (N=3), **h)** COL/DW (N=3), **i)** GAG/DNA (N=3), and **j)** COL/DNA (N=3).

3.3.4 Injury modality led to sex- based differences in inflammatory marker release

At 6 days post-injury, HMGB1 release into the media was found to be dependent on injury type (p=0.0018), but not sex (p=0.47, **Fig. 3.5a**). Therefore, looking at pooled male and female data, HMGB1 release from punctured discs (2.2 ng/g tissue) was greater than untreated (0.24 ng/g, p=0.002) and LPS injured (0.19 ng/g, p=0.002) discs (**Fig. 3.2a**). The HMGB1 release in male-punctured discs was also significantly greater than LPS injured discs (p=0.03). In female discs, a trend towards increased release of HMGB1 was observed in punctured vs. LPS discs (**Fig. 3.5a**). Cumulative NO release into the media also showed a significant effect of injury (p<0.0001), but not sex (p=0.18) or their interaction (p=0.057, **Fig. 3.5b**). LPS injury of discs led to the greatest short-term NO release into the media compared to the untreated (male: p=0.04, female: p<0.0001) and punctured (male: p=0.054, female: p<0.0001) discs (**Fig. 3.5b**). Additionally, female-LPS injured motion segments released significantly greater NO levels compared to male-LPS injured (p=0.027, **Fig. 3.5b**).

Long-term culture of male and female motion segments led to the greatest amount of NO release into the media from LPS injured discs compared to untreated discs in both sexes (p=0.006, p=0.0002, respectively, **Fig. 3.5c-e**). After 40 days in culture, male-untreated (p=0.007) and male-punctured (p=0.001) discs released significantly greater NO levels compared to their female counterparts (**Fig. 3.5e**). Male discs appeared to release significantly higher levels at NO starting at day 27 of culture (p=0.049, **Fig. 3.5c**), while female discs were responsive to LPS injury early on, at day 3 (p=0.019, **Fig. 3.5d**), contributing to significantly higher levels of NO in female-LPS discs compared to both female untreated and female-punctured discs throughout the majority of the culture period (**Fig. 3.5d**). Initially, female-LPS (day 3) and punctured (day 13) discs released more NO due to injury; however, this effect dissipated over time (day 38) (**Fig. 3.5d**).

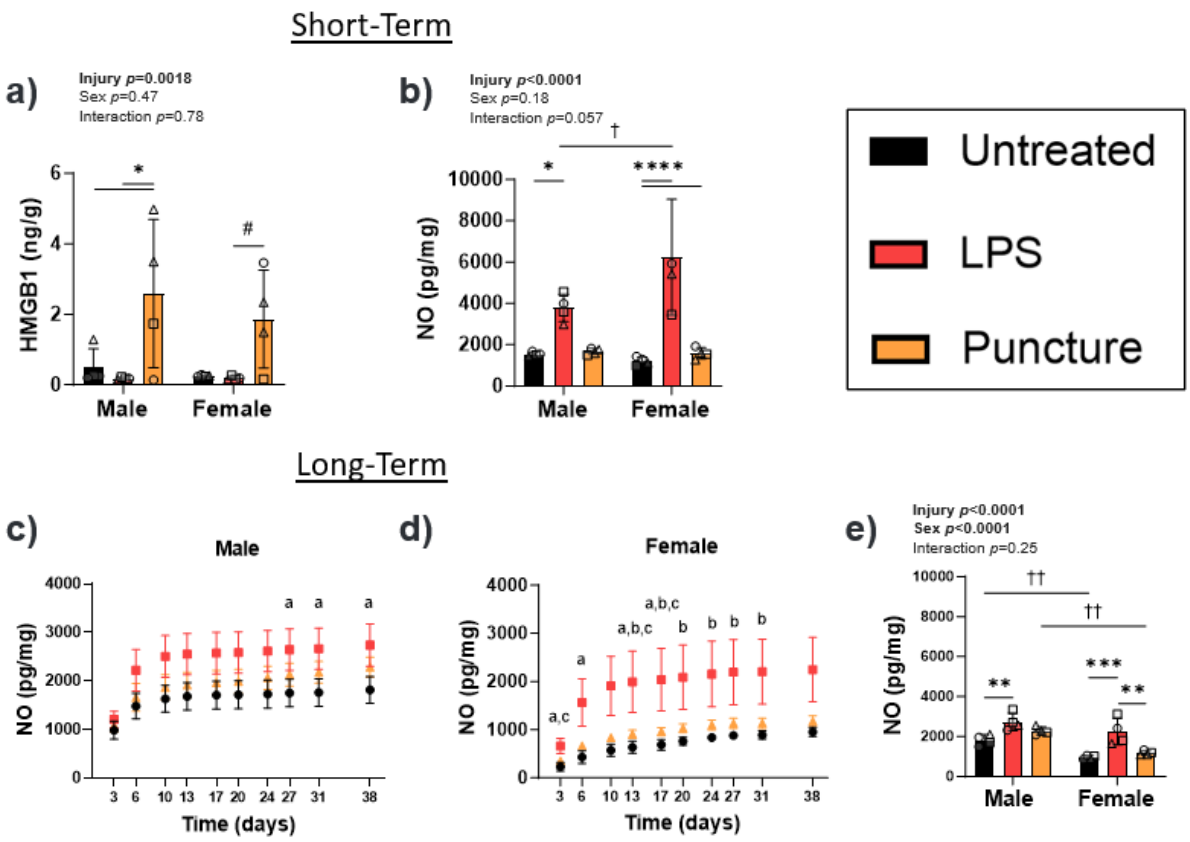

Figure 3.5: Cumulative short-term release of HMGB1 and NO into disc media.

Cumulative short-term release of **(a)** HMGB1 and **(b)** NO into disc media *p<0.05 (each symbol represents a different donor in each sex). Long-term release of NO into the media from **(c)** male and **(d)** female motion segments in each group. **(e)** Day 38 cumulative NO release (N=4, each symbol represents a different donor in each sex). *p<0.05, **p<0.01, ***p<0.001, ****p<0.0001, ^{a}p<0.05 for untreated v LPS, ^{b}p<0.05 for untreated v puncture, ^{c}p<0.05 for LPS v puncture, #p<0.1 for post hoc between injury, and †p<0.05, ††p<0.01 for post hoc between sex)

3.3.5 LDH release by sex and across all treatment groups

There were no differences in LDH or GAG loss into the media from injured discs compared to untreated discs in data separated by sex (**Fig. 3.6a, 3.6b**). However, LDH release in male long-term LPS discs seems to peak at days 3 and 6 compared to male-untreated discs ($p<0.04$, **Fig. 3.6c**), but not in female long-term treated discs (**Fig. 3.6d**). Overall, we see a significant decrease in long-term female LDH loss into the media compared to their male counterparts ($p<0.012$, **Fig. 3.6e**), which deems sex significant in LDH loss in long-term culture. GAG loss into media appears to be elevated at days 27 and 31 in punctured male discs (**Fig. 3.6f**), while we see an increase in GAG loss in female LPS treated discs at days 17 and 20 (**Fig. 3.6g**). Overall, injury modality is significant in attributing to cumulative GAG loss in both male and female discs, where puncture injury leads to the greatest GAG loss into the media compared to untreated discs ($p=0.066$, **Fig. 3.6h**).

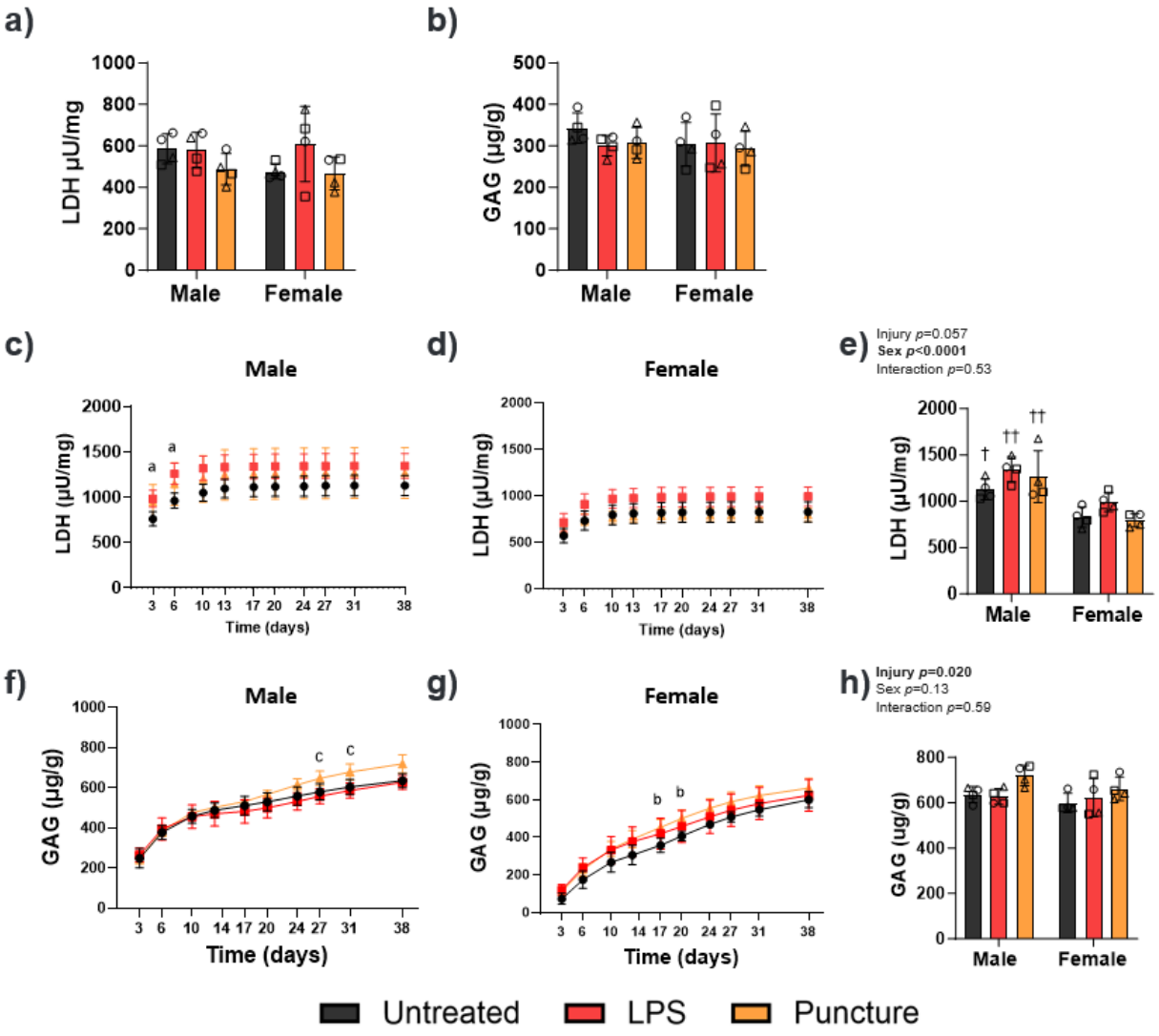

Figure 3.6: Cumulative short-term and long-term release of LDH and GAG into disc media.

Short-term release of **(a)** LDH and **(b)** GAG release into the media. Long-term LDH release over time of **(c)** male and **(d)** female as well as **(e)** cumulative LDH release at 38 days (N=4). Final cumulative GAG release over time of **(f)** male and **(g)** female as well as **(h)** cumulative GAG release at 38 days (N=4). $^{a}p<0.05$ untreated v LPS, $^{b}p<0.05$ untreated v puncture, $^{c}p<0.05$ LPS v puncture for post hoc between injury; $^{\dagger}p<0.05$, $^{\dagger\dagger}p<0.01$ for post hoc between sex.

3.3.6 Sex-based differences in biomechanical properties and regional water content

Both injury ($p<0.0001$) and sex ($p<0.0001$) were significant contributors to the dynamic modulus of discs (**Fig. 3.7a**). Sex differences were observed in the dynamic modulus of untreated motion segments (male: 4.5±0.5 MPa, female: 5.0±0.6 MPa, $p=0.0039$, **Fig. 3.7a**). This sex-dependent difference remained when LPS or puncture injury was applied to the motion segments ($p=0.0027$, $p=0.0081$, respectively). In response to injury, both male and female LPS and punctured motion segments exhibited similar decreases in dynamic modulus compared to their respective untreated discs ($p<0.0001$, **Fig. 3.7a**). Equilibrium modulus of motion segments was also both dependent on injury ($p=0.001$) and sex ($p=0.017$, **Fig. 3.7b**). However, only punctured discs from female donors exhibited a significant decrease in equilibrium modulus compared to untreated discs ($p=0.0021$, **Fig. 3.7b**).

Whole IVD water content was not significantly dependent on injury ($p=0.70$) or sex ($p=0.34$) (**Fig. 3.7c**). For NP water content, sex ($p=0.010$) but not injury ($p=0.62$), was a significant factor (**Fig. 3.7d**). AF water content exhibited a significant effect of injury ($p=0.008$) and the interaction term ($p=0.002$) (**Fig. 3.7e**). Male-untreated AFs had higher water content than female-untreated AFs ($p=0.001$, **Fig. 3.7e**). Injury from LPS and puncture significantly increased AF water compared to untreated discs in female ($p=0.0006$, $p=0.0006$, respectively, **Fig. 3.7e**) but not in male donors.

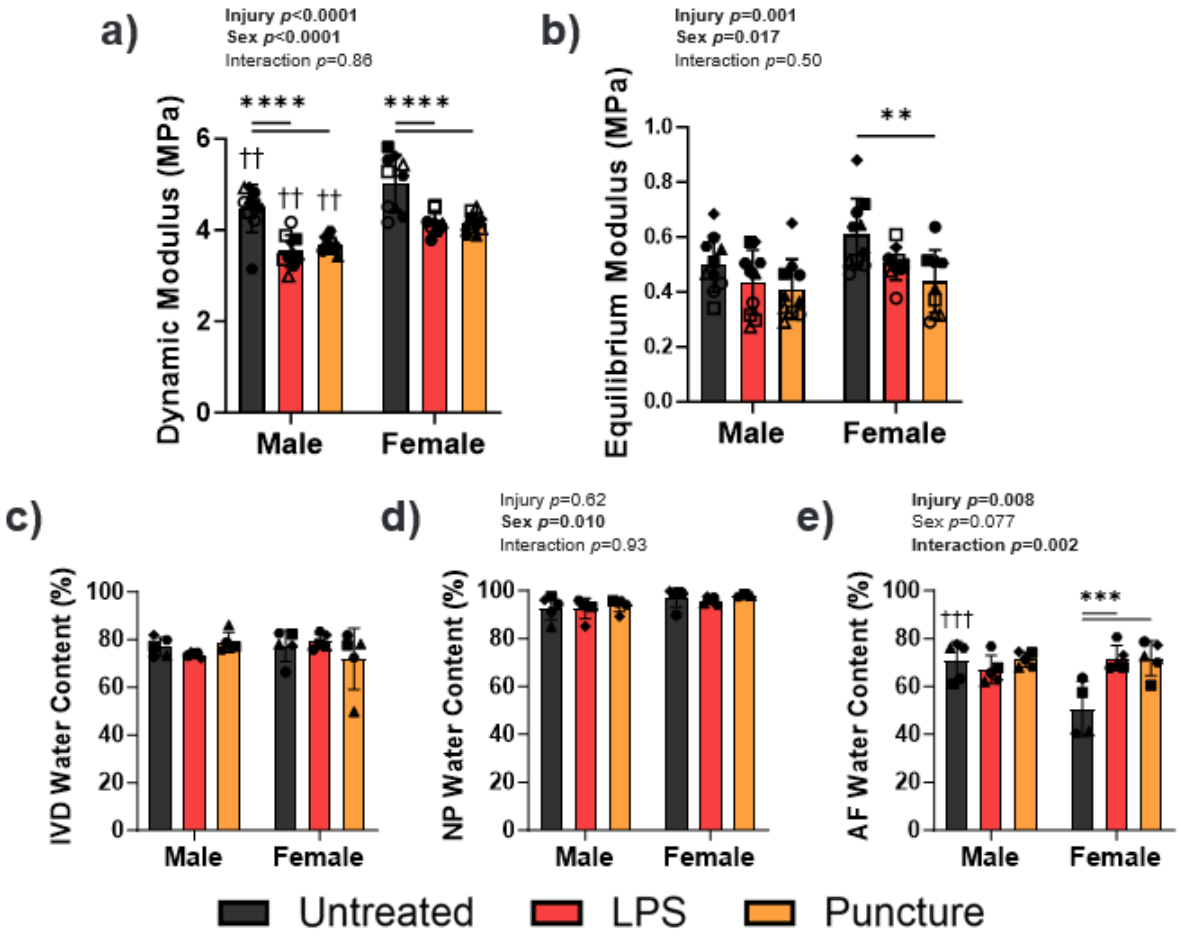

Figure 3.7: Mechanical properties and water content of long-term motion segments.

Mechanical properties and water content of long-term motion segments: **(a)** dynamic modulus (N=10) and **(b)** equilibrium modulus (N=10) and water content of **(c)** IVD (N=5), **(d)** NP alone (N=3-5), and **(e)** AF alone (N=4-5). **p<0.01, ***p<0.001, ****p<0.0001 for post hoc between injury; $^{††}p$<0.01, $^{†††}p$<0.001 for post hoc between sex. Each symbol represents a different donor in each sex.

3.3.7 Injury modality led to sex and biochemical differences in the NP

In untreated groups, sex was not a significant factor in NP biochemical content. In pooled analyses, injury was a significant contributor to NP biochemical content where GAG/DW decreased (p=0.033, **Fig. 3.2g**), and COL/DNA increased in punctured discs compared to untreated controls (p=0.012, **Fig. 3.2j**). Sex was a significant factor in NP DNA/DW (p=0.001), where puncture group had lower DNA content in male NP compared to female NP (p=0.007, **Fig. 3.8a**). Injury was a significant factor in NP COL/DNA (p=0.038); however, no significant difference between injuries was found (**Fig. 3.8e).** NP COL/DNA increased slightly in puncture vs. untreated, though this difference was not significant (p=0.091) (**Fig. 3.8e**). No significant differences in NP biochemical content were observed in LPS injured groups versus untreated.

The biochemical content of AF in untreated groups was significantly different in male and female discs. The DNA/DW of male AF was lower than female AF, regardless of injury (p<0.0001, **Fig. 3.8f**). Untreated male discs also had significantly lower GAG/DW and COL/DW content in the AF compared to untreated female discs (p=0.03, p<0.0001, **Fig. 3.8g,h**). In the AF region, injury (p=0.0007) and sex (p<0.0001) were significant factors in DNA/DW content, where LPS and puncture injury led to a decrease in DNA content compared to untreated female, but not male, AF (p=0.0015, p=0.0091, **Fig. 3.8f**). When assessing changes in GAG content, LPS decreased GAG/DW vs. untreated in female donors (p=0.045, **Fig. 3.8g**), while puncture injury significantly decreased GAG/DW content in both sexes compared to their respective untreated group (male: p=0.004, female: p<0.0001, **Fig. 3.8g**). Moreover, puncture led to lower GAG/DW than LPS injured AF in both sexes (male: p=0.0015, female: p=0.0003, **Fig. 3.8g**). Injury was not a significant factor in COL/DW content (p=0.053, **Fig. 3.8h**) of male or female discs.

Normalizing ECM content by DNA content led to further injury- and sex-dependent effects. The GAG/DNA content in AF was greater in male than female discs, regardless of injury ($p \leq 0.0002$, **Fig. 3.8i**). Sex, injury, and interaction effects were significant in AF GAG/DNA content ($p<0.0001$, $p<0.0001$, $p \leq 0.0011$ **Fig. 3.8i**). Male-LPS injured AFs exhibited a higher GAG/DNA compared to both male-untreated and male-punctured AF, respectively ($p<0.0001$, $p<0.0001$, **Fig. 3.8i**). Male-punctured AF also had greater GAG/DNA than male-untreated AF ($p=0.044$, **Fig. 3.8i**). These differences were not observed in AF GAG/DNA samples from female donors. In AF COL/DNA, injury ($p=0.0006$) and sex ($p<0.0001$) effects were observed in addition to interaction effects ($p=0.030$), where LPS and punctured discs had greater COL/DNA than untreated AF ($p=0.0006$, $p=0.0003$, **Fig. 3.8j**) in samples from male but not female donors. There was, however, significantly higher COL/DNA in male-LPS injured and punctured discs compared to corresponding female discs (LPS: $p=0.0005$, puncture: $p<0.0001$, **Fig. 3.8j**).

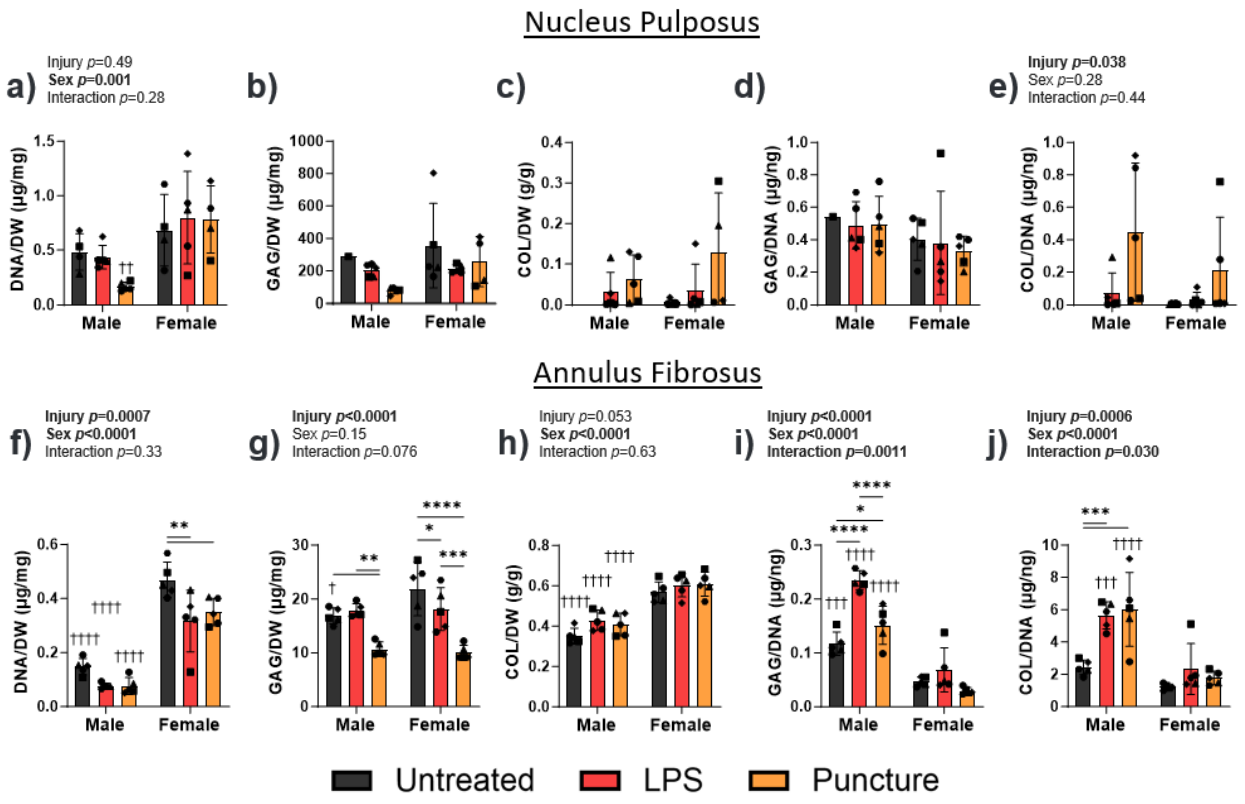

Figure 3.8: Biochemical content of long-term cultured motion segments separated by IVD region.

Biochemical content of long-term cultured motion segments separated by NP **(a-e)** and AF **(f-j)** regions. Biochemical content of the NP region of the disc is displayed as **a)** DNA/dry weight(DW), **b)** GAG/DW, **c)** COL/DW, **d)** GAG/DNA, and **e)** COL/DNA (N=4-5 for all except for COL/DW and COL/DNA graphs where samples for male untreated were lost or undetectable). Biochemical content of the AF region of the disc is displayed as **f)** DNA/DW (N=5), **g)** GAG/DW (N=5), **h)** COL/DW (N=5), **i)** GAG/DNA (N=5), and **j)** COL/DNA (N=5). For NP COL/DW and NP COL/DNA graphs, ANOVA was only conducted on LPS and puncture groups for both sexes due to missing samples. Salvaged male untreated was used for DNA and GAG analysis. *p<0.05, **p<0.01, ***p<0.001, and ****p<0.0001 for post hoc between injury; $^{\dagger}p$<0.05, $^{\dagger\dagger\dagger}p$<0.001, $^{\dagger\dagger\dagger\dagger}p$<0.0001 for post hoc between sex. Each symbol represents a different donor in each sex.

3.3.8 TLR4 inhibition on LPS-stimulated injury responses

In LPS injury groups, sex-(p<0.0001), but not TAK-treatment (p=0.26), was a significant factor in the dynamic modulus of discs (**Fig. 3.9a**). Female-LPS and female-LPST discs exhibited higher dynamic moduli compared to their male counterparts (p=0.0009, p=0.0001, **Fig. 3.9a**). For NP water content, sex was a significant factor (p=0.050) while TAK was not (p=0.57, **Fig. 3.9c**). However, there were no TAK- or sex-dependent differences in equilibrium modulus or AF water content in LPS and LPST discs (**Fig. 3.9b,d).** In the NP region of discs, there was no effect of TAK between LPS NP and LPST NP on DNA/DW, GAG/DW, COL/DW, GAG/DNA, and COL/DNA (**Fig. 3.9e-i**). Sex is a significant contributor in NP DNA/DW (p=0.0091), but there are no NP male-female differences (p>0.095, **Fig. 3.9e**). Sex also did not affect NP GAG/DW, COL/DW, GAG/DNA, or COL/DNA (**Fig. 3.9f-i**). In the AF region of LPS and LPST discs, TAK appeared not to affect DNA/DW, GAG/DW, COL/DW, GAG/DNA, and COL/DNA content (**Fig. 3.9j-n**). However, sex was a significant contributor to AF DNA/DW (p<0.0001), with lower levels found in males vs. females, independent of TAK treatment (p<0.0001, **Fig. 3.9j**). Sex was also a significant factor in COL/DW (p<0.0001, **Fig. 3.9l**) with lower levels in male vs. female samples, independent of TAK treatment (**Fig. 3.9l**). When normalizing GAG or COL by DNA content, both GAG/DNA (LPS: p<0.0001, LPST: p<0.0001) and COL/DNA (LPS: p<0.0001, LPST: p<0.0001) were significantly greater in male samples vs. female, independent of TAK treatment group (**Fig. 3.9m,n**).

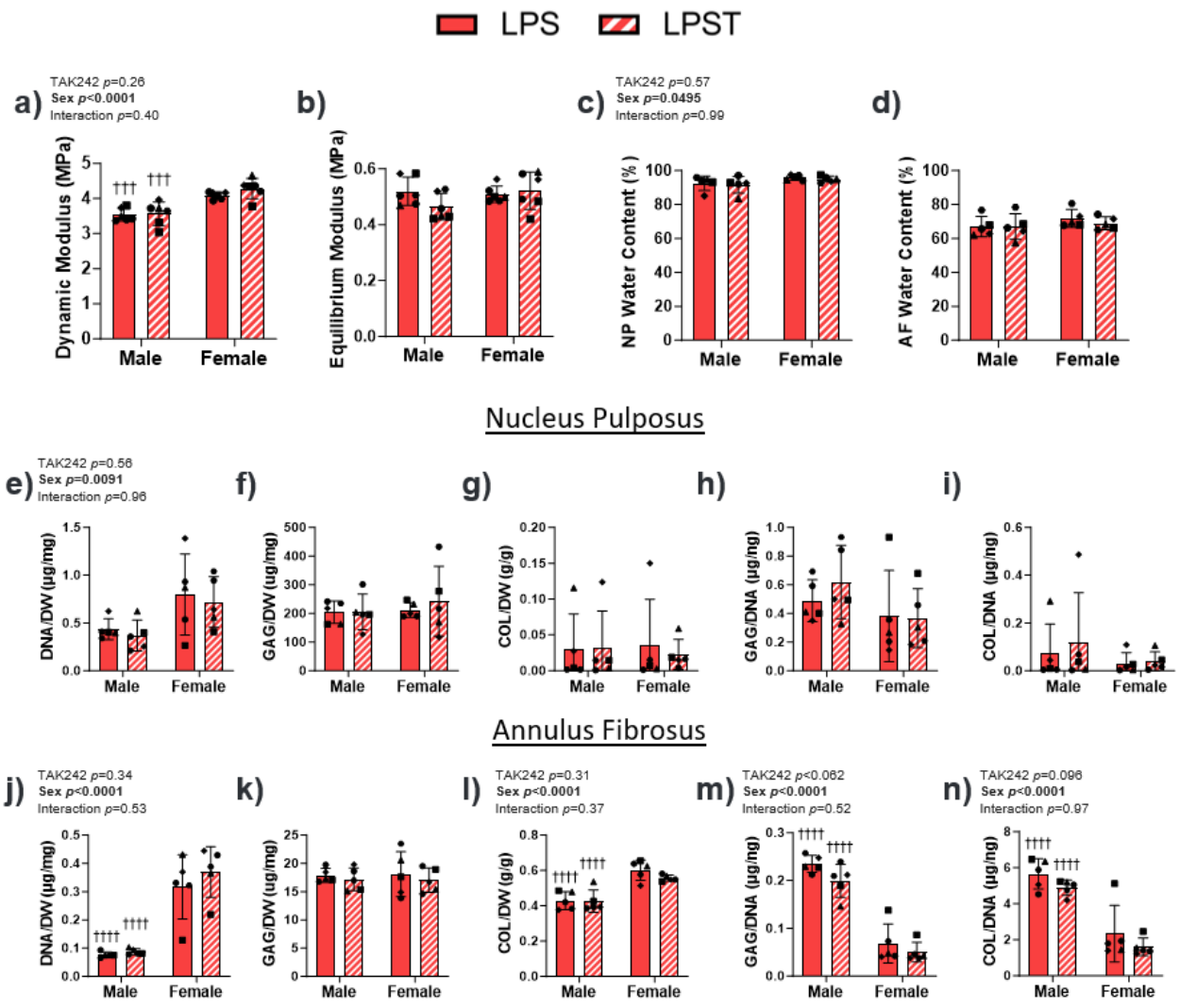

Figure 3.9: Mechanical and biochemical properties of long-term LPS and LPST treated motion segments.

Mechanical properties of long-term LPS and LPST treated motion segments: **(a)** dynamic modulus (N=6) and **b)** equilibrium modulus (N=6). Water content percentage of **(c)** NP (N=5) and **(d)** AF (N=5). Biochemical content of long-term cultured motion segments separated by NP **(e-i)** and AF **(j-n)** regions. Biochemical content of the NP region of the disc is displayed as **(e)** DNA/DW (N=5), **(f)** GAG/DW (N=5), **(g)** COL/DW (N=5), **(h)** GAG/DNA (N=5), and **(i)** COL/DNA (N=5). Biochemical content of the AF region of the disc is displayed as **(j)** DNA/DW (N=5), **(k)** GAG/DW (N=5), **(l)** COL/DW (N=5), **(m)** GAG/DNA (N=5), and **(n)** COL/DNA (N=5). $^{\dagger\dagger\dagger}p<0.001$, $^{\dagger\dagger\dagger\dagger}p<0.0001$ for post hoc between sex. Each symbol represents a different donor in each sex.

3.3.9 TLR4 inhibition on punctured disc responses

In the puncture injury groups, both TAK treatment (p=0.0021) and sex (p=0.0002) were significant factors contributing to the dynamic modulus (**Fig. 3.10a**). Male P (p=0.023) and male PT (p=0.0011) discs exhibited lower dynamic moduli compared to their female counterparts (**Fig. 3.10a**). Additionally, TAK treatment increased dynamic moduli values for females (p=0.007), not male discs (p=0.11, **Fig. 3.10a**). There were significant sex- (p=0.048), but not TAK-dependent (p=0.067), effects on equilibrium modulus of punctured discs (**Fig. 3.10b**). Both sex and TAK did not affect NP or AF water content of P and PT discs (**Fig. 3.10c,d**). In the NP region of discs, there appears to be no effect of TAK between P and PT in DNA/DW, GAG/DW, COL/DW, GAG/DNA, or COL/DNA (**Fig. 3.10e-i**). The NP DNA/DW showed a significant effect of sex (p=0.011) and sex-TAK interaction (p=0.022), with lower levels of male-NP DNA/DW in punctured discs than in corresponding female discs (p=0.0046, **Fig. 3.10e**). Furthermore, there were significant interaction terms in NP GAG/DW (p=0.0053, **Fig. 3.10f**), where TAK treatment increased punctured male-NP GAG/DW (p=0.049) but decreased female-NP GAG/DW (p=0.049, **Fig. 3.10f**). Sex was a significant factor in COL/DW (p=0.025**, Fig. 3.10g**), but no differences in group comparisons were observed (**Fig. 3.10g**). Sex (p=0.0002, **Fig. 3.10h**) and sex-TAK interaction effects (p=0.025) were significant in GAG/DNA, with higher levels of GAG/DNA in male vs female TAK-treated groups (p=0.0004, **Fig. 3.10h**).

Sex (p<0.0001) and sex-TAK interaction (p=0.037) were significant factors in AF DNA/DW, where female P and PT have higher DNA/DW content than males (p<0.0001, **Fig. 3.10j**). TAK (p=0.0084) and sex (p<0.0001) were significant factors in AF COL/DW (p<0.0001, **Fig. 3.10l**) with lower levels in male vs. female samples, independent of treatment (**Fig. 3.10l**). Due to TAK treatment, increasing trends in AF COL/DW were observed in both male and female samples

(**Fig. 3.10l**). AF GAG/DNA had significant contributions from sex (p<0.0001), TAK (p=0.0068), and sex-TAK interactions (p=0.0063, **Fig. 3.10m**), where male GAG/DNA is higher than female counterparts, regardless of TAK treatment (P: p<0.0001, PT: p=0.0005, **Fig. 3.10m**). TAK significantly decreased AF GAG/DNA vs. puncture in male (p=0.0009), but not female samples (**Fig. 3.10m**). When normalizing COL by DNA content, sex (p<0.0001, **Fig. 3.10n**) remains a significant contributor to AF COL/DNA, with higher levels in males vs. females, independent of TAK treatment (**Fig. 3.10n**).

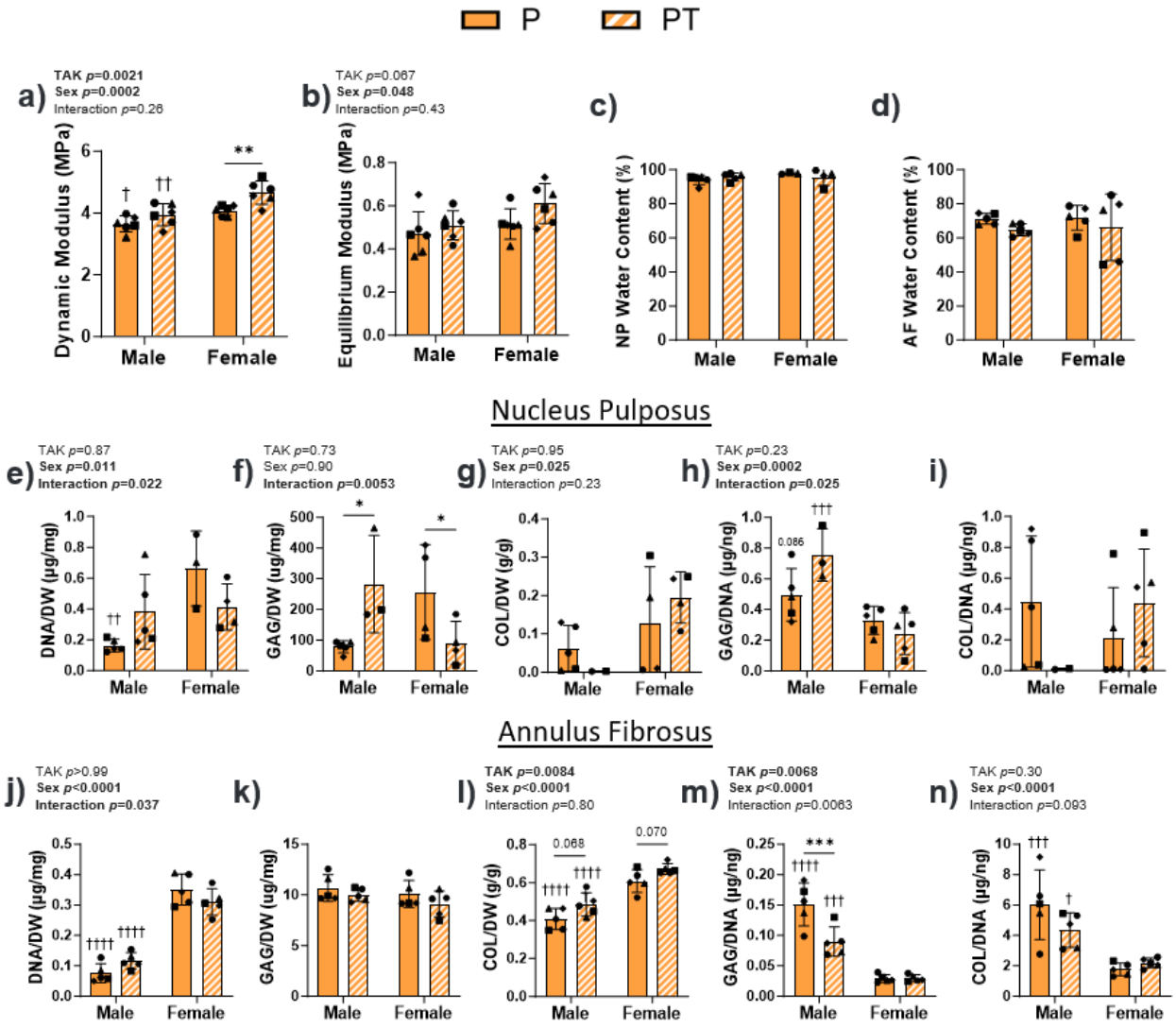

Figure 3.10: Mechanical and biochemical properties of long-term P and PT treated motion segments.

Mechanical properties of long-term P and PT treated motion segments: **(a)** dynamic modulus (N=6) and **(b)** equilibrium modulus (N=6). Water content percentage of **(c)** NP (N=5) and **(d)** AF (N=5). Biochemical content of long-term cultured motion segments separated by NP **(e-i)** and AF **(j-n)** regions. Biochemical content of the NP region of the disc is displayed as **(e)** DNA/DW (N=3-5), **(f)** GAG/DW (N=3-5), **(g)** COL/DW (N=2-5), **(h)** GAG/DNA (N=3-5), and **(i)** COL/DNA (N=2-5). Biochemical content of the AF region of the disc is displayed as **(j)** DNA/DW (N=5), **(k)** GAG/DW (N=5), **(l)** COL/DW (N=5), **(m)** GAG/DNA (N=5), and **(n)** COL/DNA (N=5). *p<0.05, **p<0.01, ***p<0.001, and ****p<0.0001 for post hoc between TAK injury, $^{\dagger\dagger\dagger}p$<0.001, $^{\dagger\dagger\dagger\dagger}p$<0.0001 for post hoc between sex. Each symbol represents a different donor in each sex. (N=6).

3.3.10 Morphological changes in both short-term and long-term injured discs

Histological staining of short- and long-term LPS and punctured discs exhibited injury-dependent differences based on Safranin O and Picrosirius Red staining. In untreated discs, the shape of the NP in male (**Fig. 3.11a,g, Fig. 3.13a,g**) and female discs (**Fig. 3.11d,j, Fig. 3.13d,j**) appeared oval with mild distortions, and exhibited similarities in vacuolated NP cell morphology and proteoglycan staining (**Fig. 3.11a,d, Fig. 3.13a,d**). With LPS injury, male (**Fig. 3.11b,h, Fig. 3.13b,h**) and female discs (**Fig. 3.11e,k, Fig. 3.13e,k**) had additional distortions to NP shape along with decreases in vacuolated NP cell morphology. However, there appears to be higher proteoglycan staining intensity in the NP region of LPS treated discs (**Fig. 3.11b,e, Fig. 3.13b,e**) compared to respective untreated controls (**Fig. 3.11a,d, Fig. 3.13a,d**). Puncture injury caused the greatest disruption to disc structure in both male (**Fig. 3.11c,i, Fig. 3.13c,i**) and female discs (**Fig. 3.11f,l, Fig. 3.13f,l**). In the puncture group, the NP became irregular in shape and smaller in area in males (**Fig. 3.11c,i, Fig. 3.13c,i**) and females (**Fig. 3.11f,l, Fig. 3.13f,l**). After puncture injury, loss of NP cellularity was also observed; the NP-AF border appeared more interrupted, and the AF appeared more distorted with greater evidence of fissures (**Fig. 3.11c,f,i,l, Fig. 3.13c,f,i,l**)., Puncture injury significantly increased the average degeneration grade compared to untreated male and female discs in short- and long-term culture (**Fig. 3.12a,3.14a**). Short-term, male-punctured discs also had a higher average degeneration score in the endplate category than their female counterparts (**Fig. 3.12j**). In long-term culture, however, no sex differences in histological grading were observed based on the grading of Safranin O and Picrosirius Red staining (**Fig. 3.14**).

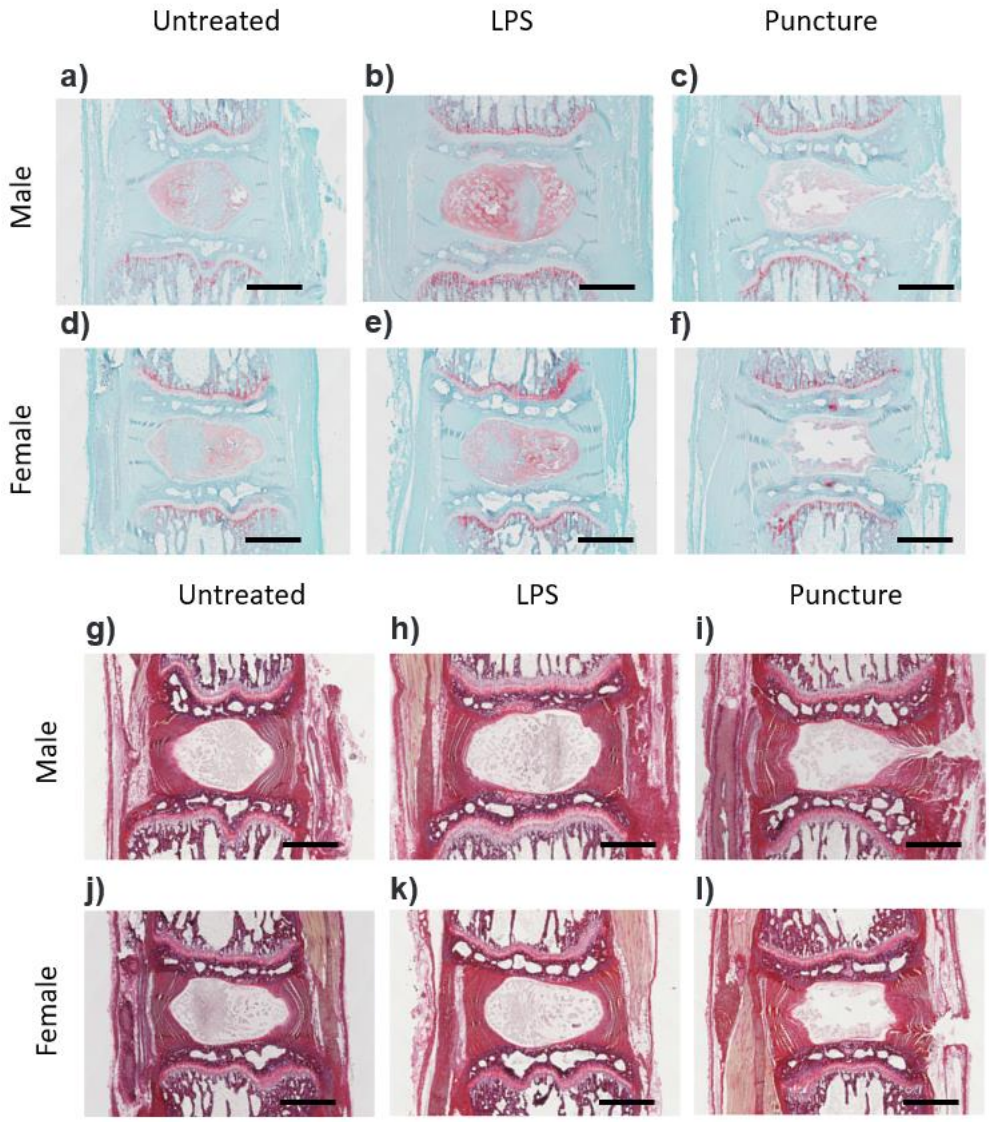

Figure 3.11: M Safranin O with Fast Green and Picrosirius Red staining of short-term male and female discs.

Safranin O with Fast Green staining of short-term male **(a)** untreated, **(b)** LPS, and **(c)** puncture and female **(d)** untreated, **(e)** LPS, and **(f)** puncture discs. Picrosirius Red staining of short-term male **(g)** untreated, **(h)** LPS, and **(i)** puncture and female **(j)** untreated, **(k)** LPS, and **(l)** puncture discs. Scale bar: 1 mm.

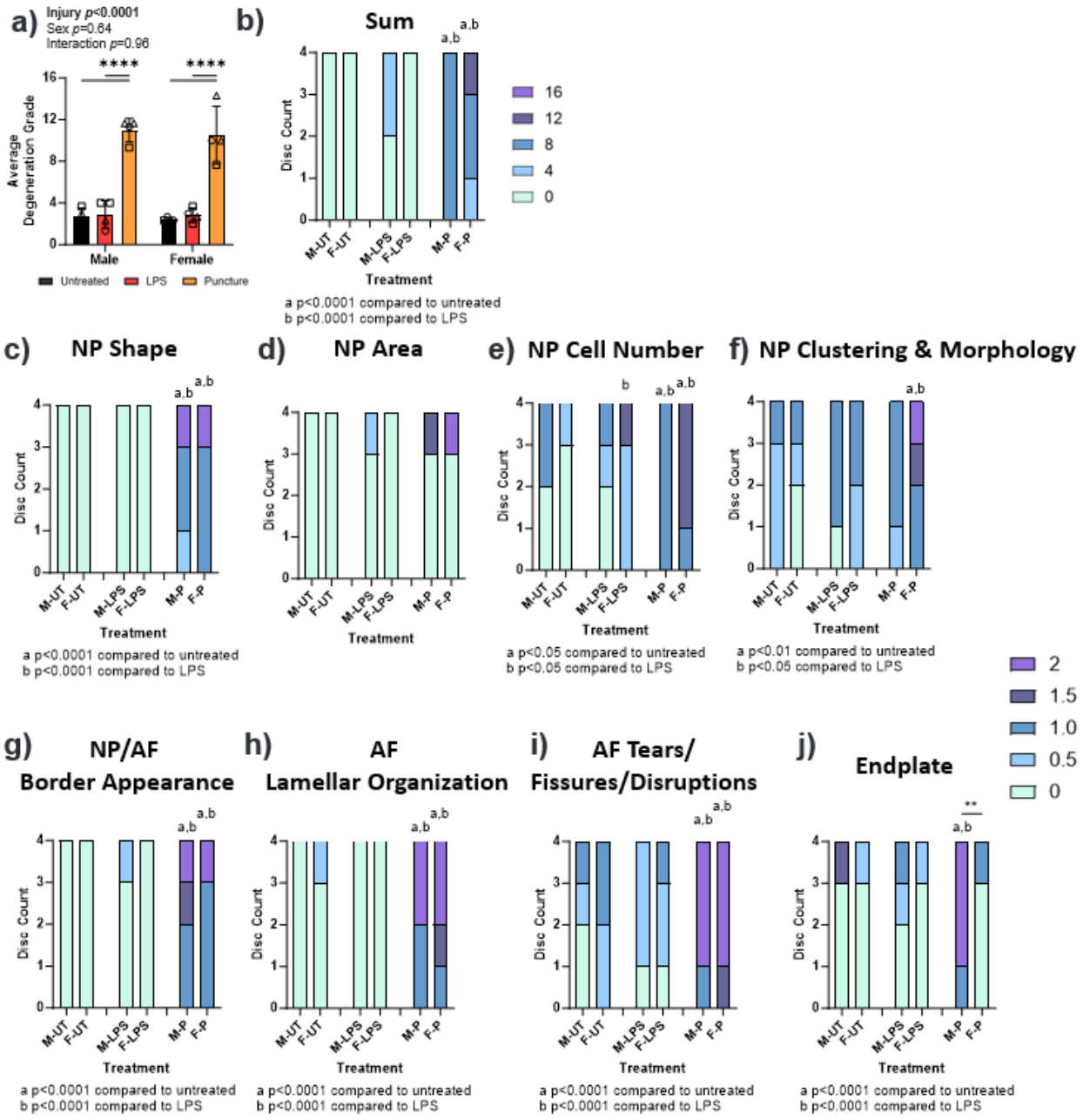

Figure 3.12: Histological grading of short-term discs.

Histological grading of short-term discs **(a)** Sum with donor distribution, **(b)** Sum, **(c)** NP Shape, **(d)** NP Area, **(e)** NP Cell Number, **(f)** NP Cell Clustering and Morphology, **(g)** NP/AF Border Appearance, **(h)** AF Lamellar Organization, **(i)** AF Tears/Fissures/Disruptions, and **(j)** Endplate. Statistical significance represented by $^{**}p<0.01$, $^{****}p<0.0001$. a or b represent significance between treatment.

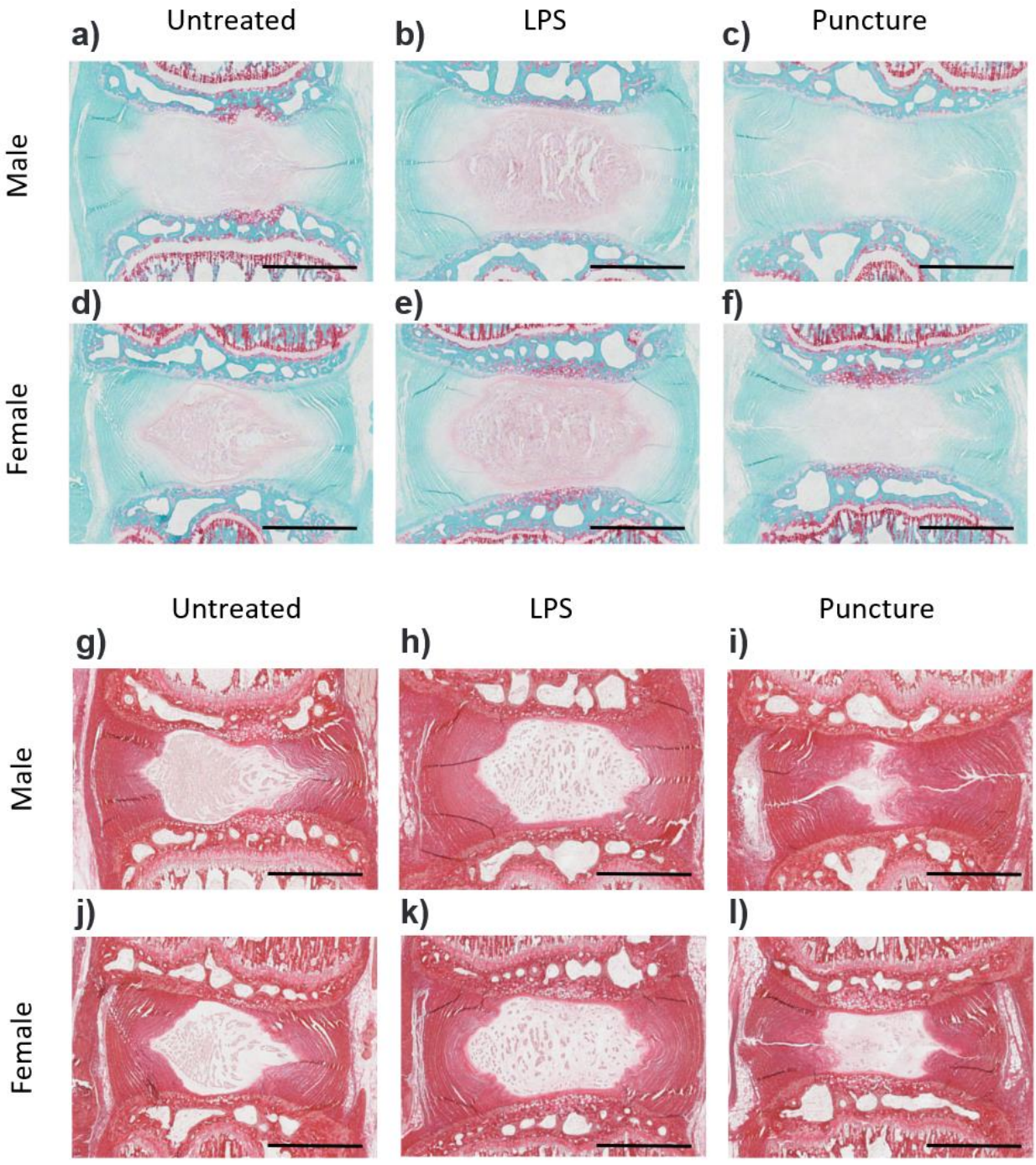

Figure 3.13: Safranin O with Fast Green and Picrosirius Red staining of long-term male and female discs.

Safranin O with Fast Green staining of long-term male **(a)** untreated, **(b)** LPS, and **(c)** puncture and female **(d)** untreated, **(e)** LPS, and **(f)** puncture discs. Picrosirius Red staining of long-term male **(g)** untreated, **(h)** LPS, and **(i)** puncture and female **(j)** untreated, **(k)** LPS, and **(l)** puncture discs. Scale bar: 1 mm.

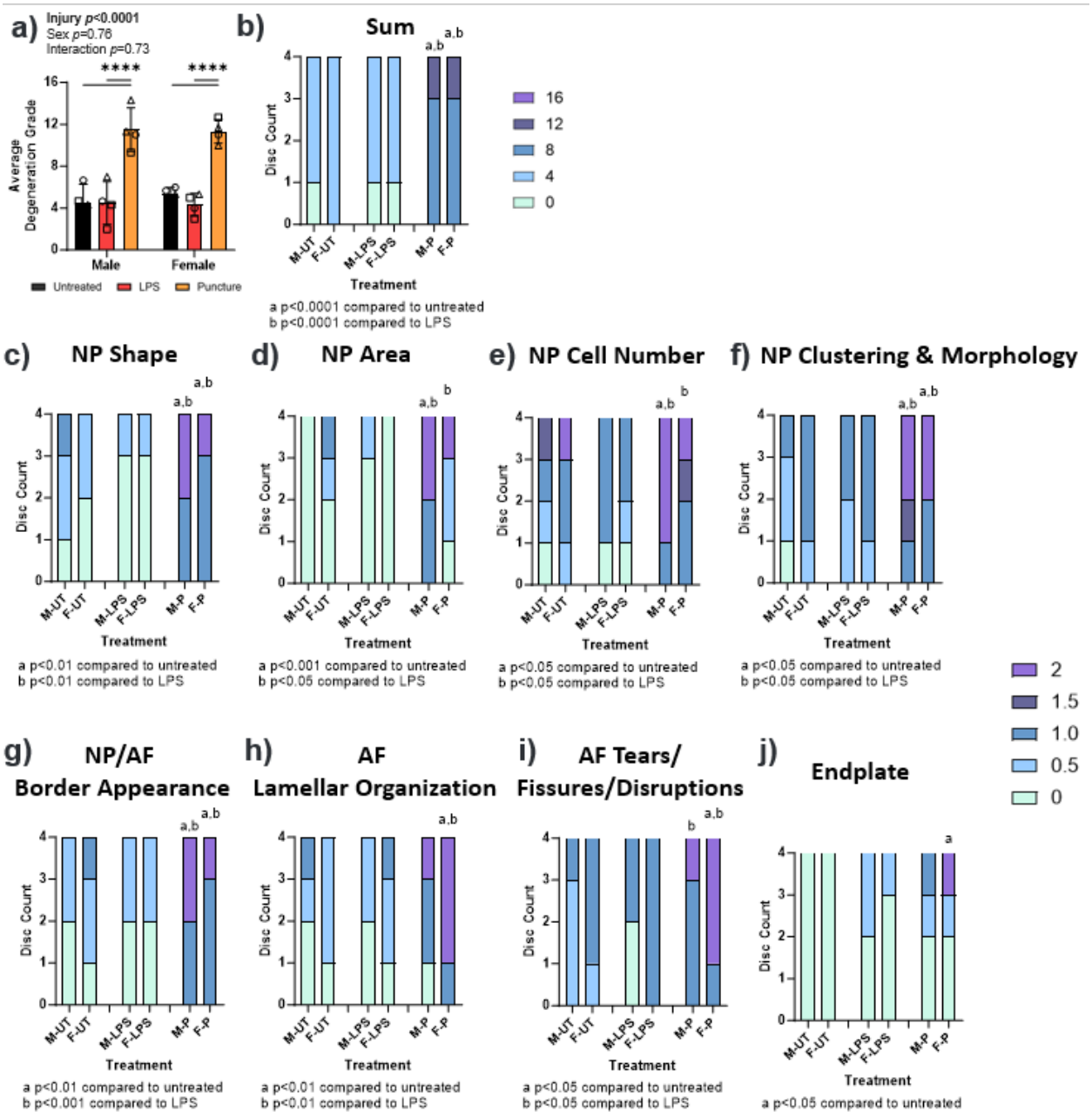

Figure 3.14: Histological grading of long-term discs.

Histological grading of long-term discs **(a)** Sum with donor distribution, **(b)** Sum, **(c)** NP Shape, **(d)** NP Area, **(e)** NP Cell Number, **(f)** NP Cell Clustering and Morphology, **(g)** NP/AF Border Appearance, **(h)** AF Lamellar Organization, **(i)** AF Tears/Fissures/Disruptions, and **(j)** Endplate. Statistical significance represented by $^{**}p<0.01$, $^{****}p<0.0001$. a or b represent significance between treatment.

3.3.11 TLR4 inhibition on histological grade of long-term cultured discs

There is decreased proteoglycan staining in the NP region in the long-term discs compared to day 0 for both female (**Fig. 3.15a,b**) and male (**Fig. 3.15c,d**) discs. However, with TAK-242, we do not see any protective effects of proteoglycan content in either female LPS treated (**Fig. 3.15e,f**) or female punctured discs (**Fig. 3.15g,h).** We also do not see any protective effects of proteoglycan content in either male LPS treated (**Fig. 3.15i,j**) or male punctured discs (**Fig. 3.15k,l)**.

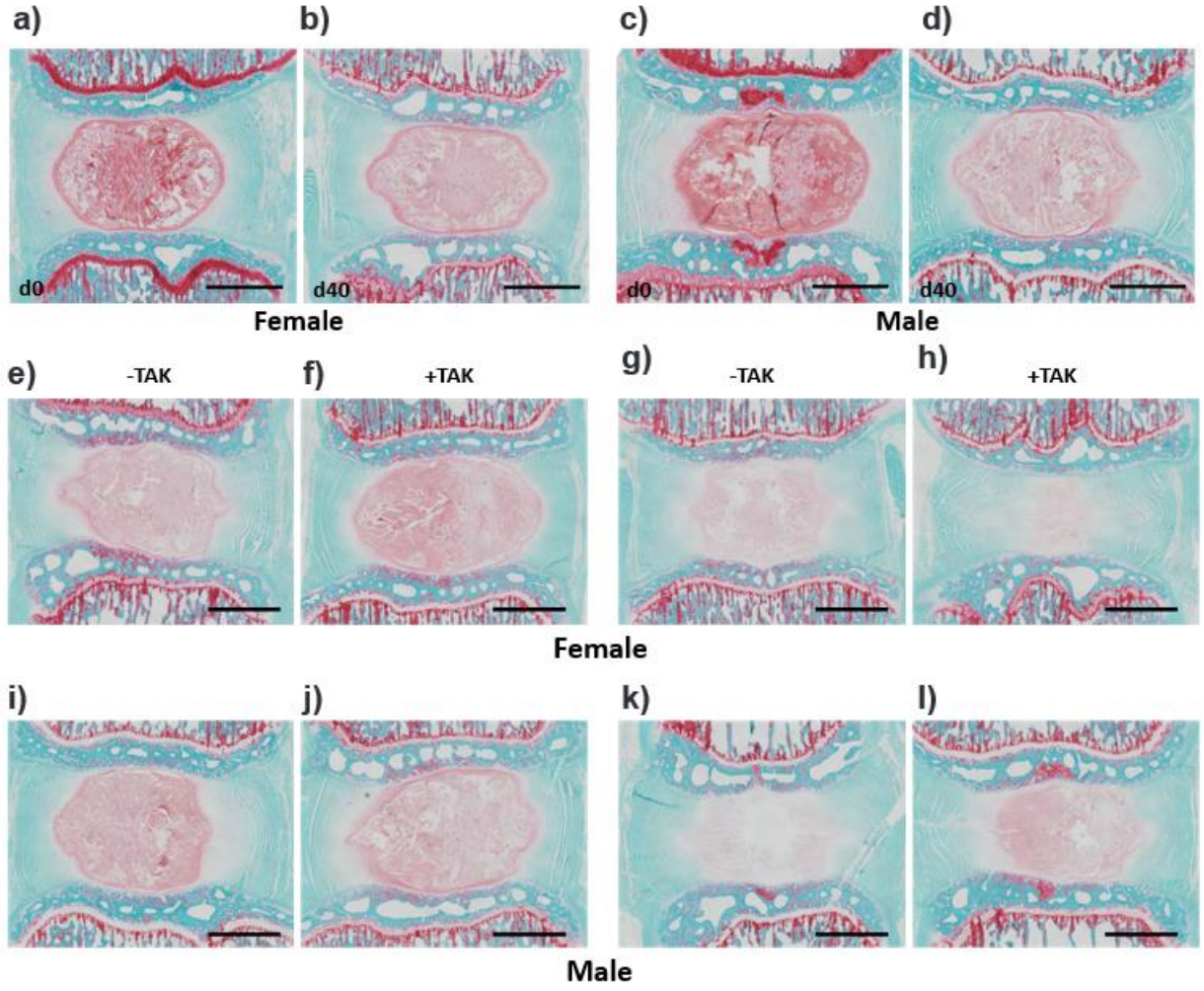

Figure 3.15: Safranin O with Fast Green staining of day 0 and long-term untreated and injured male and female discs.

Safranin O with Fast Green staining of **(a)** day 0 (d0) and **(b)** long-term female and **(c)** d0 and **(d)** long-term male discs followed by long-term female **(e)** LPS, **(f)** LPST, and **(g)** P and **(h)** PT discs in addition to male long-term **(i)** LPS, **(j)** LPST, **(k)** P and **(l)** PT discs. Scale bar: 1 mm

3.4 Discussion

This study identified sex-based differences in male and female caudal IVDs from the rat, exhibited by differences in mechanical properties, namely dynamic and equilibrium moduli, ECM biochemical content, and inflammatory response. Female untreated discs had a higher dynamic modulus compared to male untreated discs. AF of female untreated discs also had lower water content and greater DNA content suggesting greater cellularity and higher levels of GAG and COL content than in male untreated AF. The higher ECM biochemical content, thus, may contribute to the higher dynamic modulus of female discs compared to males. Moreover, chemical injury using LPS led to a greater inflammatory response in female discs than in male discs in the short-term study; yet, this difference in response is lost when looking at the long-term results. In contrast, a greater inflammatory response was seen in males compared to females in the long-term study after puncture injury. This suggests that the IVD inflammatory response to injury is sex- and time-dependent. One advantage of using this *ex vivo* approach is that it isolates sex-based differences that are specific to the IVD motion segment, the organ of interest, rather than responses dependent on systemic interaction with injury (e.g. immune system or hormone responses).

The findings of the current study extend earlier findings on sex-effects in rat IVDs. Mosley *et al.* identified some baseline distinct sex differences in IVD height where males had greater baseline IVD height than females. Likewise, additional sex-based differences were reported due to an *in vivo* 3x puncture injury [171]. While both sexes had decreased cellularity and increased fibronectin at injury sites, females had an increased degeneration grade in the outer AF compared to males. Meanwhile, male IVDs had greater torsional stiffness, torque range, and viscoelastic creep responses, while females had reduced SHG intensity compared to males post-puncture injury, suggesting that male IVDs exhibited improved healing compared to female punctured IVDs

[171]. In the current study, the response to injury, physical (puncture) or chemical (LPS), also exhibited differences between sexes. Indeed, we saw more of a sex-based response when discs were subjected to injury. Female IVDs, compared to male IVDs, appear to be more biologically responsive to LPS stimulation, indicated by their increased NO release compared to their respective untreated controls, and more susceptible to mechanical degradation, as evidenced by a significant decrease in equilibrium moduli in female-punctured compared to female untreated. However, both male and female discs were mechanically responsive to chemical and puncture injuries with decreased dynamic moduli. Chemical injury using LPS led to an increase in NO release into the media compared to untreated discs while punctured discs did not. Given the short 12 hour half-life of NO, [172], our sensitivity to observe changes in NO levels in short versus long-term experiments was different given the different time points of media collections in the experiments. Furthermore, during the short-term experiments, we see a higher release from female LPS discs than their male counterparts. Thus, females appear to be more sensitive to LPS treatment in the short-term experiment than males. However, this may not be evident in the long-term experiment due to the longer duration of the first or between media collections.

HMGB1 release was increased in punctured discs, with no sex-based effect, suggesting that cell necrosis due to puncture injury may be contributing to HMGB1 release [173]. Stratifying by sex further magnified injury effects on HMGB1 release. Interestingly, LPS stimulation did not induce significant HMGB1 release, which differs from prior findings on LPS injured human NP cells [11], indicating that presence of complex ECM may be regulating HMGB1 responses. Thus, HMGB1 release appears to be dependent on disc injury. Additionally, the daily level of HMGB1 release was so minute by day 6 of culture, rendering the disc release of HGMB1 below the

measurement range of the assay used. Like LPS, HMGB1 can serve as an agonist of TLR4 and lead to downstream NF-κβ activation [174].

Both LPS and puncture injury led to a significant decrease in dynamic modulus in male and female discs. In addition, puncture injury also reduced AF GAG content. Korecki *et al.* previously used a bovine IVD organ culture loading model to examine the effect of needle puncture injury on disc mechanics and biology. They observed decreased dynamic modulus due to needle puncture injury [175], which is consistent with the findings of this study. Interestingly, they did not detect changes in GAG release into the media. Our results demonstrate an increase in GAG loss into the media with puncture injury, along with decreased GAG content in the AF post puncture injury. The results suggest that the AF was more responsive to changes with injury, specifically GAG content, compared to the NP response to injury.

However, when looking at GAG production per AF DNA content, we see an increase in GAG content of male LPS injured and punctured AFs compared to male untreated AF, suggesting higher ECM content potentially due to lower cellular density in males. However, we do not see the same response to injury in samples from female donors, suggesting that injury response is sex-dependent. A similar effect is observed when looking at COL production per AF DNA, where there is an increase in COL/DNA in male LPS injured and punctured AF compared to their female injured counterparts. The higher GAG/DNA and COL/DNA content post-injury in male AF compared to female AFs also indicated a greater biosynthetic response post-injury, suggesting greater ECM remodeling capabilities in motion segments isolated from male donors compared to female donors. This supports the prior finding of male IVDs having improved ECM properties compared to female IVDs as reported by greater SHG intensity in the outer AF post-puncture injury [171], which represents COL integrity [161], COL organization [176], and COL fibril

diameter [177]. Lower biosynthetic responses of AF motion segments appear to be primarily driven by higher cellularity of female AF, where cells may not be responding biosynthetically to the same degree post-injury as in the male AF. However, in our study, female discs had healthier histological features than male discs 38 days post-puncture. In addition to remodeling differences in response to injury, the higher levels of AF COL and dynamic modulus in uninjured female IVDs may have protected against injury insult, compared to samples from male donors, and thus lowered the overall need to drive biosynthetic responses. Future studies are needed to directly measure the biosynthetic response of male and female AF cells and their cellular sensitivity to injury.

TAK-242 is a small molecule inhibitor of TLR4 signaling that intracellularly interferes with interactions between TLR4 and its adaptor molecules [178]. Surprisingly, TAK-242 was more effective at improving structural and functional properties of punctured discs than LPS-stimulated discs. Since HMGB1 can serve as an agonist of TLR4 and lead to downstream NF-κβ activation, the greater effectiveness on punctured IVDs may be due to the drug's blocking of TLR4 signaling through the HMGB1 ligand. Direct LPS stimulation may have overpowered the potential protective effects of TAK-242. Additionally, the puncture injury may have facilitated better diffusion of the TAK-242 drug into the motion segment. In contrast, the structural integrity of LPS injured discs was maintained, thus limiting diffusion of TAK-242 throughout the motion segment. TAK-242 appeared to improve the dynamic modulus of female punctured but not male discs, which may be evidenced by greater levels of COL/DW (albeit not significant) in female NP and AF compared to punctured-only discs. When comparing IVD geometry alone, females had lower IVD radii and height than males. However, there was no difference between the sexes when it came to IVD volume and motion segment wet weight. Nevertheless, there were differences in ECM dry weight; female AF dry weight was smaller than their male counterparts, while NP dry

weights were similar between males and females. Thus, by normalizing the GAG and COL content to wet weight or dry weights of separated NP and AF compartments, we are accounting for variation due to sex, size, or biological variability in the biochemical content of the ECM. Water content is also reported normalized to the original weight of the NP or AF; therefore, accounting for size variability due to sex or biological variation. Observations of differences in biochemical content presented normalized to wet or dry weight represent differences in the biochemical content, independent of the variation in size between male and female donors. In mechanical testing, we observed clear differences in the size of male and female motion segments and thus incorporated the size differences in our mechanical testing (as normalizing factors).

Limitations of this study include the inherent differences in male and female anatomy and physiology, such as bone density, animal size, and hormone levels. Additionally, different animal donors were used for the short-term and long-term experiments, so biological variability was observed with different study durations. Furthermore, the long-term *ex vivo* culture is limited by a lack of perfusion mimicking bodily fluids and vascularization, potentially leading to non-physiologic, deleterious effects on IVD cells. We may have lost some cartilage-like phenotype based on GAG content changes in our culture system; thus, GAG retention using media supplements like ascorbic acid could be explored in future studies. Future directions include determining how sex hormones, such as estrogen and testosterone, can influence inflammatory, biochemical, and biomechanical responses after injury [153]. This study also supports the notion for future preclinical research to consider separate male and female cohorts, as there are baseline differences in the IVD, as well as distinct sex-dependent responses to physical and chemical injury.

Chapter 4: Static and dynamic loading leads to a differential IVD response that may be mediated by TLR4

4.1 Introduction

The IVD is normally exposed to multimodal loading (e.g., compression, tension, shear, hydrostatic pressure, and osmotic pressure [13-18]. Human lumbar motion discs are estimated to experience 4.4–6.7% axial strain [19, 20] and intradiscal pressures ranging from 0.03–0.7 MPa [21] under physiologic conditions. However, both frequency and magnitude regulate whether loading is beneficial or detrimental to disc integrity [22-25]. Static loading associated with sedentary posture or dynamic activities that involve high-frequency loading (e.g. motor vehicle drivers or aircraft operators) has a higher incidence of LBP [26-33]. This may be related to the variable response of the IVD to different loading profiles.

It is also well established that loading profiles regulate IVD cell response in a magnitude- and frequency-dependent manner, where prolonged static loading or dynamic loading above 1 Hz promotes matrix degradation *in vivo*, and loading at or below 0.5 Hz exhibits anabolic effects on the disc [22, 23, 69, 70, 179-184]. While the anabolic effects of mechanical loading on the IVD have been extensively studied *in vitro*, resulting inflammatory cascades have not been well characterized, although studies suggest that they are also influenced by the loading profile [23, 76, 77]. NP cells secreted IL-1β and TNFα and upregulated matrix-related genes COL2A1, ACAN, and MMP3 in response to compressive loading [23, 76, 77]. Zhou *et al.* compressed bovine caudal discs at 50% of IVD height using a single injurious insult and saw increases in MMP expression and NO release versus physiological loading [185]. Additionally, they observed greater temporal inflammatory response post-1 day versus 8 days of loading. Nevertheless, changes in inflammatory

cytokine profiles of whole bone-disc-bone motion segments in response to loading remain understudied.

Recent studies have highlighted a significant role of innate immune activation, particularly TLRs, in IVD degeneration [4, 5, 7, 8]. TLR4 is involved in the pathogenesis of the IVD, where expression of TLR4 increases with increasing degeneration severity and mediates catabolic and inflammatory processes [4-8]. Activation of TLR4 has been shown to induce a pro-inflammatory cascade in IVD cells with subsequent loss of IVD matrix integrity [7]. Additionally, DAMPs such as HMGB1 have degenerative effects on disc cells mediated by TLR signaling [9, 10, 186, 187]. Furthermore, HMGB1 signaling increases expression of TLR4 suggesting a possible feedback signal [12]. While these studies identify TLR4 as a critical regulator of joint pathology, the potential contribution of TLR4 to mechanically-induced inflammatory signaling of the IVD is unknown.

The goals of this study were to characterize the inflammatory signaling changes in response to IVD static and dynamic loading and investigate contributions of TLR4 signaling in response to mechanical loading. We hypothesized that loading profiles would modulate the inflammatory response depending on frequency and amplitude and that TAK-242, a small molecule inhibitor of TLR4 signaling, would reduce pro-inflammatory signaling and promote anti-inflammatory gene expression. Thus, bone-disc-bone motion segments were used in a loading organ culture model to characterize IVD morphological, inflammatory, and histological responses when subjected to distinct loading profiles with and without TAK-242.

4.2 Materials and Methods

4.2.1 Study design

Having seen distinct sex differences based on Chapter 3, Chapter 4 only used male rats to simplify the analysis of loading-induced effects. Previous *in vitro* loading studies have shown mechanical stiffness, viscoelastic relaxation, and water content in discs recovered after 18 hours of cyclic loading [175, 188]. Thus, we decided to measure the effects of loading on inflammation within 9 hours post loading to understand the inflammatory cascade while the disc is still experiencing the physical effects of loading.

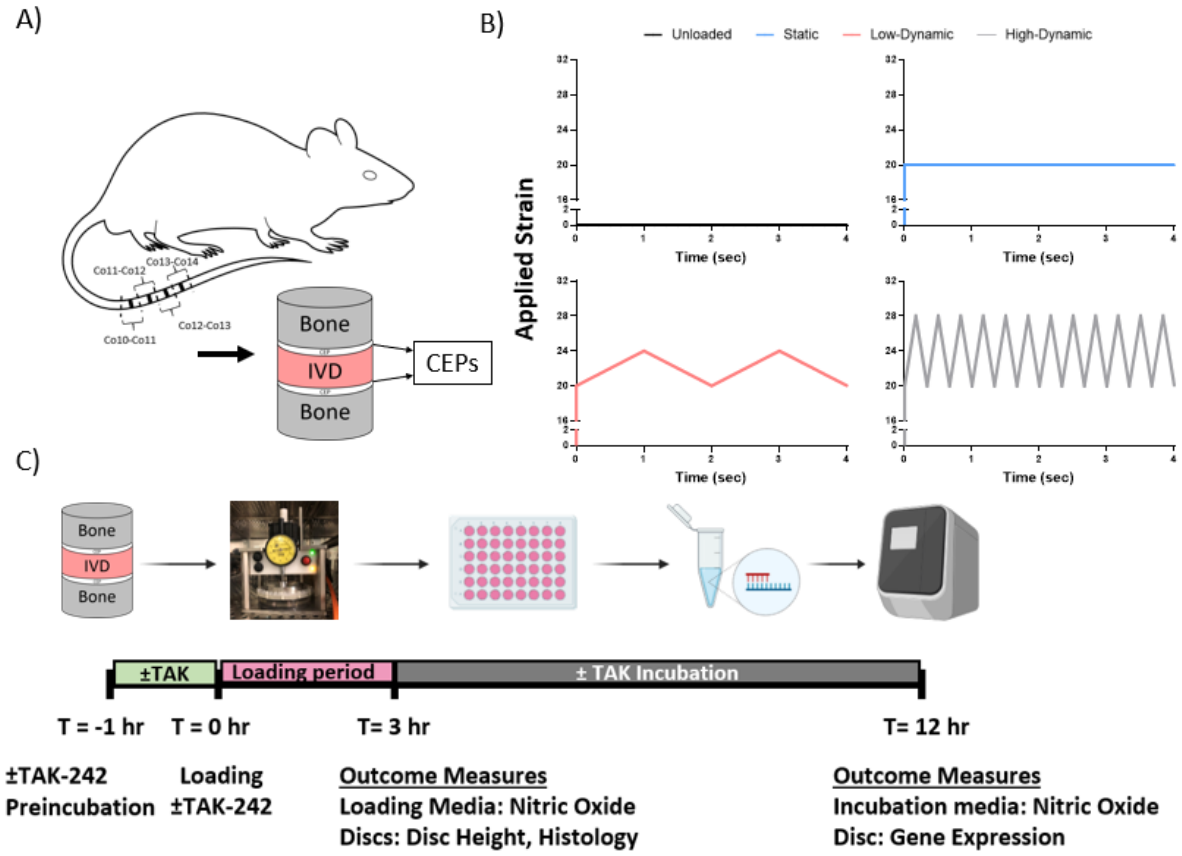

Figure 4.1: Experimental plan of Chapter 4.

A) Dissection of caudal motion segments from male Sprague-Dawley rats. **B)** Loading profiles applied to motion segments for a duration of 3 hr. **C)** Timeline and study design. Created with Biorender.com

4.2.2 Sample isolation and tissue culture of discs

Caudal (Coccygeal/Co) bone-disc-bone motion segments (N=104) were isolated from 26 mature male Sprague-Dawley rats (300 – 500 g). Segments were allocated consistently by level, unloaded: Co13-Co14, static: Co11-Co12, low dynamic: Co12-Co13, and high-dynamic: Co10-Co11, and washed in 1x PBS with 1% antibiotic-antimycotic (AA) (**Fig 4.1A**). Cuts were made mid vertebral body to separate levels, and samples were submerged in Dulbecco's Modified Eagle Medium (DMEM), 10% FBS, 1% AA. Motion segments were then cultured in chemically defined media (CM: phenol-free DMEM without L-glutamine, 100 µg/mL sodium pyruvate, 50 µg/mL L-proline, 1% AA, 1% ITS Premix)[167].

4.2.3 IVD motion segment loading conditions

Samples were loaded for 3 hours using a custom-made displacement control device to apply static and dynamic loading profiles with varying magnitudes and frequencies. A tare compressive strain of ~20% of segment height (1.75 mm) was applied to the static group to retain contact between the loading platen and sample to eliminate liftoff. The low- and high-dynamic groups were loaded with a 20% static strain plus an additional dynamic strain (low-dynamic: 4% dynamic strain (0.35 mm) applied at 0.5 Hz, high-dynamic: 8% dynamic strain (0.70 mm) applied at 3Hz). Unloaded segments were cultured as free-swelling controls. To assess whether inflammatory signaling persists with recurring, long-term loading, a group of samples was loaded daily using the above protocol for 5-days. To assess the effect of applied strain magnitude on responses, we also compared samples loaded with static to high-static (20% tare + 8% static strain). Three segments were loaded simultaneously while submerged in CM. After collecting loading media (LM), motion segments were then transferred to individual wells and incubated with fresh CM for 9 hours. Individual sample incubation media was collected for analysis. IVDs were snap-

frozen after the removal of adjacent vertebrae for RNA extraction. Greiss Reagent System Assay was used to measure NO levels in loading and incubation media.

4.2.4 Disc and motion segment height changes

Radiographic analysis of IVDs was performed using a BenchTop Labscope. Pre- and post-loading images were acquired, and disc height change from pre-load to post-load of each sample was analyzed using ImageJ [168]. Five equally-spaced measurements were taken across the width for each sample and averaged.

To assess tissue recovery during the 9-hour post loading culture period, we measured disc height changes by comparing dimensions from pre-load to end of loading (3 hrs) and end of the 9-hour rest period (12 hours). Motion segment dimensions were measured using a digital caliper on the same set of samples over the 3 time points.

4.2.5 TLR4 inhibition of loaded discs

TAK-242, or Resatorvid, was dissolved in DMF and further diluted in media. A pilot study was conducted to identify an efficacious TAK-242 dose for IVD motion segments. Control segments were cultured with LPS (1 μg/ml) with or without TAK-242 (at 1 or 10 μM) for 24 hours. The resulting NO release into the media informed the TAK-242 dosing selected for loaded IVD samples. Segments were incubated with TAK-242 at 1.0 μM throughout the experiment, starting from 1 hour prior to loading, during loading, and 9-hours post-loading incubation.

4.2.6 Histology

To evaluate changes in IVD morphology, a subset of samples was fixed in 10% buffered formalin phosphate overnight at 4°C and stored in 70% ethanol. Motion segments were decalcified in EDTA for two weeks. Decalcified discs were paraffin-embedded and sectioned (7 μm). Slides

were stained with Alcian Blue (pH=1.0, GAG), Picrosirius Red (collagen), and H&E (cellularity). Images were taken using a Zeiss Axio Observer Z1 and an Axiocam 503 color camera.

4.2.7 qPCR preparation

IVD tissues were minced and processed for RNA extraction with TRIzol and a stick homogenizer, followed by phase-lock separation. RNA precipitation was performed using Qiagen miRNeasy columns. cDNA was synthesized using iScript cDNA Synthesis Kit. Gene specific master mixes were prepared using designed primers (**Table 4.1**) and iTaq Universal SYBR Green Supermix. RT-qPCR was run on a QuantStudio™ 6 Flex Real-Time PCR System. *Gapdh* was used as the housekeeping gene. Samples were normalized to the unloaded controls without TAK-242 using the $2^{-\Delta\Delta Ct}$ method.

Table 4.1: qPCR Primer Sequences.

Gene	FWD Primer Sequence	REV Primer Sequence	Amplicon Size (bp)
Acan	GGA TCT ATC GGT GTG AAG TGA TG	AGT GTG TAG CGT GTG GAA ATA G	112
Arg1	CCA AGC CAA AGC CCA TAG A	CCA GGC CAG CTT TCC TTA AT	102
Col1a1	GCT TGA AGA CCT ATG TGG GTA TAA	GGG TGG AGA AAG GAA CAG AAA	89
Col2a1	CAT AGG GCC TGT CTG TTT CTT	CCA TTC AGT GCA GAT CCT AGA G	117
Gapdh	GCA AGG ATA CTG AGA GCA AGA G	GGA TGG AAT TGT GAG GGA GAT G	98
Hmgb1	TCG GCC TTC TTC TTG TTC TG	GTT GTT CCA CAT CTC TCC TAG TT	108
Ifng	GTG AAC AAC CCA CAG ATC CA	GAA TCA GCA CCG ACT CCT TT	111
Il10	CTG CAG GAC TTT AAG GGT TAC T	TTT CTG GGC CAT GGT TCT C	103
Il1b	TCT GAC AGG CAA CCA CTT AC	CAT CCC ATA CAC ACG GAC AA	128
Il6	GAA GTT AGA GTC ACA GAA GGA GTG	GTT TGC CGA GTA GAC CTC ATA G	105
Mmp3	CCT GAT AGC TCT TCC TCT GAA AC	GGT TGA CTG GTG CCA TAT GTA	104

Mmp12	CTG GTT CGG TTG TTA GGA AGA	CCC TGA GCA TAC AGT GGA TAT G	90
Nos2	CAA CTA CTG CTG GTG GTT ACA	AAG GTA TGC CCG AGT TCT TTC	107
Tlr4	CAG AGC CGT TGG TGT ATC TT	AGC AAG GAC TTC TCC ACT TTC	110
Tnfa	CCC AAT CTG TGT CCT TCT AAC T	CAG CGT CTC GTG TGT TTC T	105

4.2.8 Long-term motion segment loading conditions

To validate the effect of single vs. extended loading on inflammatory outcomes, we loaded rat caudal IVDs daily for 5 days using the same unloaded, static, and high-dynamic protocols as the 1 day (3 hr) loading and measured resulting gene expression at the end of the organ culture period. These long-term "5-day loading" results were compared to the short-term "1-day loading" results. Segment collection occurred from three rats, as noted in Section 4.2.2. Motion segments were loaded for 3 hours daily followed by a 24-hour incubation period for 5-days using the unloaded, static, and high-dynamic loading profiles. LM and individual disc incubation media were collected and analyzed for NO content, and IVDs were prepared for RNA extraction and PCR.

4.2.9 High-static loading condition to assess matrix compaction

To investigate the possibility that matrix compaction may be limiting the ability of TAK-242 to diffuse into the high-dynamic loaded discs, we performed an additional experiment where the applied magnitude of static strain was increased to that of the high-dynamic group (termed as high-static loading) to investigate the effect of TAK-242 in these conditions.

In the high-static group, an 8% static strain (0.7 mm) was superimposed to the 20% tare strain applied to the motion segments, mimicking the applied magnitude of the high-dynamic group. The average height loss of high-static discs was achieved using a fluoroscope. Motion

segments were loaded using high-static loading with and without TAK-242, as described in Section 4.2.5. LM and individual disc incubation media were collected and analyzed for NO content, and IVDs were prepared for RNA extraction and PCR.

4.2.10 Statistical analysis

One-way ANOVAs with Holm-Sidak post-hoc tests were conducted comparing changes in disc height and NO release into LM. Spearman correlations were conducted to analyze the effects of applied strain and frequency on NO release into LM. Student t-tests were conducted on the gene expression of loaded versus unloaded discs. Student t-tests were also conducted to compare the effect of TAK-242 in each loading group versus no TAK-242 analog. Two-way ANOVA with Holm-Sidak post-hoc tests were also conducted comparing long-term NO release into LM between loading profiles across time points. Student t-tests were conducted on gene expression of long-term loaded versus long-term unloaded discs. Student t-tests were also conducted to compare gene expression of 5-day loaded versus 1-day loaded discs. Kruskal-Wallis and Mann-Whitney non-parametric tests were used with non-normal data as indicated by the Shapiro-Wilk test. Outliers were excluded from analysis as determined by ROUT(Q=1%). Statistical significance was set at $^{*}p<0.05$ where $\alpha=0.05$, and any trends where $^{\#}p<0.1$ were noted using GraphPad Prism 9.2.0.

4.3 Results

4.3.1 IVD height changes with loading

The average disc height increased by 8.5±9% in unloaded and significantly decreased by 17±12%, 36±22%, and 61±13% in static (p=0.001), low-dynamic ($p<1.0\times10^{-4}$), and high-dynamic ($p<1.0\times10^{-4}$) groups versus unloaded (**Fig. 4.2E**). Disc height change in high-dynamic was significantly greater than low-dynamic (p=0.012) and static ($p<1\times10^{-4}$), which were also different from each other (p=0.022).

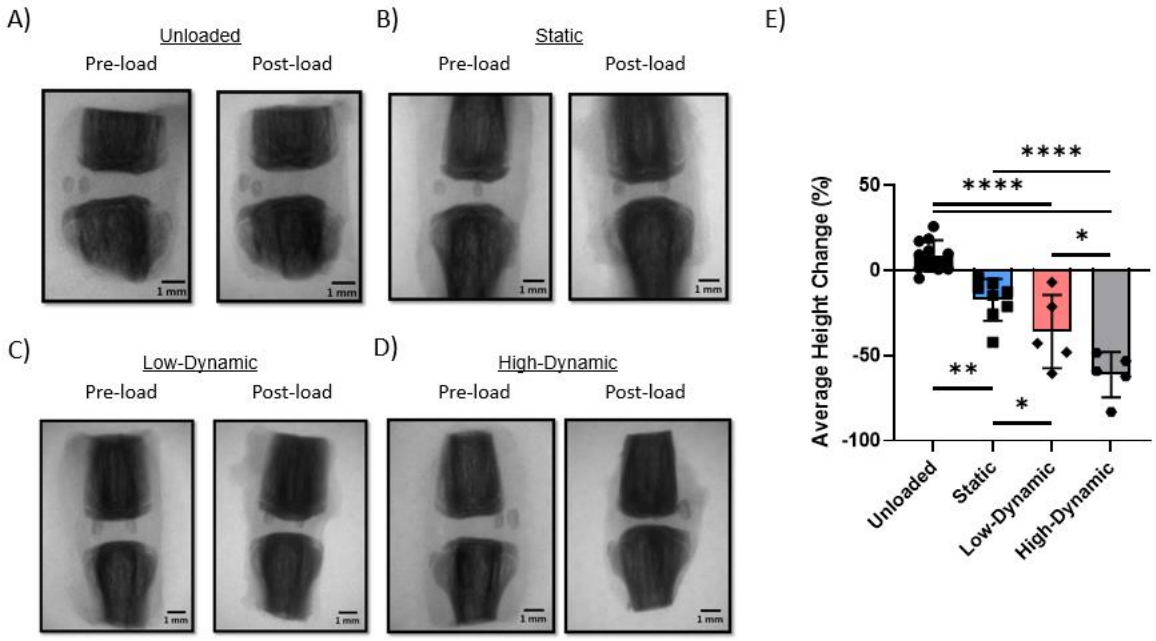

Figure 4.2: Disc height analysis post 3 hr loading.

Representative fluoroscope images of **A)** an unloaded Co10-Co11 motion segment which exhibited an ~ 8.54 ± 9.3% increase in disc height, **B)** a static loaded Co9-Co10 motion segment where frequency was set at 0 Hz which exhibited a ~ -17.3 ± 12.3% decrease in disc height, **C)** a low-dynamic loaded Co9-Co10 motion segment at 0.5 Hz which exhibited a ~ -36.0 ± 21.5% decrease in disc height, **D)** a high-dynamic loaded Co10-Co11 motion segment at 3 Hz which exhibited a ~ -61.3 ± 13.3% decrease in disc height. **E)** Average IVD height change experienced under each loading profile (N=11,8,5,5, respectively). ****$p < 0.0001$, **$p < 0.01$, and *$p < 0.05$.

4.3.2 Motion segments recover disc height 9 hours post loading

Unloaded discs did not significantly change in segment height at T=3 or 12 hrs compared to pre-load (p=0.16). Static-loaded discs had height loss at the end of loading (T=3 hrs, -2.45%) that recovered to a level comparable to pre-load by T=12 hrs (+0.19%) (p=0.18). High dynamic exhibited a decrease in height at T=3 hrs (-7.58%) that also recovered significantly but partially back toward pre-load levels (-3.04%) (p=0.040, N=3). Therefore, tissue swelling during 9 hours post culture incubation allowed samples to recover to pre-load conditions based on the loading group differentially; however, it did not result in swelling beyond the original segment height (**Fig. 4.3B**).

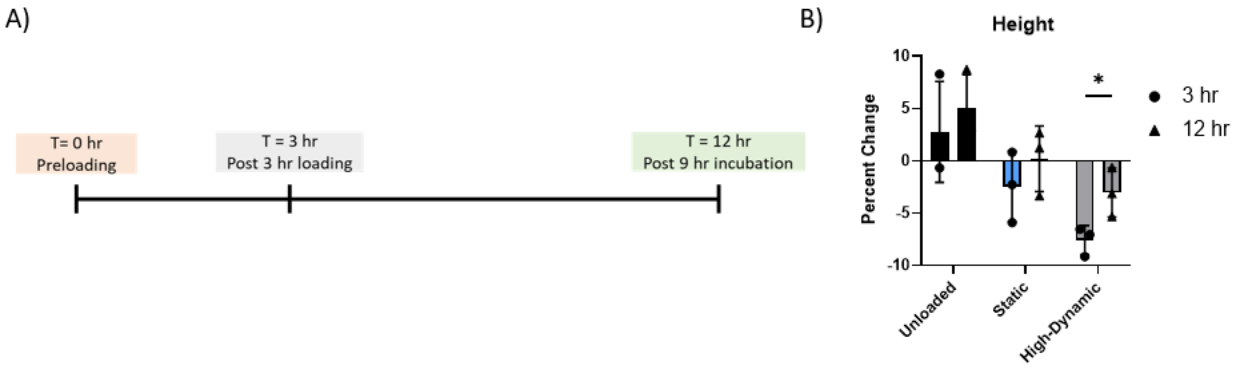

Figure 4.3: Motion segment swelling study on short-term loaded discs.

A) Timeline of one-time loading insult ranging from preload (T=0 hr), post-loading (T=3 hr), and post 9 hr tissue incubation (T=12 hr). **B)** Percent change in whole bone-disc-bone motion segment height at T=3 hr and T=12 hr compared to T=0 hr (preload). *p< 0.05

4.3.3 NO and gene expression of loaded IVDs

NO release into low-dynamic (p=0.016) and high-dynamic ($p<1.0\times10^{-4}$) LM was significantly higher compared to unloaded (**Fig. 4.4A**). NO release during static loading was significantly lower compared to low- (p=0.016) and high-dynamic loading ($p<1.0\times10^{-4}$). Low-dynamic loading released less NO than high-dynamic loading (p=0.017) (**Fig. 4.4A**). NO release during loading was dependent on both applied strain ($p<1.0\times10^{-4}$, r=0.86) and frequency ($p<1.0\times10^{-4}$, r=0.89) (**Fig. 4.4Bi-ii.**). There were no differences in NO release from individual discs during incubation (p=0.67) (**Fig. 4.4C**).

When looking at gene expression in loaded IVDs, pro-inflammatory genes *Nos2* (p=0.025), *Tnfa* ($p=1.0\times10^{-4}$), and *Il1b* (p=0.020) were upregulated in the high-dynamic loaded discs versus unloaded. *Tlr4* (p=0.028) and *Hmgb1* ($p=3.0\times10^{-4}$) expression also increased in the high-dynamic group versus unloaded. Anti-inflammatory *Il10* (p=0.0036) and *Arg1* (p=0.023) expression also significantly increased in high-dynamic versus unloaded (**Fig. 4.4D-F,H-I,K-L).** Expression of ECM genes *Col1a1* (p=0.032), *Col2a1* (p=0.0019), *Acan* (p=0.0011), and *Mmp3* (p=0.030) was downregulated in high-dynamic loading versus unloaded discs (**Fig. 4.4M**). Under static loading, gene expression of *Nos2* (p=0.030), *Tnfa* (p=0.0026), *Il1b* (p=0.046), *Ifng* (p=0.0098), *Tlr4* (p=0.012), *Hmgb1* (p=0.0079), *Il10* (p=0.0073), and *Arg1* (p=0.017), was upregulated versus unloaded discs (**Fig. 4.4D-F,H,I,K,L**). Expression of *Col1a1* (p=0.0071), *Col2a1* (p=0.0022), *Acan* ($p=8.0\times10^{-4}$), and *Mmp3* (p=0.018) was also downregulated under static loading versus unloaded (**Fig. 4.4M**). Low-dynamic loading had significantly lower expression of *Arg1* (p=0.033) and *Acan* (p=0.032) versus unloaded (**Fig. 4.4L,M**).

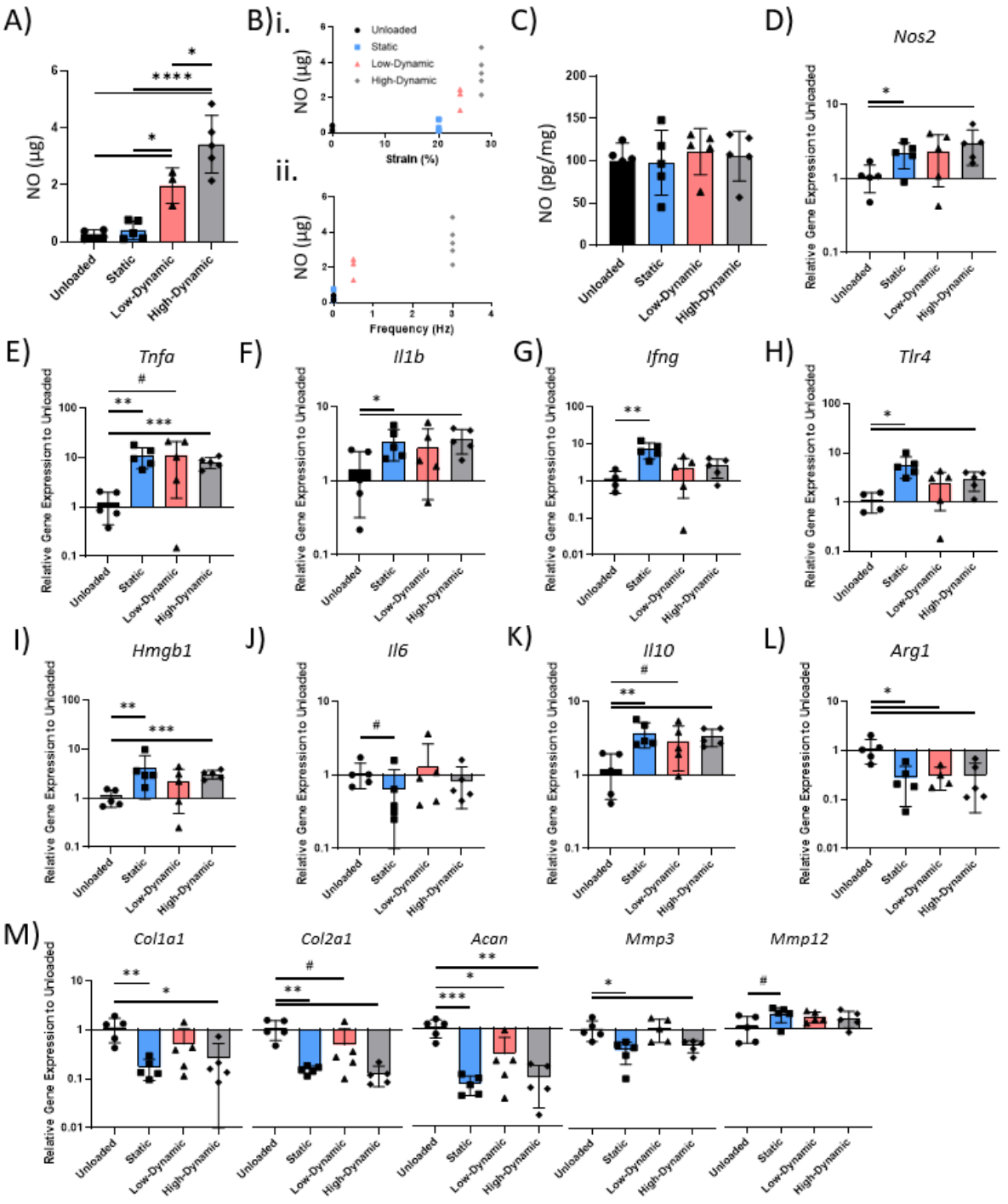

Figure 4.4: Inflammatory cytokine profiles of loaded discs.

A) NO released into loading media of unloaded, static, low-dynamic, and high-dynamic conditions (N=4,3,3,5), **B)** NO release represented by applied **i.** strain and **ii.** frequency (N=3-5), and **C)** NO release into media 9 hr post-loading (N=5). Gene expression 9 hr post-loading of **D)** *Nos2* (N=5), **E)** *Tnfa* (N=5), **F)** *Il1b* (N=5), **G)** *Ifng* (N=4,5,5,5), **H)** *Tlr4* (N=4,5,5,5), **I)** *Hmgb1*

(N=5), **J)** *Il6* (N=5), **K)** *Il10* (N=5), **L)** *Arg1* (N=5,5,4,5), in addition to ECM genes **M)** *Col1a1*, *Col2a1*, *Acan*, *Mmp3*, and *Mmp12* (N=5). ****p< 0.0001, ***p< 0.001, **p< 0.01, *p< 0.05, and #p< 0.1

4.3.4 Effect of TAK-242 on unloaded IVDs

In unloaded discs stimulated with LPS, TAK-242 reduced NO production at both 1 and 10 μM (p=0.0020) (**Fig. 4.5A**). The addition of TAK-242 to the media of the unloaded discs did not affect NO release in the first 3 hours (p=0.23) (**Fig. 4.5B**), but it did reduce subsequent NO release in the incubation media (p=2.0×10^{-4}) (**Fig. 4.5C**). TAK242+unloaded significantly decreased *Il6* (p=0.0023) and *Arg1* (p=0.027) versus unloaded discs (**Fig. 4.5D**). ECM genes *Col1a1* (p=0.037), *Col2a1* (p=0.0037), and *Acan* (p=0.0028) were also significantly downregulated (**Fig. 4.5E**).

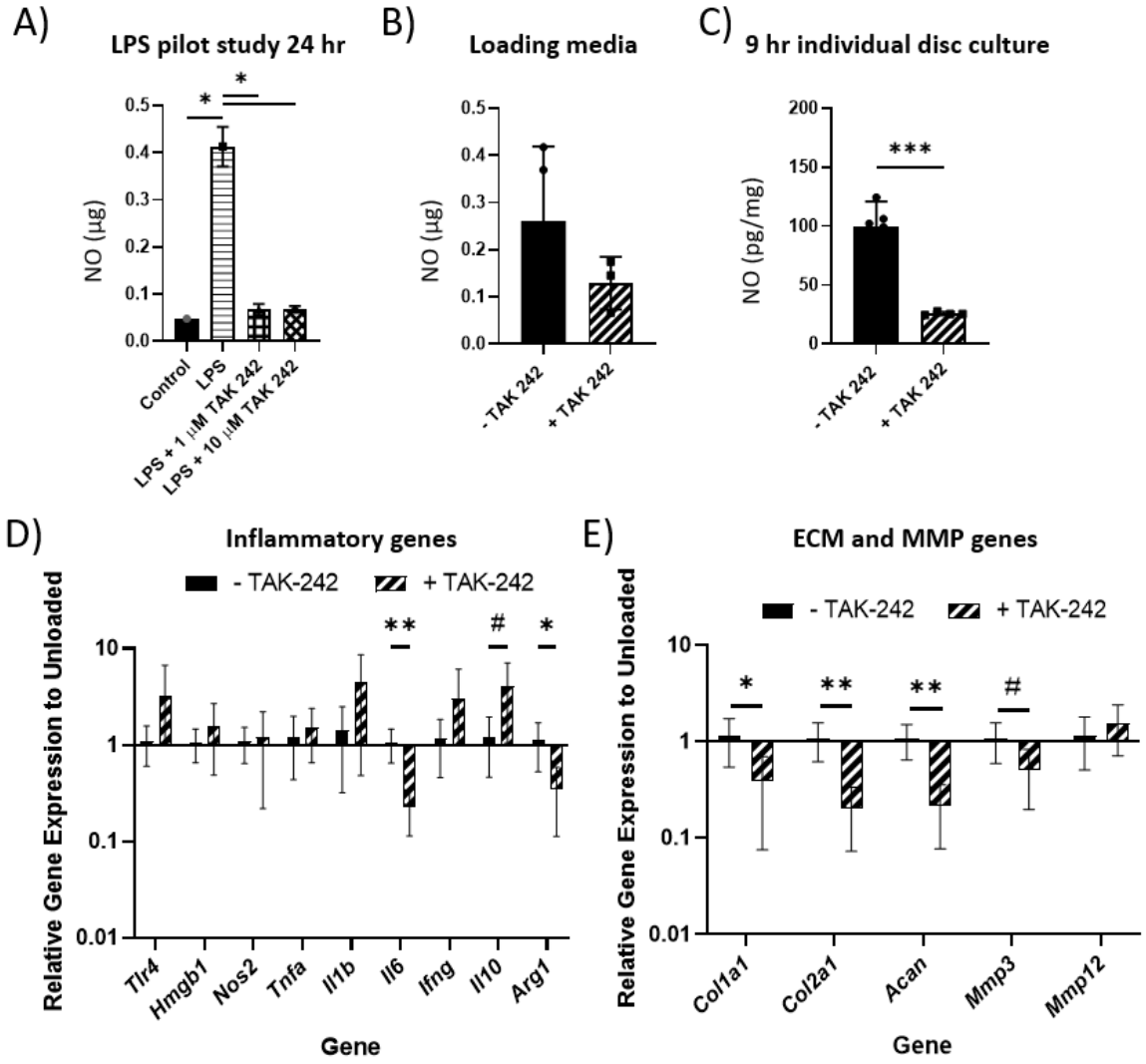

Figure 4.5: Inflammatory and ECM environment of unloaded discs.

A) NO release of unloaded discs stimulated with LPS and cultured with 1 µM and 10 µM TAK for 24 hr (N=2), **B)** 3 hr NO release into media with unloaded discs ± 1 µM TAK-242 (N=4,3), and **C)** NO release from individual discs 9 hr post-loading (N=5). **D)** Inflammatory gene expression (N=5) and **E)** ECM gene expression 9 hr of unloaded discs ± 1 µM TAK-242 (N=5). ***$p < 0.001$, **$p < 0.01$, *$p < 0.05$, and #$p < 0.1$

4.3.5 Effect of TAK-242 on loaded IVDs

TAK-242 did not alter NO release into the static LM (p=0.26) (**Fig. 4.6A**) but did reduce NO release into the post-static loading individual disc media (p=0.021) (**Fig. 4.6B**). *Tlr4* (p=0.018), *Tnfa* (p=0.020), and *Ifng* (p=0.010) expression significantly decreased in static+TAK242 versus static (**Fig. 4.6C**). *Arg1* (p=0.039), *Col1a1* (p=0.0079), *Col2a1* (p=0.026), *Acan* (p=0.016), *Mmp3* (p=0.0065), and *Mmp12* (p=0.045) expression significantly increased in static+TAK242 versus static (**Fig. 4.6C-D**).

During low- and high-dynamic loading, NO release into LM (p=0.81, p=0.85) (**Fig. 4.6E,I**) and incubation media (p=0.22, p=0.22) (**Fig. 4.6F,J**) was not significantly different from their no TAK-242 counterparts. However, there were significant increases in *Il6* (p=0.0063) and *Arg1* ($p=9.5\times10^{-4}$) gene expression in high-dynamic+TAK242 versus high-dynamic (**Fig. 4.6K**).

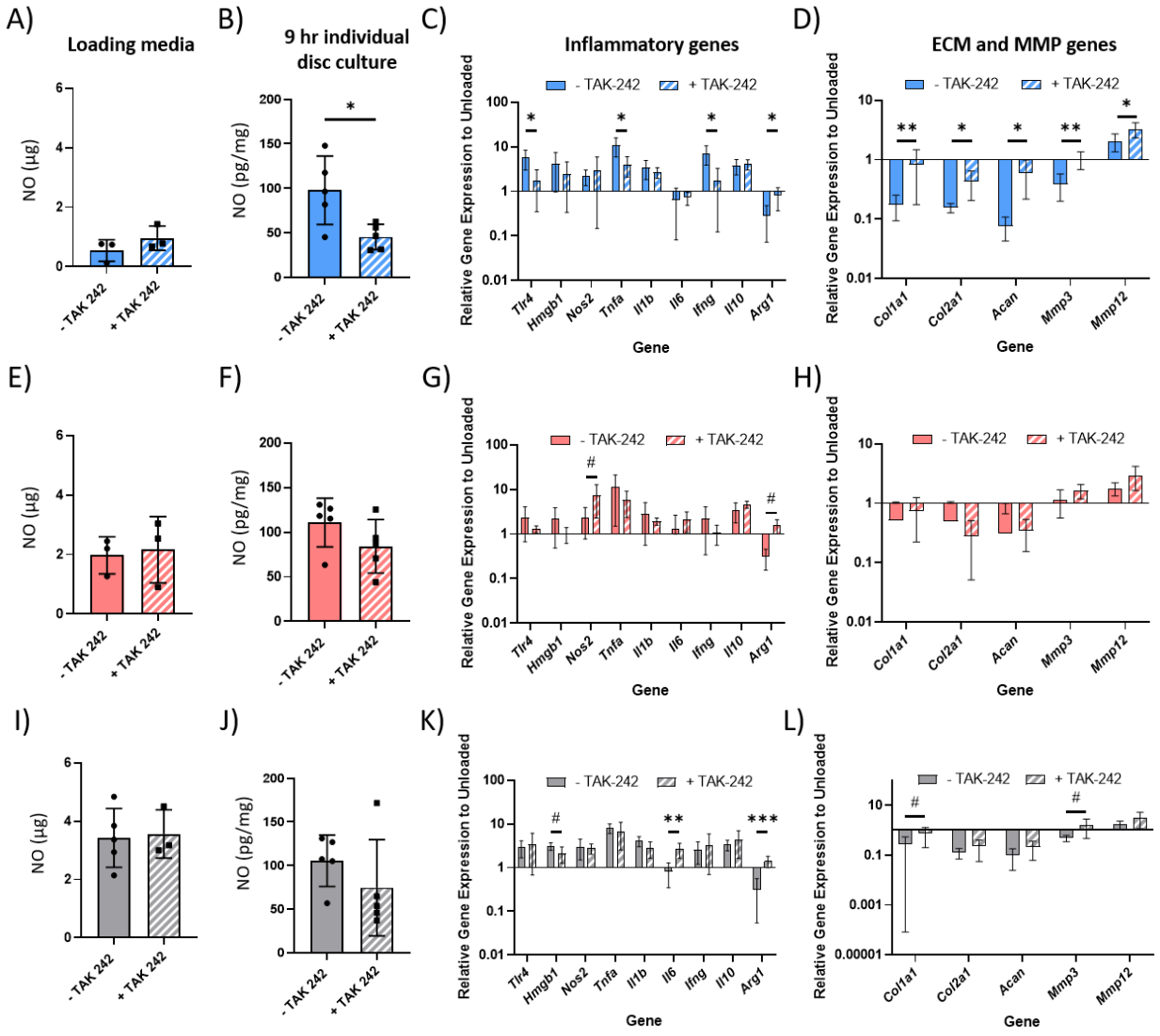

Figure 4.6: Inflammatory and ECM environment for static, low-dynamic, and high-dynamic discs.

A) 3 hr NO release into media (N=3), **B)** NO release from individual discs 9 hr post-loading (N=5), **C)** inflammatory gene expression (N=4-5), and **D)** ECM gene expression 9 hr post-loading (N=5) ± 1 µM TAK-242 for static discs. **E)** 3 hr NO release into media (N=3), **F)** NO release from individual discs 9 hr post-loading (N=5), **G)** inflammatory gene expression (N=3-5), and **H)** ECM gene expression 9 hr post-loading (N=3-5) ± 1 µM TAK-242 for low-dynamic discs. **I)** 3 hr NO release into media (N=3-5), **J)** NO release from individual discs 9 hr post-loading (N=5), **K)** inflammatory gene expression (N=4-5), and **L)** ECM gene expression 9 hr

post-loading (N=5) ± 1 µM TAK-242 for high-dynamic discs. ***p< 0.001, **p< 0.01, *p< 0.05, and #p< 0.1

4.3.6 Histology

In unloaded discs, the NP appeared round and constituted much of the disc cross-sectional area (**Fig. 4.7A-C**). About 80% of NP cells were large and vacuolated, surrounded by a GAG-rich matrix (**Fig. 4.7D**). The NP-AF border was distinct (**Fig. 4.7A-C**). The AF comprised of well-organized collagen-rich discrete lamellae bulging outward (**Fig. 4.7E**). Under static loading, the NP region appeared compacted and displaced by an AF-like collagen matrix, with little evidence of NP vacuolated cells (**Fig. 4.7D**). The AF lamellae were distorted (serpentine) or ruptured, and the NP-AF border was indistinguishable (**Fig. 4.7E**). In low- and high-dynamic groups, the NP appeared round but asymmetric and convex (**Fig. 4.7D**), with a pronounced irregular shape observed in high-dynamic. Fewer clustered vacuolated cells were observed in low-dynamic versus unloaded, while the AF appeared to be distorted, with observations of lamella infolding and NP-AF border disruptions (**Fig. 4.7A-C**). In high-dynamic, the NP was full of GAG-rich clusters and was surrounded by a mildly disrupted inner AF (**Fig. 4.7D**). The outer AF exhibited disruption in collagen lamellae with increased fissures (**Fig. 4.7E**).

In unloaded+TAK242, the NP maintained its round, oval shape (**Fig. 4.7F-H**), with ~60% of NP cells appearing large and vacuolated (**Fig. 4.7I**), and AF morphology remained intact. In static+TAK242, the NP shape was round and vacuolated, while the AF appeared less distorted than in static. In dynamic+TAK242 loaded discs, no qualitative differences were observed versus no TAK242 counterparts.

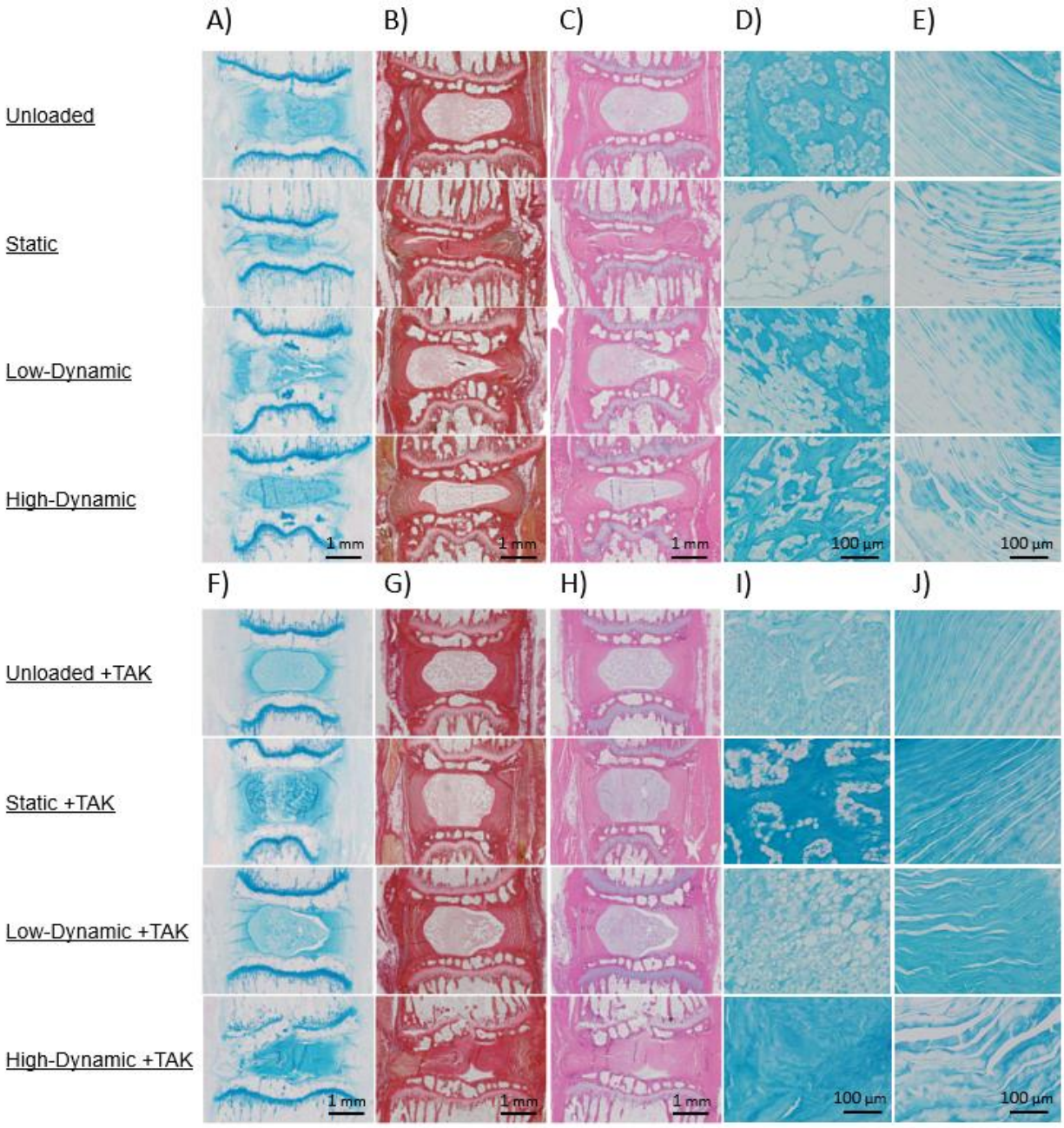

Figure 4.7: Histological differences in ±TAK-242 post-loaded discs.

Histology on discs post 3 hr loading without TAK-242 **A-E)** and with TAK-242 **F-J)** from unloaded, static, low-dynamic, and high-dynamic conditions. **A,F)** Alcian Blue, **B,G)** Picrosirius Red, **C,H)** H&E, **D,I)** NP region, and **E,J)** AF region.

4.3.7 Inflammatory response of long-term high-dynamic loaded discs led to the greatest release of NO throughout 5-days of loading

Daily NO release into LM ranged from 0.00-0.21 µg for unloaded, 0.48-0.98 µg for static, and 1.7-2.3 µg for high-dynamic (**Fig. 4.8A,** N=1). After 5-day loading, cumulative NO release from high-dynamic discs at 3163±330 pg/mg was significantly higher than static at 2214±238 pg/mg (p=0.019) and unloaded discs at 914±46 pg/mg (p=0.019) (**Fig. 4.8B**). Gene expression in 5-day loaded IVDs showed pro-inflammatory gene *Nos2* trending upward (p=0.054) in high-dynamic compared to unloaded discs, while other pro-inflammatory genes such as *Tnfa* (p=0.11), *Il1b* (p=0.99), *Ifng* (p=0.86), and *Il6* (p=0.56) were not significantly different from unloaded discs (**Fig. 4.8C-F,I**). *Tlr4* (p=0.046) and *Hmgb1* (p=0.017) expressions decreased in the high-dynamic group versus unloaded (**Fig. 4.8G-H**). Anti-inflammatory *Arg1* (p=0.023) expression did not significantly change in high-dynamic versus unloaded (**Fig. 4.8J).** Expression of ECM genes *Col1a1* was trending downwards (p=0.082) while *Acan* (p=0.019) and *Mmp3* (p=0.002) were significantly upregulated in high-dynamic loading versus unloaded discs (**Fig. 4.8K**). There was no change in *Col2a1* (p=0.13) for high-dynamic compared to unloaded (**Fig. 4.8K**). Under static loading, there was no difference in gene expression of *Nos2* (p=0.15), *Tnfa* (p=0.17), *Il1b* (p=0.25), *Ifng* (p=0.12), *Tlr4* (p=0.19), *Hmgb1* (p=0.36), or *Il6* (p>0.99) versus unloaded discs (**Fig. 4.8C-I**). However, *Arg1* was significantly upregulated in static versus unloaded discs post 5-day loading (p=0.0011, **Fig. 4.8J**). Expression of *Col1a1* (p=0.062) was trending downwards under static loading versus unloaded, while *Mmp3* (p=0.020) was significantly upregulated under static loading versus unloaded (**Fig. 4.8K**). There was no difference in ECM gene expression of *Col2a1* (p=0.36) and *Acan* (p=0.55) in static discs post 5-day loading (**Fig. 4.8K**). In the 5-day loading study,

cumulative NO levels increased at a greater rate in high-dynamic vs. static, where both loading profiles resulted in increased NO versus unloaded **(Fig. 4.8)**.

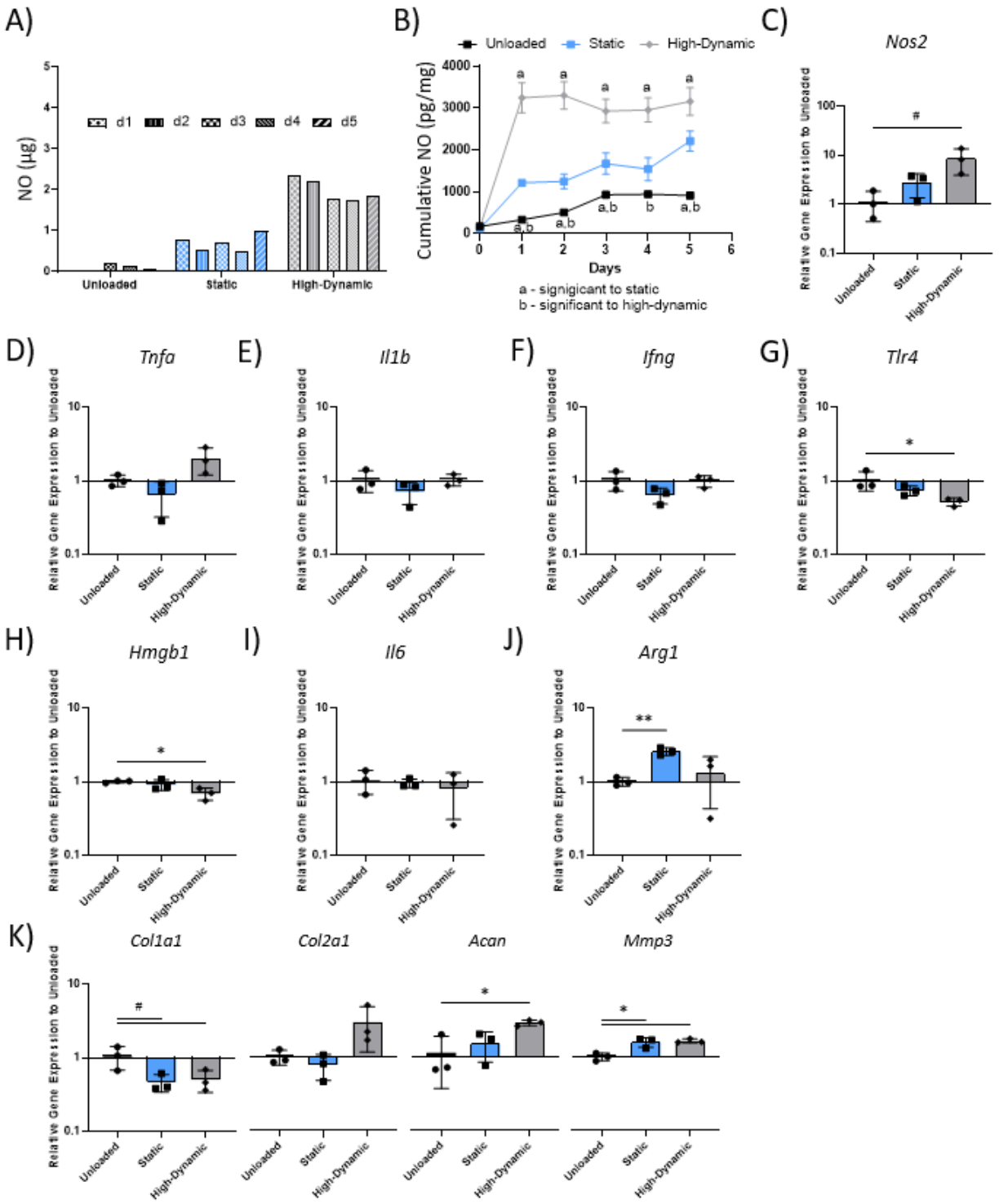

Figure 4.8: Inflammatory cytokine profiles of long-term (5-day) loaded discs normalized to long-term 5-day unloaded discs.

A) NO release into LM of unloaded, static, and high-dynamic conditions (N=1), **B)** cumulative NO release of individual motion segments over 96 hr (N=3, a represents $p < 0.05$ compared to

static, b represents $p < 0.05$ compared to high-dynamic), and gene expression 24 hr post 5-day loading of **C)** *Nos2* (N=3), **D)** *Tnfa* (N=3), **E)** *Il1b* (N=3), **F)** *Ifng* (N=3), **G)** *Tlr4* (N=3), **H)** *Hmgb1* (N=3), **I)** *Il6* (N=3), **J)** *Arg1* (N=3), in addition to ECM genes **K)** *Col1a1*, *Col2a1*, *Acan*, and *Mmp3* (N=3) compared to 5-day unloaded gene expression. **p< 0.01, *p< 0.05, and #p< 0.1

4.3.8 Inflammatory response of long-term loaded discs was mitigated, and ECM remodeling increased with 5-day loading compared to 1-time loaded discs

In Figure 4.8B, results from Figure 4.7B were normalized to the 1-day loading results presented in the manuscript. For the 5-day unloaded discs, there was higher inflammatory gene expression of *Tlr4* (p=7.8×10^{-3}), *Hmgb1* (p=5.0×10^{-3}), and *Tnfa* (p=0.017) versus the 1-day unloaded discs (**Fig. 4.9B**). *Nos2* was downregulated in 5-day versus 1-day loaded discs (p=0.049) (**Fig. 4.9B**). Gene expression of *Il1b* (p=0.090) and *Ifng* (p=0.056) was trending upwards in 5-day versus 1-day unloaded discs (**Fig. 4.9B**). There was no significant change in inflammatory gene expression of *Il6* (p=0.14) and *Arg1* (p=0.16) (**Fig. 4.9B**). Gene expression of *Col1a1* (p=0.023) and *Col2a1* (p=0.019) was downregulated in 5-day unloaded discs compared to 1-day unloaded discs (**Fig. 4.9C**). However, *Acan* (p=0.29) and *Mmp3* (p=0.83) gene expression did not differ between 5-day and 1-day unloaded discs (**Fig. 4.9C**).

For the 5-day static discs, there was no difference in inflammatory gene expression of *Tlr4* (p=0.10), *Hmgb1* (p=0.28), *Il1b* (p=0.21), and *Il6* (p=0.83) versus the 1-day static-loaded discs (**Fig. 4.9D**). *Tnfa* (p=0.023) and *Ifng* (p=0.030) gene expression was significantly downregulated while *Nos2* was trending downwards in 5-day versus 1-day static-loaded discs (p=0.062) (**Fig. 4.9D**). *Arg1* inflammatory gene expression was significantly upregulated in 5-day versus 1-day static loaded discs (p=1.1×10^{-4}) (**Fig. 4.9D**). Gene expression of *Col1a1* (p=0.025) was downregulated while *Acan* (p=0.0028) and *Mmp3* (p=2.1×10^{-4}) expression was upregulated in 5-day static loaded compared to 1-day static loaded discs (**Fig. 4.9E**). However, *Col2a1* (p=0.84) gene expression did not differ between 5-day and 1-day static loaded discs (**Fig. 4.9E**).

For the 5-day high-dynamic discs, there was no difference in inflammatory gene expression of *Tlr4* (p=0.19), *Nos2* (p=0.97), *Tnfa* (p=0.17), *Il1b* (p=0.43), *Il6* (p=0.31), *Ifng* (p=0.84), and

Arg1 (p=0.12) versus the 1-day unloaded discs (**Fig. 4.9F**). However, *Hmgb1* (p=0.0050) gene expression was significantly downregulated in 5-day versus 1-day high-dynamic loaded discs (**Fig. 4.9F**). Gene expression of *Col2a1* (p=0.026), *Acan* ($p<1.0\times10^{-4}$), and *Mmp3* ($p=1.0\times10^{-4}$) was upregulated in 5-day high-dynamic discs compared to 1-day high-dynamic discs (**Fig. 4.9G**). However, *Col1a1* (p=0.19) gene expression did not differ between 5-day and 1-day high-dynamic discs (**Fig. 4.9G**).

Our results demonstrate decreased gene expression of various genes, such as *Tnfa and Ifng*, in 5-day statically loaded discs compared to the 1-day loaded discs (**Fig. 4.9D**). There was also an increase in ECM and related remodeling genes such as *Acan* and *Mmp3* gene expression in discs post-5-day static and high-dynamic loading versus 1-day loading (**Fig.4.9E,G**). Overall, inflammatory gene expression was more upregulated in response to 1-day of loading when compared to 5-day loading, and inhibition in ECM gene expression due to loading appeared to recover with 5-day loading (**Fig. 4.8,4.9**), suggesting that 5-day loading simulated IVD remodeling.

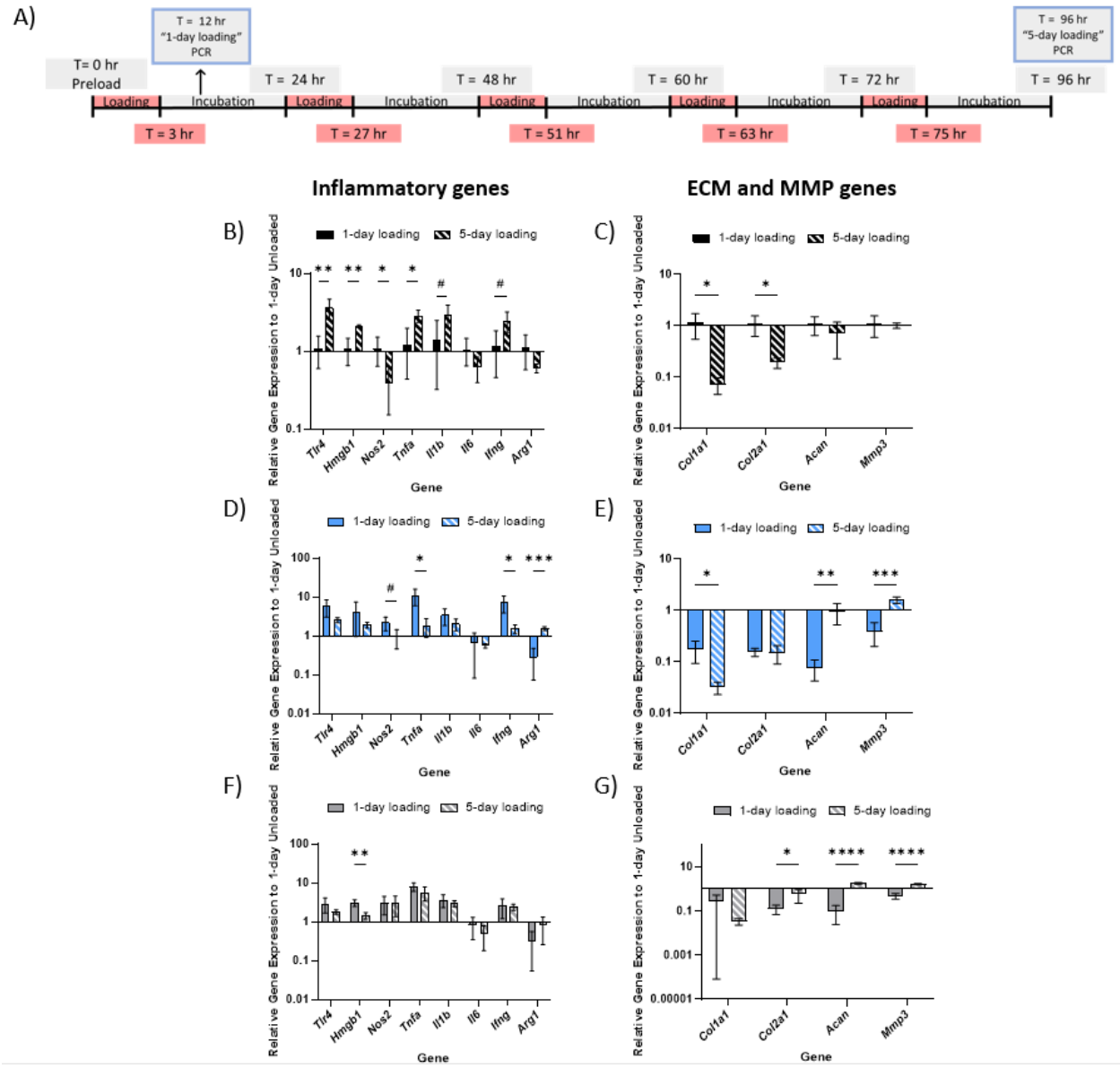

Figure 4.9: Inflammatory cytokine profiles of long-term (5-day) loaded discs normalized to short-term (1-day) loaded discs.

A) Experimental timeline for long-term 5-day loading. Inflammatory and ECM environment for 5-day loaded compared to 1-day loaded discs for **B-C)** unloaded discs (N=4-5), **D-E)** static discs (N=5), and **F-G)** high-dynamic discs (N=5). ***$p < 0.001$, **$p < 0.01$, *$p < 0.05$, and #$p < 0.1$

4.3.9 Matrix compaction did not occur in high-static loading despite affecting the inflammatory response of discs

Average disc height change for the high-static group was calculated to be -22 ± 26%, where it was not significantly different from the static group (p=0.57), but high-static was still significantly greater in height loss compared to unloaded (p=2.0×10^{-4}) (**Fig. 4.10B-C**, N=6-11). When comparing high-static to unloaded discs, expression of *Tlr4*, *Hmgb1*, *Il1b*, and *Ifng* was upregulated with *Tnfa* trending upwards (p=9.5×10^{-4}, 3.6×10^{-3}, 0.012, 0.034, and 0.094, respectively) (**Fig. 4.10H,** N=3-5). There was no significant change in *Nos2*, *Il6*, *Il10*, and *Arg1* gene expression between high-static and unloaded groups (p=0.19, 0.42, 0.25, and 0.97, respectively) (**Fig. 4.10H**, N=3-5). ECM gene expression of *Acan* and degradative enzyme *Mmp12* was significantly increased in high-static compared to unloaded discs (p=1.7×10^{-3}, 0.018, respectively) (**Fig. 4.10I,** N=3-5). Meanwhile, *Col1a1* and *Mmp3* were trending downwards (p=0.052, 0.089, respectively) (**Fig. 4.10I,** N=3-5), and *Col2a1* gene expression was not significantly altered in high-static discs compared to unloaded discs (p=0.26) (**Fig. 4.10I,** N=3-5). Thus, when assessing the effect of loading magnitude, the high-static group exhibited a similar profile of elevated pro-inflammatory gene expression to static loading.

In high-static loading, TAK-242 did not significantly alter NO release from LM (p=0.68) (**Fig. 4.10D**, N=2). TAK-242 also did not reduce NO release from individual discs post-incubation (p=0.65) (**Fig. 4.10E**, N=3). There was no significant change in gene expression of *Tlr4*, *Hmgb1*, *Tnfa*, *Ifng*, and *Arg1* between high-static groups with and without TAK-242 (p=0.20, 0.25, 0.90, 0.31, and 0.37, respectively) (**Fig. 4.10F**, N=3). *Nos2*, *Il1b*, and *Il6* were significantly downregulated with the addition of TAK-242 for high-static loading (p=0.013, 0.013, and 0.0086, respectively) (**Fig. 4.10F**, N=3). *Il10* trended upwards with TAK-242 compared to no TAK-242

high-static loaded discs (p=0.087) (**Fig. 4.10F**, N=3). There was no difference in ECM gene expression of *Col1a1*, *Col2a1*, *Acan,* or degradative enzyme *Mmp3* with the use of TAK-242 (p=0.89, 0.34, 0.19, and 0.56, respectively) (**Fig. 4.10G**, N=3). However, *Mmp12* was significantly downregulated with the addition of TAK-242 (p=0.0057) (**Fig. 4.10G**, N=3).

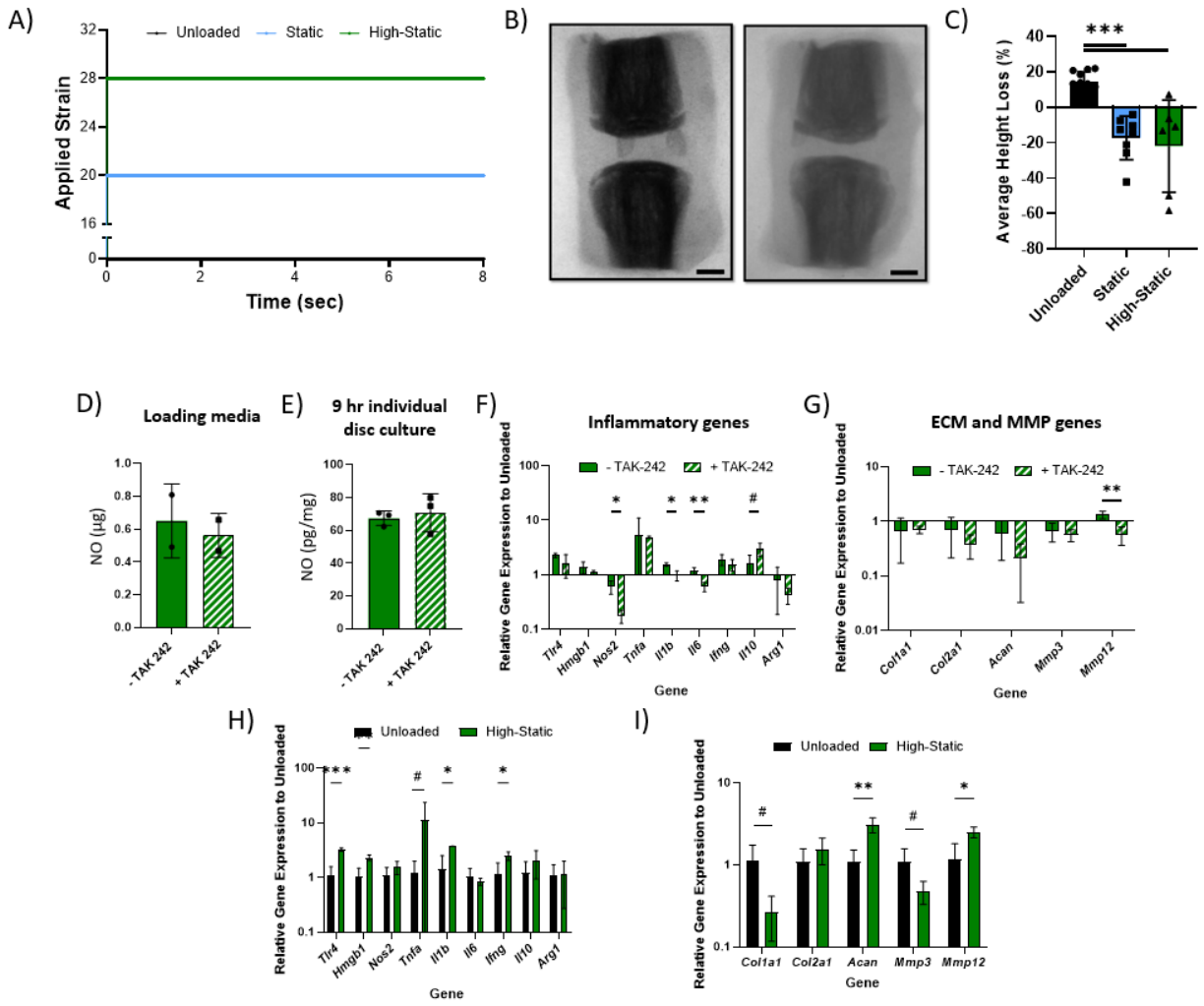

Figure 4.10: Physical and inflammatory characterization of high-static loaded discs.

A) Loading profiles of unloaded, static, and high-static groups. **B)** Disc height change with high-static loading from pre-load to post-load. Bar represents 1 mm. **C)** Average height change of discs under static and high-static conditions compared to unloaded (N=5-11). Inflammatory environment of high-static discs where **D)** represents the 3 hr NO release into LM for high-static loading ± TAK-242 (N=3) and **E)** is the NO release from individual discs 9 hr post-loading (N=3). **F)** Inflammatory and **G)** ECM gene expression 9 hr post high-static loading ± 1 µM TAK-242 (N=3). **H)** Inflammatory and **I)** ECM gene expression of high-static discs compared to unloaded discs (N=3-5). ***p< 0.001, **p< 0.01, *p< 0.05, and #p< 0.1

4.4 Discussion

The goals of this study were to characterize the inflammatory signaling changes in response to static and dynamic loading and to investigate the contributions of TLR4 to mechanically-induced inflammatory signaling using an organ culture model of bone-disc-bone motion segments. NO release into the LM was highly correlated with applied frequency and strain magnitude across different loading profiles. Static and high-dynamic loading significantly increased TLR4 and HMGB1 expression, which was not observed in the more physiologically relevant low-dynamic loading. The current study also investigated the efficacy of TAK-242, a drug that inhibits pro-inflammatory TLR4 signaling. While co-treatment with TAK-242 significantly decreased NO release in unloaded groups, its effects on loaded IVDs differed by loading profiles, where TAK-242 decreased pro-inflammatory expression in static but not dynamic loaded groups. This suggests that TLR4 plays a direct role in mediating inflammatory responses of IVD to static compression.

Solute transport associated with different loading profiles may also affect NO release. The cyclic nature of dynamic loading may be modulating the transport of cytokines into the media, possibly through convection-aided transport [44]. NO release was higher in low- and high-dynamic loading conditions, possibly due to higher NO production and/or greater solute convection at these frequencies. Despite the significant increase in iNOS gene expression with static loading, NO media levels did not change, potentially due to the lack of fluid flow convection. Matrix compaction due to static loading may have also hindered NO diffusion from the disc into the media [189]. Although motion segments largely recovered to pre-load height during incubation (**Fig. 4.3**), NO release during incubation was similar across loading groups. Over time, 5-day loading led to a nonlinear increase in cumulative NO release, driven primarily by increases in NO levels during earlier loading events (**Fig. 4.8**).

The catabolic IVD tissue response to static and high-dynamic loading suggests that non-physiological loading elicits a similar molecular profile, including significant increases in TNFα and IL-1β expression. TNFα and IL-1β are key pro-inflammatory cytokines elevated in human degenerated disc samples [190]. Though IL-6 is also associated with advanced degeneration [134, 191, 192], we did not see significant increases in either short- or long-term loading protocol (**Fig. 4.8,4.9**). TNFα also promotes IL-10 secretion, which serves as negative feedback on pro-inflammatory cytokines to mitigate damage [193-195]. Indeed, we observed TNFα upregulation and IL-10 upregulation in injurious loading conditions. However, the 5-day loading study showed decreased TNFα inflammatory gene expression compared to 1-day loading (**Fig. 4.9D**), which may be a consequence of IL-10 feedback. Since IL-10 was upregulated in static and high-dynamic loading, this suggests that anti-inflammatory signaling is activated in the same post-loading timeline as pro-inflammatory activation.

Static and high-dynamic loading resulted in similar alterations to pro-inflammatory cytokines and ECM gene expression, whereas the low-dynamic group was considered more physiologically relevant since it did not lead to significant pro-inflammatory upregulation of cytokines. When assessing the impact of loading magnitude, the high-static group also exhibited a similar profile of elevated inflammatory genes to static and high-dynamic groups (**Fig. 4.10**). Interestingly, IFNγ increased in static and high-static but not high-dynamic loading. IFNγ is an important mediator of immunity and inflammation [196]. The results of this study differ from literature, which found distinct inflammatory responses to static and dynamic loading. In Wang *et al.,* greater levels of IL-1β and TNFα expression were found under static loading (0.5 MPa) compared to dynamic loading (0.5 – 1.0 MPa with either 0.1 or 1 Hz) [77]. These findings are consistent with our findings using low-dynamic loading. Some studies show that dynamic loading

was more detrimental to IVD integrity than static loading when higher frequencies were applied, leading to greater cell death, which was not examined directly in the current study [197, 198]. Although their pro-inflammatory profiles were similar, we observed differences in histological changes of the IVD in static and high-dynamic vs. unloaded. Specifically, versus unloaded discs, static loading led to more morphological disruption than low-and high-dynamic discs. This suggests that fluid pressurization from dynamic loading may have protected against NP cell or tissue rupture.

TLR4 was upregulated in static and high-dynamic loading versus unloaded discs. Activation of TLR4 can enhance the production of mediators such as HMGB1, which can also augment the inflammatory response [7, 174]. High HMGB1 levels can promote GAG loss in discs, which contribute to the GAG loss observed in the histological analyses of static and high-dynamic loading [186].

The current study also investigated the efficacy of TAK-242, a drug that inhibits intracellular TLR4 signaling and decreases downstream NF-κB activation in response to inflammatory stimuli [178, 199]. While co-treatment with TAK-242 post-injury significantly decreased NO release in unloaded discs, its effects on loaded IVD motion segments differed by loading profiles. TAK-242 co-treatment decreased pro-inflammatory expression in unloaded and static, but not dynamic loaded groups, suggesting that TLR4 plays a direct role in mediating inflammatory responses of IVD to static loading. There was a slight qualitative difference in the representative histology of +TAK static loaded discs in which the ECM was better conserved compared to the -TAK counterpart. This is consistent with gene expression results where TAK-242 mitigated the effects of static loading. However, during loading, NO release was not affected by TAK-242. Thus, TLR4 may mediate post-injury rather than during injury inflammatory

responses. Some reasons for this may be that the loading period is too short for the drug to penetrate and influence cells within a compacted ECM during compression.

Findings indicated that TAK-242 effectively mitigated post-injury response when loading increased TLR4 levels (i.e., static loading). Indeed, TAK-242 significantly decreased levels of TLR4 and decreased pro-inflammatory cytokines TNFα and IFNγ gene expression under static loading. A concomitant increase in macrophage-related factors, ARG1 and MMP12, was observed in TAK-242-treated statically loaded discs. COL1A1, COL2A1, and ACAN also increased significantly with TAK-242, suggesting TLR4 inhibition promoted an anabolic remodeling response due to increased MMP3 expression. Findings are consistent with our prior study that showed how TAK-242 abrogated HMGB1-induced MMP-1 expression in addition to mitigating NF-κB signaling in human NP cells *in vitro* [11]. The increase in ARG1 expression also supports additional anti-inflammatory effects of TLR4 inhibition [178, 200], further demonstrating the potential of decreasing the pro-inflammatory response for static loading.

Limitations of this study include discs being exposed to different loading profiles and orientations compared to an *in vivo* setting due to soft tissue removal during dissection and an absence of systemic circulation *in vitro*. Furthermore, gene expression reported in this study represents contributions of heterogeneous IVD tissue, including NP, AF, and CEPs, with media analyses including contributions of surrounding vertebral bone. Maintenance of the intact IVD, including uninterrupted CEP to bone interface, was necessary to maintain motion segment integrity for applied loading. We aimed to minimize the potential for herniation of the NP from the loaded IVD by keeping an intact interface with surrounding bone. However, bone presence may have interfered with diffusion of molecules into the media post-loading.

Chapter 5: Secretome of loaded IVDs can prime MSCs for cell therapy

5.1 Introduction

Mechanisms of IVD degeneration are not fully understood; however, cytokines are thought to play primary roles within the degenerative signaling cascade [201]. Few studies have examined how the secretome of tissue, such as the IVD, can influence resident or transplanted cells in the disease microenvironment and how physical factors, such as mechanical loading, may influence the secretome. DAMPS, such as HMGB1 or glycoproteins [202], have been shown to have degenerative effects in disc cells, including increased expression of inflammatory cytokines and matrix degrading enzymes by signaling through TLRs [9-11]. However, it is unclear if such DAMPs are secreted from a loaded IVD. The first goal of this study is to investigate how loading influences the secretome of IVD motion segments using unbiased proteomics analysis.

The second goal of this study is to evaluate the potential of using IVD secretome, or CLM, to prime MSCs as a form of cell therapy. One primary function of MSCs in tissue repair is their anti-inflammatory abilities in modulating disease microenvironments. Prior studies have shown that priming human MSCs with IFNγ or poly I:C-leads to pro- or anti-inflammatory effects, respectively [136]. Studies have also emphasized the importance of the MSC secretome and the benefits of immunomodulation from MSC conditioned medium (CM) [96, 137, 138], where primed MSC secretome led to immunomodulatory effects on IL-1β-stimulated chondrocytes [139]. However, few studies have examined how a tissue's secretome, such as the IVD, can influence MSC phenotype and immunomodulation. One study in the literature analyzed CM derived from healthy, traumatic, and degenerated human IVDs and used the IVD secretome to analyze its effect on MSC secretion, proliferation, viability, and metabolic activity [138]. The IVD

secretome exhibited distinct profiles among different tissue sources, and MSCs exhibited slight differences in response to sources of conditioned media [138]. Thus, the second goal of this study is to investigate how the secretome of IVD motion segments exposed to different loading profiles can affect MSC immunomodulatory responses.

This study's third and fourth goal revolves around assessing the functional aspects of primed MSCs for their eventual use as cell therapy. The ISCT suggests guidelines for the assessment of regulatory properties of human MSCs; thus, we will implement them in this rat MSC model for good practice. It is recommended that a functional analysis of cells be conducted to provide mechanistic insights on the inter-study variance in the clinical response among patients. The IDO response should also be interrogated as part of an *in vitro* licensing assay [203]. This chapter will follow these guidelines.

MSCs are likely to be functional if they have immunosuppressive abilities and can protect against ECM degradation. Our lab has also injected naïve MSCs in punctured caudal disc segments and evaluated the impact of varying the therapeutic window on the efficacy and fate of an MSC injection *in vivo* via either 3-, 14-, or 30- days post-injury injection. It was observed that an MSC injection 3 days post-injury was crucial in maintaining MSC signal intensity and improving GAG content in injured discs [204]. However, now our goal was to evaluate if primed MSCs can be immunomodulatory and protect ECM content in a manner greater than naïve MSCs alone.

MSCs are likely to be functional if they have immunosuppressive abilities and can protect against ECM degradation. Hence, there are 4 hypotheses for this study design. **Study 1:** Hypothesis 3.1) IVD motion segment secretome is dependent on loading profile with varying applied frequency and compression magnitude. Hypothesis 3.2) Exposure to the IVD secretome would result in an altered MSC immunomodulatory response compared to the naïve MSC response

and that distinct differences exist in the MSC response to the IVD secretome that is dependent on magnitude and frequency of the loading profile. **Study 2:** Hypothesis 3.3) Injurious CLM-MSCs will exhibit the greatest immunosuppressive ability compared to naïve MSCs, evidenced by inhibition of T-cell proliferation. **Study 3:** Hypothesis 3.4) Injection of injurious CLM-MSCs into an *ex vivo* punctured disc will lead to improved immunosuppression and regeneration than punctured discs.

This chapter builds onto the findings of the previously described methods and findings in Chapter 3 (puncture injury) and Chapter 4 (loading) using a novel *ex vivo* whole organ loading IVD model system similar to the ones mentioned in the literature [194–196], which allow for microenvironmental parameters to be independently controlled, prior to clinical translation.

5.1.1 Study design

This overarching study looks at the potential of CLM as a therapy alone, the use of CLM with cell therapy, and the efficacy of primed MSCs in an *ex vivo* puncture model similar to the one discussed in Chapter 3. Study 1 investigates the secretome of CLM and its ability to alter CLM-MSCs' immunosuppressive and regenerative abilities (**Fig. 5.1A**). Study 2 tests the functional aspect of CLM-MSCs by conducting a standardized T-cell proliferation assay (**Fig. 5.1B**). Study 3 tests the functional aspect of CLM-MSCs in an *ex vivo* puncture model to assess immunomodulation and regeneration (**Fig. 5.1C**).

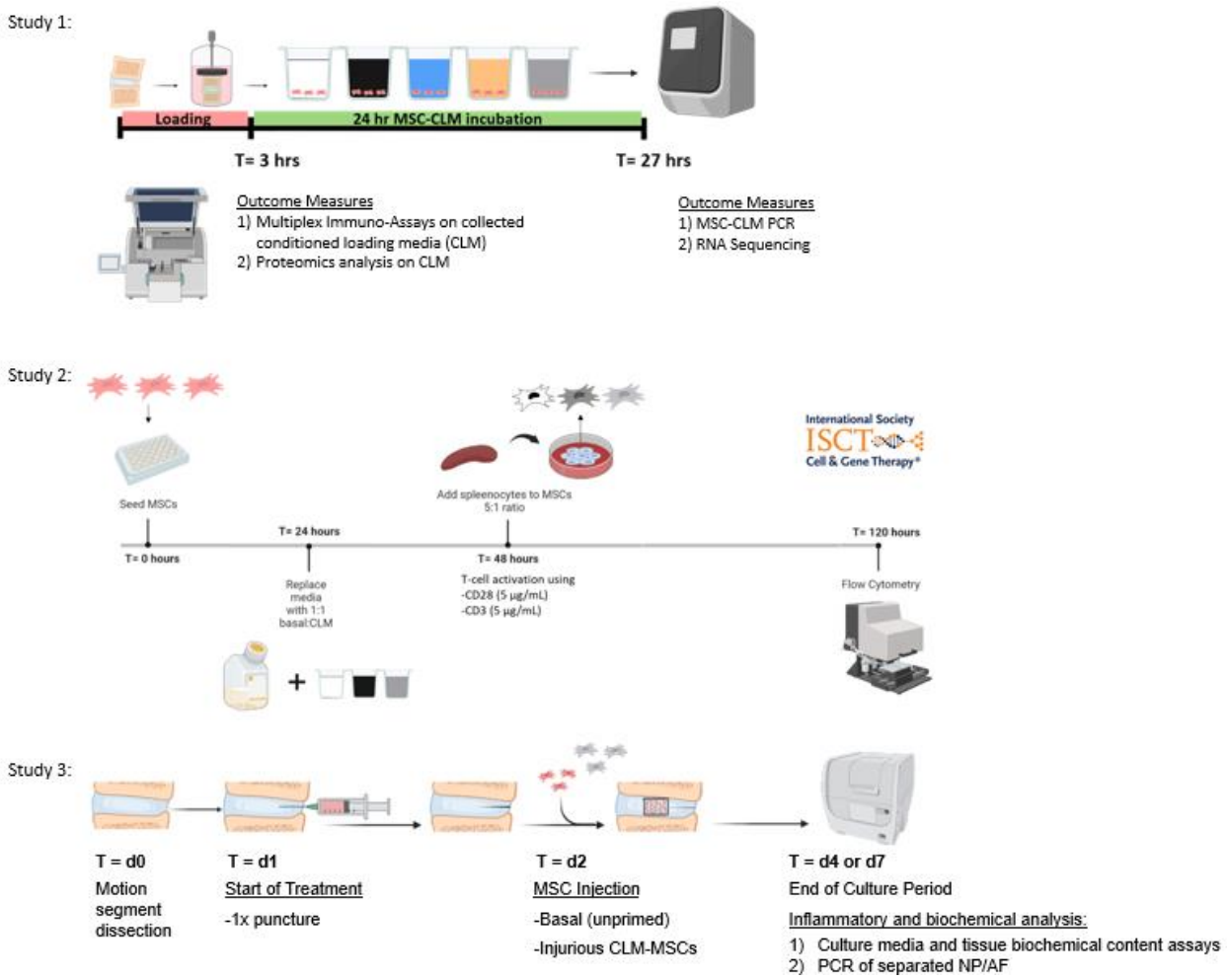

Figure 5.1: Experimental plan of Chapter 5.

Experimental design of studies **A)** Study 1 investigates the secretome of CLM and it can alter CLM-MSCs' immunosuppressive and regenerative abilities. **B)** Study 2 tests the functional aspect of CLM-MSCs by conducting a standardized T-cell proliferation assay. **C)** Study 3 tests the functional aspect of CLM-MSCs in an *ex vivo* puncture model to assess immunomodulation and regeneration. Created with Biorender.com

5.2 Material and Methods

5.2.1 IVD loading to generate CLM

48 caudal IVD motion segments were dissected from the caudal (Co10 to Co14) region of 12 male, mature Sprague-Dawley rats (IACUC-approved). IVD motion segments were submerged in phenol-free chemically defined media post-overnight equilibration and loaded for 3 hours using a mechanical loader to generate CLM. A tare compressive strain of ~20% of segment height was applied to the static group to retain contact between the loading platen and sample to eliminate liftoff. One important note is that from this point on, the high-dynamic group previously coined in Chapter 4 will be renamed as injurious in Chapter 5 and hereafter.

The physiologic and injurious groups were loaded with a 20% static strain plus an additional dynamic strain (physiologic: 1.1% dynamic strain applied at 0.125 Hz, injurious: 8% dynamic strain applied at 3 Hz). Unloaded (UL) segments were cultured as free-swelling controls. Average height changes of discs were confirmed using previously described methods in Section 4.2.4. The protein content of CLM of discs was measured using a standard Bradford protein assay (Bio-Rad). A dedicated analysis (using 6 male Sprague-Dawley rats) was also conducted on CLM from unloaded and injuriously loaded discs to characterize HMGB1 release using an ELISA (Tecan).

5.2.2 Multiplex Immuno-Assays of CLM

Cytokine release in CLM was measured using a custom-defined multi-plex immune assay using analytes from the Biolegend Legendplex Rat Th Cytokine Panel V02 measuring IL-6, TNFα, IFNγ, CXCL1, GM-CSF, IL-17A, IL-1β, IL-10, and MCP-1. Additionally, nonactivated IDO levels were measured using a colorimetric assay established in the literature [145, 205-207].

5.2.3 Proteomics profile of CLM

Protein was extracted using trichloroacetic acid and washed with acetone to form protein pellets [208]. Samples were then submitted to the Columbia University Proteomics and Macromolecular Crystallography Shared Resource. Pellets were denatured in 8 M urea and 0.1 M ammonium bicarbonate, followed by disulfide bond reduction using 5 mM DTT (56°C, 30 minutes) and alkylation with 10 mM iodoacetamide (RT, 30 minutes in the dark). After quenching, samples were diluted, digested overnight at 37°C, and halted with 1% TFA. LC-MS/MS analysis utilized a Thermo Scientific™ UltiMate™ 3000 RSLCnano system linked to an Orbitrap Fusion™ Tribrid™ mass spectrometer. MaxQuant was employed for label-free quantification (LFQ) and database searches against the human proteome.

5.2.4 Transcriptomic profile of CLM-primed MSCs

MSCs were isolated from 4 male Sprague-Dawley rats' bone marrow and expanded in culture. P3-P5 MSCs (60,0000 per well, N=6 per group) were cultured in 1:1 ratio of IVD CLM (CM: phenol-free DMEM without L-glutamine, 100 µg/mL sodium pyruvate, 50 µg/mL L-proline, 1% AA, 1% ITS Premix) and naïve MSC media (phenol free DMEM+10% FBS, 1% AA, 4mM GlutaMax). A naïve MSC group was also used as a control. After 24 hours, CLM-MSC media was collected for NO analysis. RNA was also isolated from the MSCs. Total RNA was retrieved using 2-Mercaptoethanol and RLT buffer, followed by ethanol precipitation using the RNeasy Mini Kit

(Qiagen). RNA quality and integrity were assessed via microspectrophotometry (NanoDrop) and microelectrophoresis (Columbia Molecular Pathology Core). High-purity samples (OD260/280>1.9, RNA integrity number>9.0) were submitted for RNA sequencing (Columbia Bioinformatics Core) (N=4 for each CLM run #1-4).

PCR was conducted on CLM-MSCs (only from MSCs treated with CLM from one of the donors) for gene expression analysis of anti-inflammatory mediators (*Ido1*, *Tgfb1*, *Arg1*, *Il10)*, a chemokine associated with anti-inflammatory responses (*Rantes)*, and pro-inflammatory mediators *(Nos2*, *Il1b*, *Il6*, *Tnfa*, and *Ifng)*. RNA was converted to cDNA using the iScript cDNA Synthesis Kit (Bio-Rad) and diluted to a 1 ng/µL concentration for PCR. Gene specific master mixes were prepared using designed primers at a 400 nM concentration (**Table 5.1**) and iTaq Universal SYBR Green Supermix (Bio-Rad, Philadelphia, PA). RT-qPCR was run on a QuantStudio™ 6 Flex Real-Time PCR System (Applied Biosystems™, Waltham, MA).

Table 5.1: Primers used for CLM-MSC PCR analysis

Gene	Forward Sequence	Reverse Sequence
Gapdh	GCA AGG ATA CTG AGA GCA AGA G	GGA TGG AAT TGT GAG GGA GAT G
Rantes	CCT GTC ATT GCT TGC TCT AGT C	GCC ATA GGA GAG GAC ACA GTT A
Il6	GAA GTT AGA GTC ACA GAA GGA GTG	GTT TGC CGA GTA GAC CTC ATA G
Tnfa	CCC AAT CTG TGT CCT TCT AAC T	CAG CGT CTC GTG TGT TTC T
Ifng	GTG AAC AAC CCA CAG ATC CA	GAA TCA GCA CCG ACT CCT TT
Ido1	GGA ACT TCC TCT CCT CCT TAG A	AGG CCA TTC ACA CAC TCA TTA T
Tgfb1	CTG AAC CAA GGA GAC GGA ATA C	GTT TGG GAC TGA TCC CAT TGA

5.2.5 T-cell proliferation assay on CLM-MSCs

For the T-cell proliferation assay [209], 60,000 MSCs were plated in 24-well plates and allowed to attach overnight. Cells were then stimulated in a 1:1 ratio of IVD CLM (CM) : naïve

MSC media, described in Section 5.2.4, with either unloaded or injurious CLM. A naïve MSC group (no conditioned media) was also used as a control.

After 24 hours, T-cells were collected from 1 freshly collected spleen from a Sprague Dawley rat (repeated for each CLM donor). The spleen was removed from the rat and mashed between two glass slides in a 1x ice-cold PBS suspension. The suspension was strained with a 100 µm strainer and pelleted by spinning at 450G for 5 minutes. Spleen cells were resuspended in red blood cell (RBC) lysis buffer 1:10 in UltraPure water and incubated at room temperature for 5 minutes. Cells were then pelleted again by spinning at 450G for 5 minutes and resuspended in αMEM + 10% FBS, 1% AA. Cells were dyed with 5 µM CFSE Cell Division Tracker Kit (BioLegend) for 20 minutes to monitor the proliferation of the T-cells in culture with MSCs. Spleen cells were strained throughout the process using a 100 µm strainer to avoid clumps.

Spleen cells were then added to the primed CLM-MSCs at a ratio of 1:5 (300,000 spleen cells/well). T-cell growth was stimulated by adding 5 µg/mL CD3 and 5 µg/mL CD28 antibodies to the media in culture. Cultures were allowed to proliferate for 72 hours before the suspended spleen cells were removed and stained for CD4, a T-cell marker, and dead cells with propidium iodide (PI) antibodies. Flow cytometry was performed on a Novocyte Quanteon by gating spleen cells for live (negative for PI) and T-cells (positive for CD4) and observing the proliferation curves and the Division Index measure reported by the Quanteon software.

5.2.6 Injection of injuriously primed CLM-MSCs in a puncture disc model

48 caudal IVD motion segments were dissected from the caudal (Co5 to Co14) region of 4 male, mature Sprague-Dawley rats (IACUC-approved). Motion segments were then cultured in chemically-defined media (CM: phenol-free DMEM without L-glutamine, 100 µg/mL sodium pyruvate, 50 µg/mL L-proline, 1% AA, 1% ITS Premix, and a 4 mM concentration of GlutaMax

for 24 hours [167]. After the 1-day equilibration period, samples were allocated into 1 of 4 groups: control (CM alone), puncture, puncture with naïve MSCs, or puncture with injurious CLM-MSCs. Motion segments were punctured using a 20-gauge needle inserted 4 mm into the IVD and held in place for 15 seconds before the culture duration in CM. After another 1-day equilibration period, naïve or injurious CLM-MSCs (10,000 cells in a 2 µL volume) were injected into the designated motion segments using a Hamilton 33-gauge needle along with a 27-gauge needle as a guide (where the 4 mm mark was noted via a needle stopper). Samples from all groups were then incubated for 4 to 7 days in CM for analysis post-cell therapy.

5.2.7 NO and IDO assays on ex vivo punctured discs injected with CLM-MSCs

Greiss Reagent System Assay was used to measure NO levels throughout the 4–7-day culture period of *ex vivo* punctured discs injected with CLM-MSCs. Additionally, nonactivated IDO levels were measured using the colorimetric assay established in the literature [145, 205-207].

5.2.8 PCR of ex vivo punctured discs injected with CLM-MSCs

NP and AF compartments of the IVD motion segment were dissected post-culture and dipped in RNAlater prior to -80°C storage. For homogenization, samples were transferred on ice to Trizol in round bottom tubes and then pulverized using a stick homogenizer (IKA). Total RNA was retrieved using a high salt solution with isopropanol precipitation and the RNeasy Mini Kit (Qiagen). RNA quality was assessed via methods in microspectrophotometry (NanoDrop OD260/280>1.6), and thus, high-quality samples were used in this analysis. RNA was converted to cDNA using the iScript cDNA Synthesis Kit (Bio-Rad) and diluted to a 1 ng/µL concentration for PCR. Gene specific master mixes were prepared using designed primers at a 400 nM concentration (**Table 5.2**) and iTaq Universal SYBR Green Supermix (Bio-Rad, Philadelphia,

PA). RT-qPCR was run on a QuantStudio™ 6 Flex Real-Time PCR System (Applied Biosystems™, Waltham, MA).

Table 5.2: Primers used for *ex vivo* punctured discs injected with CLM-MSC PCR analysis

Gene	Forward Sequence	Reverse Sequence
Gapdh	GCA AGG ATA CTG AGA GCA AGA G	GGA TGG AAT TGT GAG GGA GAT G
Ido1	GGA ACT TCC TCT CCT CCT TAG A	AGG CCA TTC ACA CAC TCA TTA T
Nos2	AAC CCA AGG TCT ACG TTC AAG	GCA CAT CGC CAC AAA CAT AAA
Il6	GAA GTT AGA GTC ACA GAA GGA GTG	GTT TGC CGA GTA GAC CTC ATA G
Il13ra1	CCT AGT GGA GCA GGA AAT ACT C	GGC TCA CAG GGA AGT TGT AA
Ill3	AAC AGC AGC ATG GTA TGG AG	TGG CAT TGC AAC TGG AGA T
Cxcl1	GCA CCC AAA CCG AAG TCA TA	GGG ACA CCC TTT AGC ATC TTT
Il4r	CTC CGT GAG CTG TCT GAT TT	CGT AGA AGT GCG GAT GTA GTC
Il4	GTC ACT GAC TGT AGA GAG CTA TTG	CTG TCG TTA CAT CCG TGG ATA C

5.2.9 Statistical analysis

One-way ANOVAs were conducted for average height loss, CLM protein content, and cytokine release of loaded motion segments. When warranted by the result of the normality test, a non-parametric Kruskal-Wallis ANOVA was performed using Dunn's multiple comparisons test for group comparisons. For HMGB1 release from motion segments, a Mann-Whitney test was conducted since data did not follow a normal distribution. Statistical significance was set at $p<0.05$ where $\alpha=0.05$ using GraphPad Prism 9.2.0.

For proteomics, results were analyzed using log2 fold change or "difference relative to UL" of LFQ intensities with the Perseus software. Statistical significance was determined using False

Discovery Rate (FDR) set at 0.05 for Perseus. Significant proteins and their "difference relative to UL" were input into Reactome for pathway analysis.

RNAseq analysis of CLM-MSCs compared to naïve MSCs was conducted where differential expression of genes was computed using DESeq2. Pathway analysis was performed using Reactome on data sets by inputting significant genes and their fold change, demonstrating individual gene up- or downregulation with $p<0.05$ and FDR entities <0.07 [210].

For PCR analysis of CLM-MSCs (using 6.17.22 CLM), a Kruskal-Wallis test with a Dunn's post-hoc test was used to analyze the MSC-CLM NO release. One-way ANOVAs were performed with Holm-Sidak post hoc tests to analyze the effect of CLM on MSC gene expression. To compare CLM-MSCs vs naïve MSCs, student t-tests were used. Statistical significance was set at $p<0.05$ where $\alpha=0.05$ using GraphPad Prism 9.2.0.

Additionally, for NO, IDO, and gene expression results, statistical significance was set at $p<0.05$ where $\alpha=0.05$ using GraphPad Prism 10.1.0 using one-way or two-way ANOVAs depending on analysis of whole motion segment or separated NP vs AF data.

5.3 Results

5.3.1 Injurious loading led to the greatest release of cytokines

The average disc height in static (-17.3%, N=8), physiologic (-8.9%, N=6), and injurious loading (-61.3%, N=5) groups was significantly different from the UL condition (8.5%, N=11) and from each other ($p<0.01$) (**Fig. 5.2B**). Injurious CLM (N=3) led to the greatest release of protein content into the media compared to physiologic ($p=0.0004$, N=4), static ($p=0.0013$, N=4), and UL CLM ($p=0.0002$, N=4) (**Fig. 5.2C**). HMGB1 release was greatest in injurious CLM (20.3 ng, N=5), although it was not significantly upregulated ($p=0.90$) compared to UL CLM (1.5 ng, N=4) (**Fig. 5.2D**). IDO activity in CLM was the greatest in physiologic CLM compared to unloaded ($p=0.015$, N=4) (**Fig. 5.2E**). Notably, 25% of cytokine/protein release into the media is assumed to come from the IVD alone. In comparison, the remaining 75% comes from the bone, corresponding to individual IVD and bone tissue wet weights (data not shown).

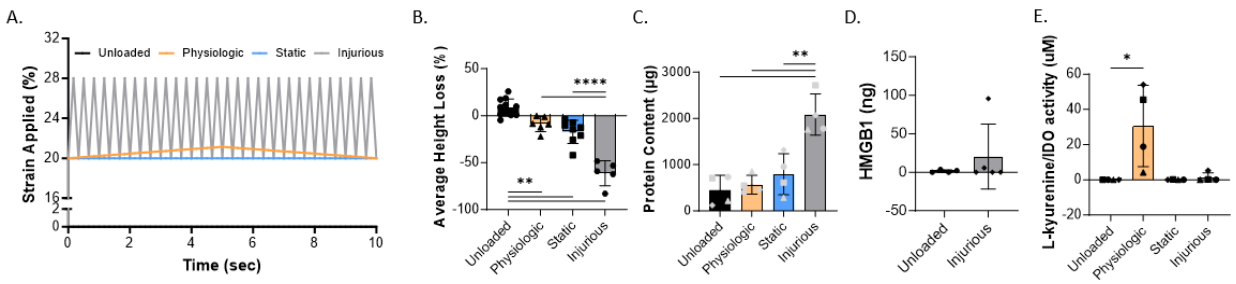

Figure 5.2: Loading of IVD motion segments leads to decreased disc height and increased protein content into CLM.

Loading of IVD motion segments leads to decreased disc height and increased protein content into CLM. **A)** Loading profiles **B)** Average IVD height loss in loaded motion segments **C)** Protein content released in CLM **D)** HMGB1 release in injuriously loaded discs **E)** IDO activity in CLM

NO release into injurious CLM (p=0.034) was significantly higher than unloaded CLM (**Fig. 5.3A**). IL-6 release during injurious loading was also significantly higher compared to UL (p=0.046), physiologic (p=0.046), and static (p=0.038) CLM (**Fig. 5.3B**). TNFα release during injurious loading was also significantly higher compared to UL (p<0.0001), physiologic (p<0.0001), and static (p<0.0001) CLM (**Fig. 5.3C**). IFNγ release during injurious loading was also significantly higher compared to UL (p=0.020) and physiologic (p=0.020) CLM (**Fig. 5.3D**). CXCL1 release during injurious loading was also significantly higher compared to UL (p=0.017), physiologic (p=0.0069), and static (p=0.013) CLM (**Fig. 5.3E**).

Interestingly, GM-CSF release from unloaded discs was significantly higher compared to physiologic (p=0.0014), static (p=0.037), and injurious (p=0.012) CLM (**Fig. 5.3F**). The same trend follows for IL-17A and IL-1β where IL-17A release from unloaded discs was higher compared to physiologic (p=0.016) CLM (**Fig. 5.3G**), and IL-1β release from unloaded discs was higher than physiologic (p=0.011) CLM (**Fig. 5.3H**). MCP-1 release from injurious CLM (p=0.020) was significantly higher compared to physiologic CLM (**Fig. 5.3I**). However, there was no difference in IL-10 release among CLM (**Fig. 5.3J**).

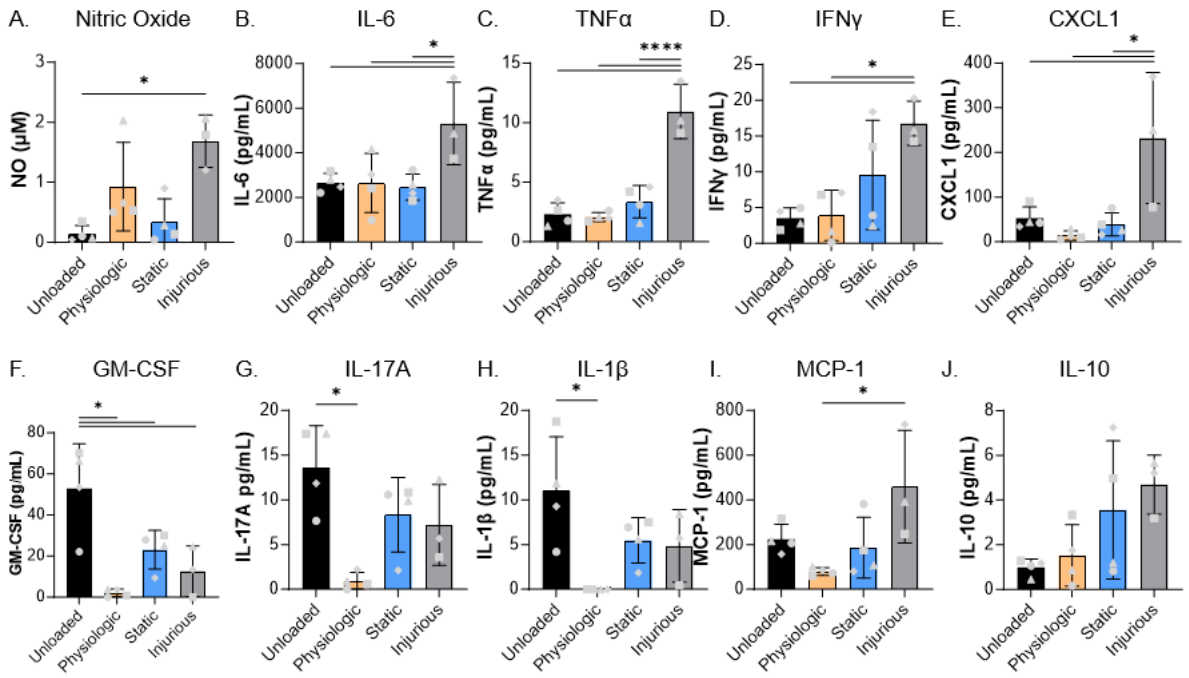

Figure 5.3: Cytokine release in CLM.

Cytokine release in CLM **A)** NO, **B)** IL-6, **C)** TNFα, **D)** IFNγ, **E)** CXCL1, **F)** GM-CSF, **G)** IL-17A, **H)** IL-1β, **I)** MCP-1, and **J)** IL-10 in CLM of unloaded, static, physiologic, and injurious loading conditions (N=3-4). ****$p< 0.0001$ and *$p< 0.05$

5.3.2 Proteomics analysis exhibited the greatest protein presence in injurious CLM

Proteomics analysis yielded 1, 0, and 37 proteins that were differentially expressed in physiologic (**Fig. 5.4 i**), static (**Fig. 5.4 ii.**), injurious CLM (**Fig. 5.4 iii.**), respectively, compared to UL CLM. The four most significant pathways for the secretome of injuriously loaded discs were related to the immune system (12 proteins), innate immune system (8 proteins), neutrophil degranulation (6 proteins), and RHO GTPase Effectors (4 proteins). Differentially expressed proteins involved in innate immune system signaling include upregulated major vault protein (MVP), Actin-related protein 3 (ACTR3), galectin-3 (LGALS3), fatty acid-binding protein-5 (FABP5), phosphoglycerate mutase (PGAM1), and V-type proton ATPase subunit B (ATP6V1B2) and downregulated glycogenin-1 (GYG1) and Neutrophil degranulation include the downregulation of Lysozyme C-1 (LYZ1) along with 4 other proteins involved in the general immune system (upregulated dynactin subunit 2 (DCTN2), annexin A1 (ANXA1), endoplasmic reticulum aminopeptidase 1 (ERAP1), and downregulated ubiquitin-conjugating enzyme E2 variant-2 (UBE2V2)). Six proteins were explicitly involved in neutrophil degranulation: GYG1, LYZ1, MVP, LGALS3, FABP5, and PGAM1 in the secretome of injurious CLM compared to UL CLM. Additionally, it appears that four proteins: (Tyrosine 3-Monooxygenase/Tryptophan 5-Monooxygenase Activation Protein Theta) YHWAQ, Protein phosphatase 1 regulatory inhibitor subunit 14A (PPP1R14A), ACTR3, and profilin-2 (PFN2) are RHO GTPase Effectors and are related to actomyosin contractility. Levels of ECM proteins, such as CHAD, were upregulated, while nidogen-1 (NID1) and EFEMP1 were downregulated in injurious CLM compared to UL CLM (**Fig. 5.4B**). Additionally, physiologic CLM led to the significant downregulation of chemokine C-X-C motif ligand 1 (CXCL1) compared to unloaded CLM.

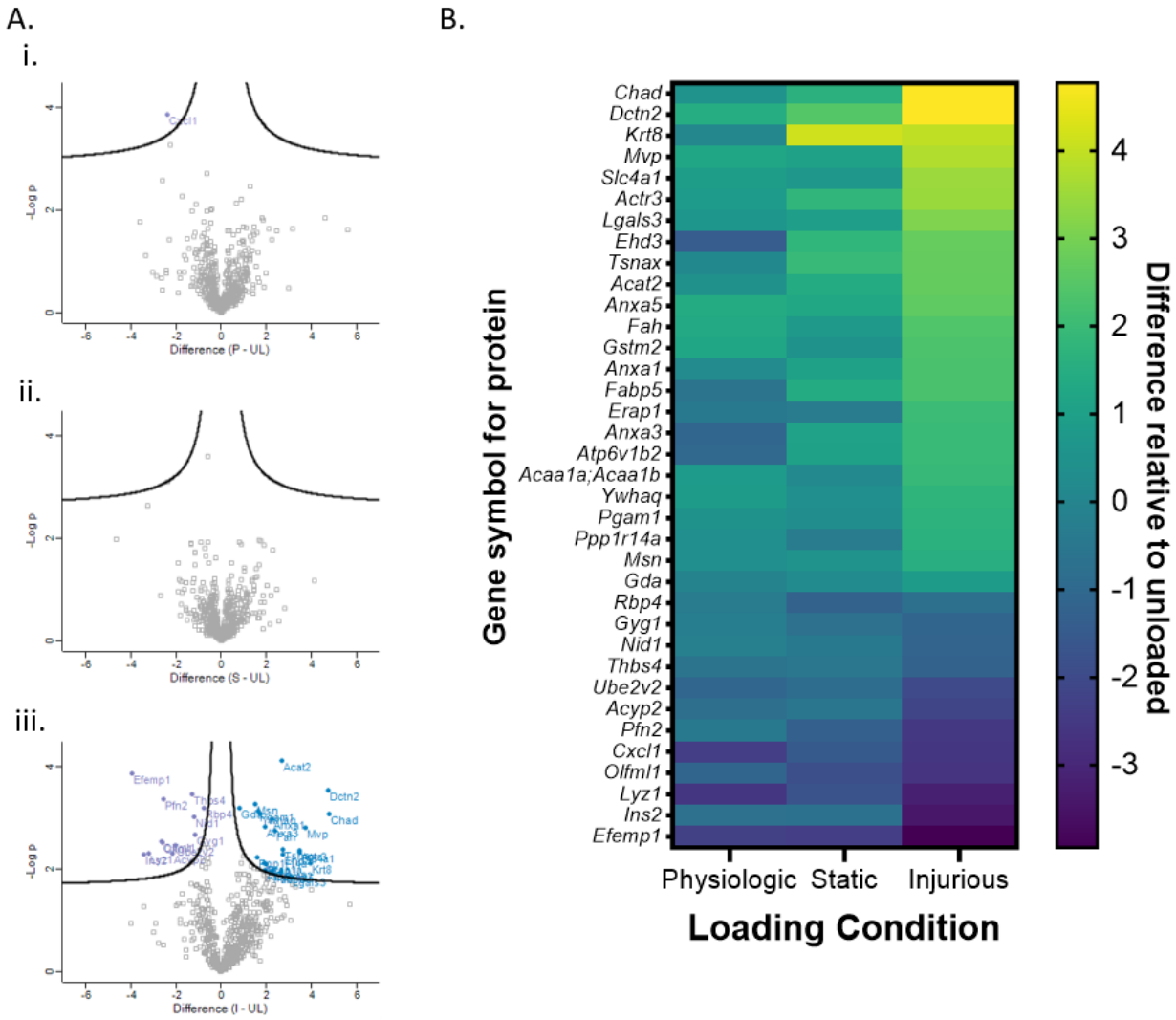

Figure 5.4: Volcano plots and heat map of significant proteins released.

Proteomic analysis of CLM showing **A)** volcano plots representing the difference in i. physiologic – UL CLM ii. Static – UL CLM, and iii. injurious – UL CLM and **B)** heatmap representing genes of proteins which displayed significant fold changes in the secretome of injuriously loaded IVD motion segments.

5.3.3 Injurious CLM led to regulation of various pathways implicated in proteomics

RHO GTPase Effectors, Neutrophil degranulation, and G2M DNA damage checkpoint were downregulated in injurious CLM compared to unloaded CLM (total difference: 0.56, 0.54, 0.48) (Entities FDR: 0.035, 0.035, 0.041, respectively) (**Fig. 5.5A**).

However, the following pathways were upregulated in injurious CLM compared to unloaded CLM: RUNX2 regulates genes involved in differentiation of myeloid cells (difference: 3.09, entities FDR: 0.035), RUNX1 regulates transcription of genes involved in differentiation of myeloid cells (difference: 4.83, Entities FDR: 0.035), Immune System (difference: 1.16, entities FDR: 0.035), Regulation of localization of FOXO transcription factors (difference: 1.73, Entities FDR: 0.035), Chk1/Chk2(Cds1) mediated inactivation of Cyclin B:Cdk1 complex (difference: 1.73, Entities FDR: 0.035), Activation of BAD and translocation to mitochondria (difference: 1.73, Entities FDR: 0.038), RHO GTPases activate PKNs (difference: 1.68, Entities FDR: 0.041) (**Fig. 5.5A**).

Proteins implicated in RHO GTPase Effectors include the downregulation of PFN2, and the upregulation of PPP1R14A, YHWAQ, and ACTR3 (**Fig. 5.5B**). Proteins implicated in RHO GTPases activating PKNs include PPP1R14A and YHWAQ (**Fig. 5.5C**). Proteins implicated in Neutrophil degranulation include the downregulation of LYZ1, CXCL1, and GYG1, and the upregulation of PGAM1, FABP5, LGALS3, and MVP (**Fig. 5.5D**). Differentially expressed proteins involved in the immune system signaling included downregulated LYZ1, CXCL1, UBE2V2, and GYG1, and upregulated moesin (MSN), PGAM1, ATP6V1B2, ERAP1, FABP5, ANXA1, LGALS3, ACTR3, MVP, and DCTN2 **(Fig. 5.5E**). Proteins implicated in G2/M DNA damage checkpoint include downregulated UBE2V2 and upregulated YWHAQ (**Fig. 5.5F**).

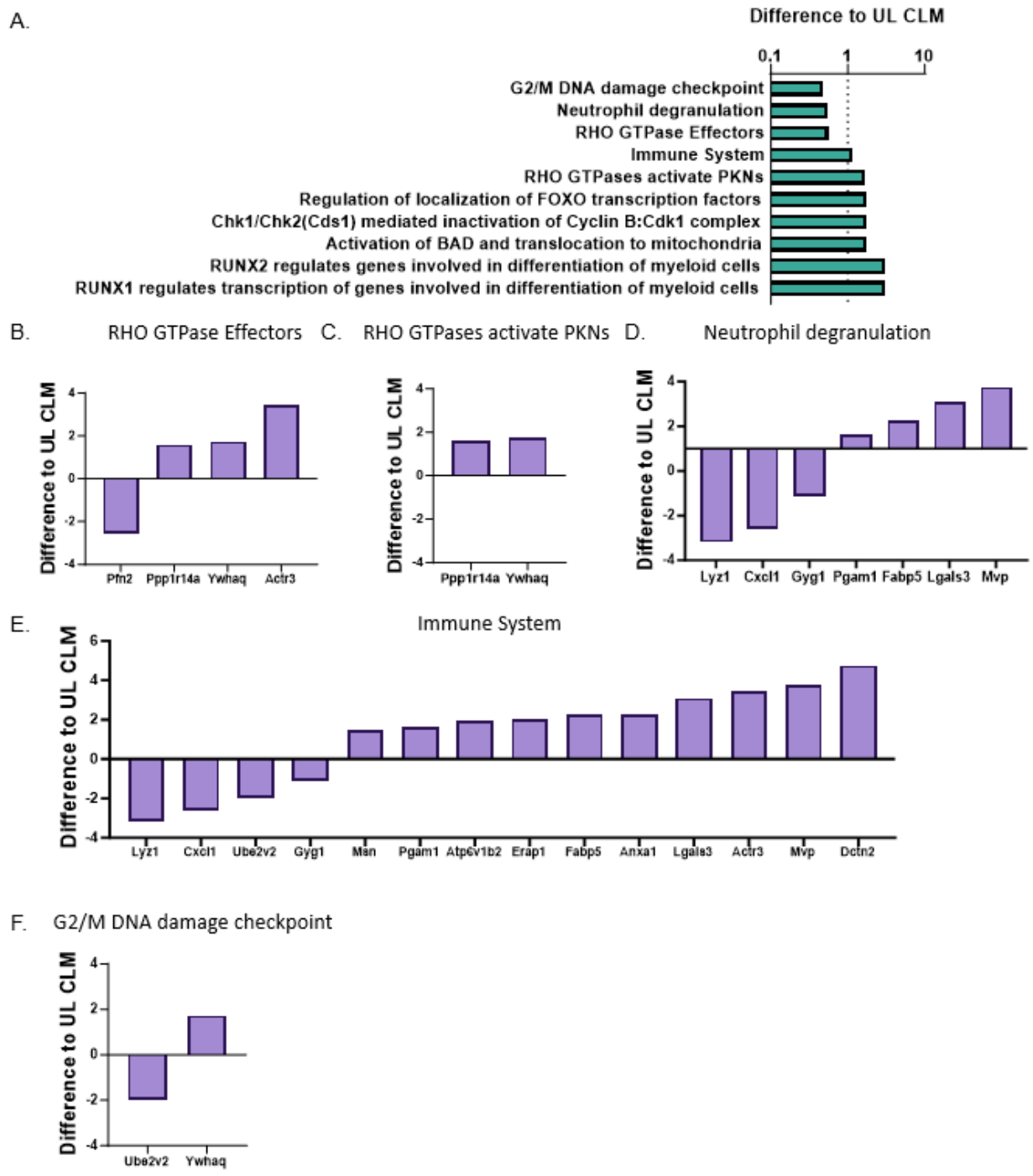

Figure 5.5: Pathways and genes of proteins implicated in injurious CLM.

A) Pathways and **B-H)** genes of proteins implicated in injurious CLM. **A)** Overall pathway representing the difference in injurious – UL CLM as well as genes implicated in the following pathways: **B)** RHO GTPase Effectors, **C)** RHO GTPases activate PKNs, **D)** Neutrophil degranulation, **E)** Immune System, and **F)** G2/M DNA damage checkpoint

5.3.4 Priming of injurious CLM-MSCs exhibited the greatest immunomodulatory and regenerative potential

The volcano plot of injurious CLM-MSCs versus naïve MSCs shows significance for a few genes (**Fig. 5.6A**). The following pathways were downregulated in injurious CLM-MSCs compared to naïve MSCs: NOTCH3 Intracellular Domain Regulates Transcription (fold change: 0.22, entities FDR: 0.0035), Signaling by NOTCH3 (fold change: 0.23, entities FDR: 0.012), NOTCH4 Intracellular Domain Regulates Transcription (fold change: 0.25, entities FDR: 0.021), Signaling by NOTCH1 HD+PEST Domain Mutants in Cancer (fold change: 0.33, entities FDR: 0.012), Signaling by NOTCH1 PEST Domain Mutants in Cancer (fold change: 0.33, entities FDR: 0.012), Constitutive Signaling by NOTCH1 HD+PEST Domain Mutants (fold change: 0.33, entities FDR: 0.012), Constitutive Signaling by NOTCH1 PEST Domain Mutants (fold change: 0.33, entities FDR: 0.012), Signaling by NOTCH1 in Cancer (fold change: 0.33, entities FDR: 0.012), Elastic fiber formation (fold change: 0.41, entities FDR: 0.062), NOTCH1 Intracellular Domain Regulates Transcription (fold change: 0.45, entities FDR: 0.012), and Signaling by NOTCH1 (fold change: 0.51, entities FDR: 0.012) (**Fig. 5.6B**).

However, the following pathways were upregulated in injurious CLM-MSCs compared to naïve MSCs: Signaling by Interleukins (fold change: 3.87, entities FDR: 0.066), and Interleukin-10 Signaling (fold change: 7.93, entities FDR: 0.012) (**Fig. 5.6B**).
Genes implicated in Signaling by Interleukins include downregulated *Il18r1*, *Ptpn14*, *Dcp2*, *Ikbkg*, and *Rap1b*, along with upregulated *Ifnlr1*, *Bcl6*, *Hmox1*, *Clcf1*, *Hif1a*, *Il4r*, *Irak3*, *Ccr1*, *Il7r*, *Il13ra1*, *Sod2*, *Il1rn*, *Cxcl1*, *Il6*, *Cxcl2*, *and Csf3* (**Fig. 5.6C**). Genes implicated in Interleukin-10 Signaling include upregulated *Ccr1*, *Il1rn*, *Cxcl1*, *Il6*, *Cxcl2*, and *Csf3* (**Fig. 5.6D**). Genes implicated in Signaling by NOTCH3 include downregulated *Hes1*, *Jag1*, *Notch3*,

Hey2, *Heyl*, and *Hey1* (**Fig. 5.6E**). Genes implicated in Elastic Fiber Formation include downregulated *Loxl1*, *Loxl2*, *Fbn2*, *Tgfb3*, and *Eln* (**Fig. 5.6F**).

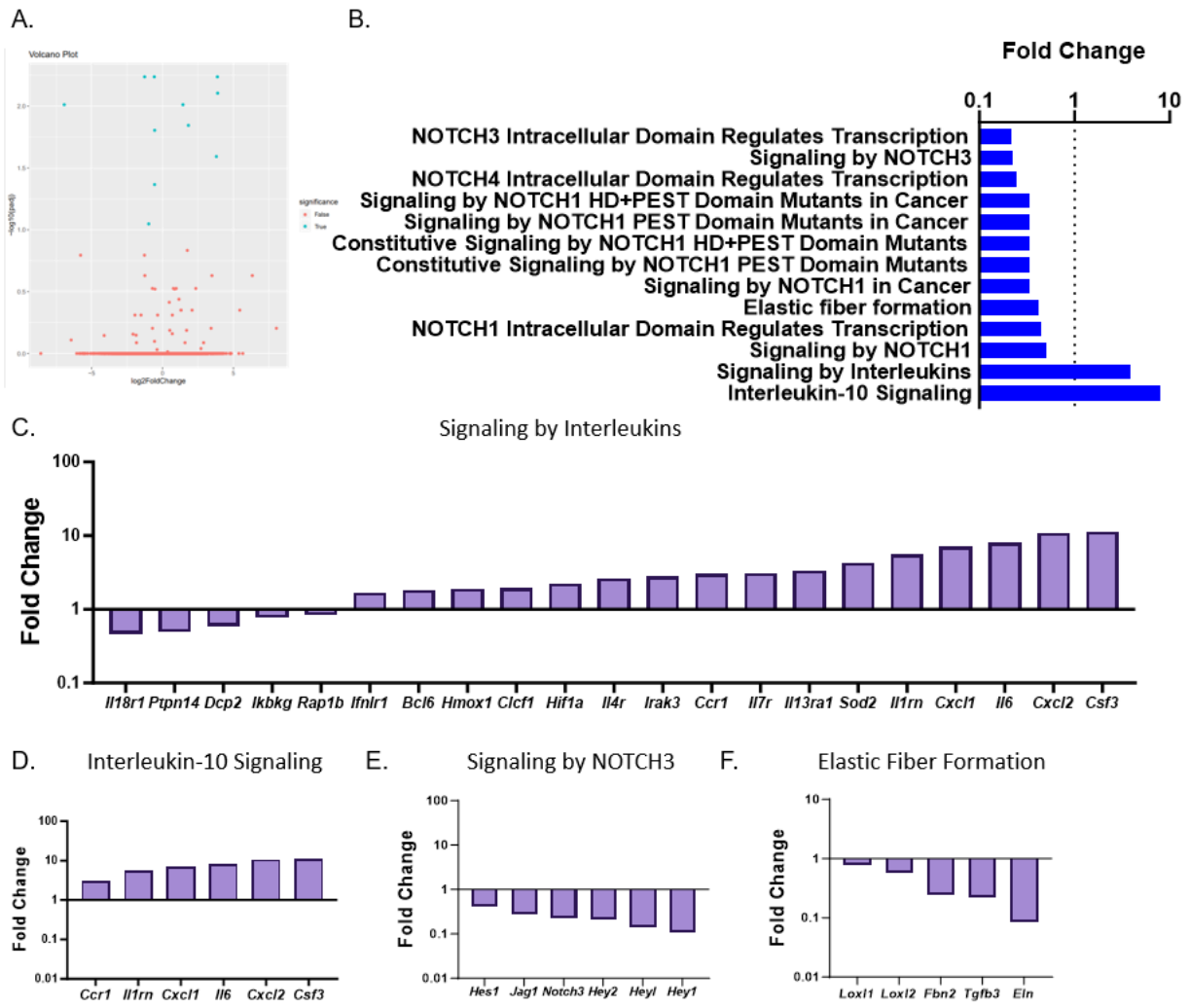

Figure 5.6: Pathways and genes implicated in injurious CLM-MSCs compared to naïve MSCs.

A) Volcano plot of injurious CLM-MSCs versus naïve MSCs. Pathways and genes implicated in priming of injurious CLM-MSCs compared to naïve MSCs. **B)** Overall pathway representing the difference in injurious CLM-MSCs compared to naïve MSCs, as well as genes implicated in the following pathways: **C)** Signaling by Interleukins, **D)** Interleukin-10 Signaling, **E)** Signaling by NOTCH3, and **F)** Elastic Fiber Formation

5.3.5 Static CLM-MSCs led to a change in immunomodulatory activity compared to naïve MSCs

The volcano plot of static CLM-MSCs versus naïve MSCs only shows one significant gene (**Fig. 5.7A**). However, when analyzing an FDR entity <0.05, the following pathways were upregulated in static CLM-MSCs compared to naïve MSCs: CD163 mediating an anti-inflammatory response (fold change: 9.66, entities FDR: 0.013), and Interleukin-10 Signaling (fold change: 4.20, entities FDR: 0.0036) (**Fig. 5.7B**). Genes implicated in Interleukin-10 Signaling include upregulated *Csf3*, *Il6*, and *Cd86* (**Fig. 5.7C**), while genes implicated in CD163 mediating an anti-inflammatory response include upregulated *Myh9*, *Il6*, and downregulated *Plk2* (**Fig. 5.7D**).

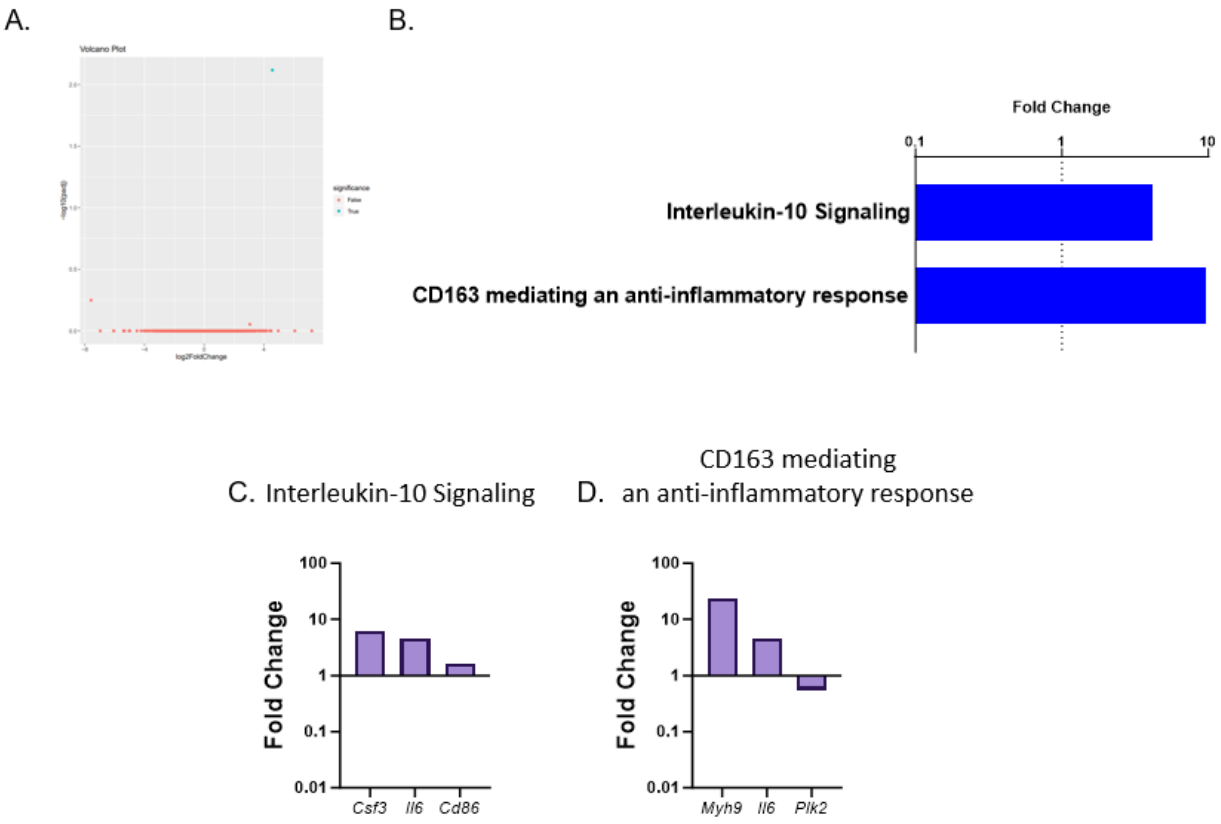

Figure 5.7: Pathways and genes implicated in static CLM-MSCs compared to naïve MSCs.

A) Volcano plot of static CLM-MSCS versus naïve MSCS. Pathways and genes implicated in priming of static CLM-MSCs compared to naïve MSCs. **B)** Overall pathway representing the difference in static CLM-MSCs and naïve MSCs, as well as genes implicated in the following pathways: **C)** Interleukin-10 Signaling, and **D)** CD163 mediating an anti-inflammatory response

5.3.6 Physiologic CLM-MSCs led to a change in an upregulation of heme signaling, although not significant, compared to naïve MSCs

The volcano plot of physiologic CLM-MSCs versus naïve MSCs shows no significant gene compared to naïve MSCs (**Fig. 5.8A**). The following pathways were upregulated in physiologic CLM-MSCs compared to naïve MSCs, albeit not significant, via entities FDR: CD163 mediating an anti-inflammatory response (fold change: 9.66, entities FDR: 0.013), and Heme signaling (fold change: 2.90, entities FDR: 0.42) (**Fig. 5.8B**). Like static CLM-MSCs, CD163 mediating an anti-inflammatory response was upregulated in physiologic CLM-MSCs compared to naïve MSCS, although not significant based on entities FDR<0.05). Genes implicated in CD163 mediating an anti-inflammatory response include upregulated *Il6*, *Myh9*, and *Adam17* (**Fig. 5.8C**), while genes implicated in Regulation of HMOX1 expression and activity include *Hmox1* (**Fig. 5.8D**). Genes implicated in Heme signaling include upregulated *Ppargc1a* and *Hmox1* (**Fig. 5.8E**).

This finding corresponds to IDO activity levels in physiologic CLM since IDO is an inducible heme-containing enzyme, and its levels are the highest in physiologic CLM, as seen in Figure 5.1.

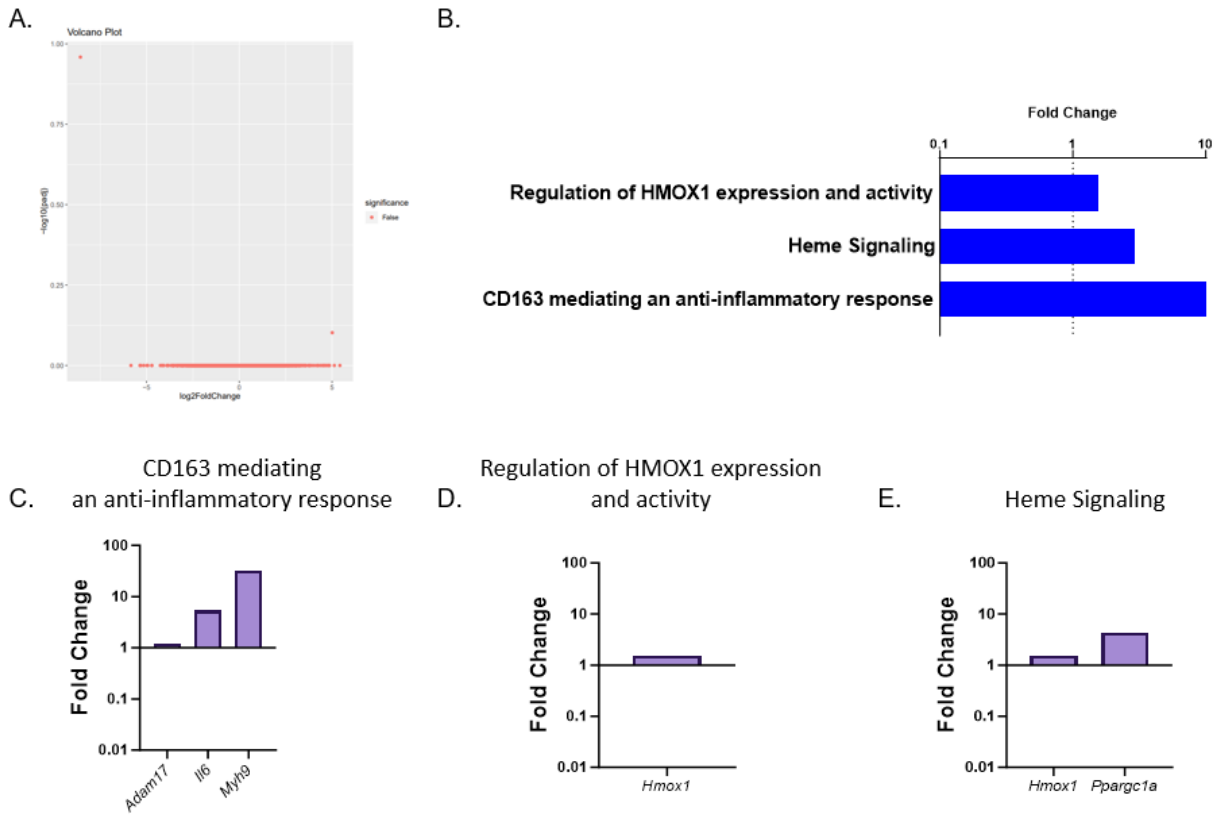

Figure 5.8: Pathways and genes implicated in physiologic CLM-MSCs compared to naïve MSCs.

A) Volcano of physiologic CLM-MSCs versus naïve MSCs. Pathways and genes implicated in priming of physiologic CLM-MSCs compared to naïve MSCs. **B)** Overall pathway representing the difference in physiologic CLM-MSCs and naïve MSCs, as well as genes implicated in the following pathways: **C)** CD163 mediating an anti-inflammatory response **D)** Regulation of HMOX1 expression, activity, and **E)** Heme signaling

5.3.7 NO and PCR of CLM-MSCs confirms immunomodulatory phenotype of injurious CLM-MSCs

NO release into the CLM by the MSCs was statistically greater for injurious loading compared to unloaded ($p<0.02$), static ($p<0.0002$), and naïve media ($p<0.0001$, **Fig. 5.9A**). NO release by MSCs in unloaded, physiologic, and injurious CLM was also statistically greater than NO release from naïve MSCs ($p<0.02$, $p<0.002$, $p<0.0001$, respectively, **Fig. 5.9A**). Exposure of MSCs to unloaded IVDs led to an upregulation of pro-inflammatory genes *Nos2*, *Il1b*, *Il6*, *Tnfa*, and downregulation of *Ifng* ($p=0.014$, $p=0.0006$, $p<0.0001$, $p=0.0026$, $p=0.043$, respectively) (**Fig. 5.9B**), yet no difference in gene expression among anti-inflammatory genes *Ido1*, *Tgfb1*, *Arg1*, and *Il10* compared to naïve MSCs (**Fig. 5.9C**). Injurious CLM-MSCs led to an increase in *Rantes* compared to static CLM ($p<0.004$) (**Fig. 5.9D**), an increase in *Il6* compared to unloaded, static, and physiologic CLM ($p<0.0001$, $p<0.0001$, $p<0.03$, respectively) (**Fig. 5.9E**), and an increase in *Ifng* ($p<0.03$) (**Fig. 5.9G),** an increase in *Ido1* compared to static and physiologic CLM ($p<0.002$, $p<0.03$, respectively) (**Fig. 5.9H**), and an increase in *Tgbf1* compared to unloaded, static, and physiologic CLM ($p<0.04$, $p<0.0002$, $p<0.004$, respectively) (**Fig. 5.9I**). Meanwhile, static CLM-MSCs led to a downregulation of *Rantes* ($p<0.05$) (**Fig. 5.9D**), *Tnfa (*$p<0.03$) (**Fig. 5.9F**), and *Tgfb1* ($p<0.04$) (**Fig. 5.9I**) compared to unloaded CLM. Physiologic CLM-MSCs resulted in a comparable immunomodulatory profile as naïve MSCs, specifically *Rantes* ($p=0.18$) (**Fig. 5.9D**), *Ido1* ($p=0.14$) (**Fig. 5.9H**), and *Ifng* ($p<0.83$) (**Fig.5.9G**), yet upregulated *Il6* ($p<0.003$) (**Fig. 5.9E**) expression and downregulated *Tnfa* ($p<0.0008$) (**Fig. 5.9F**) expression.

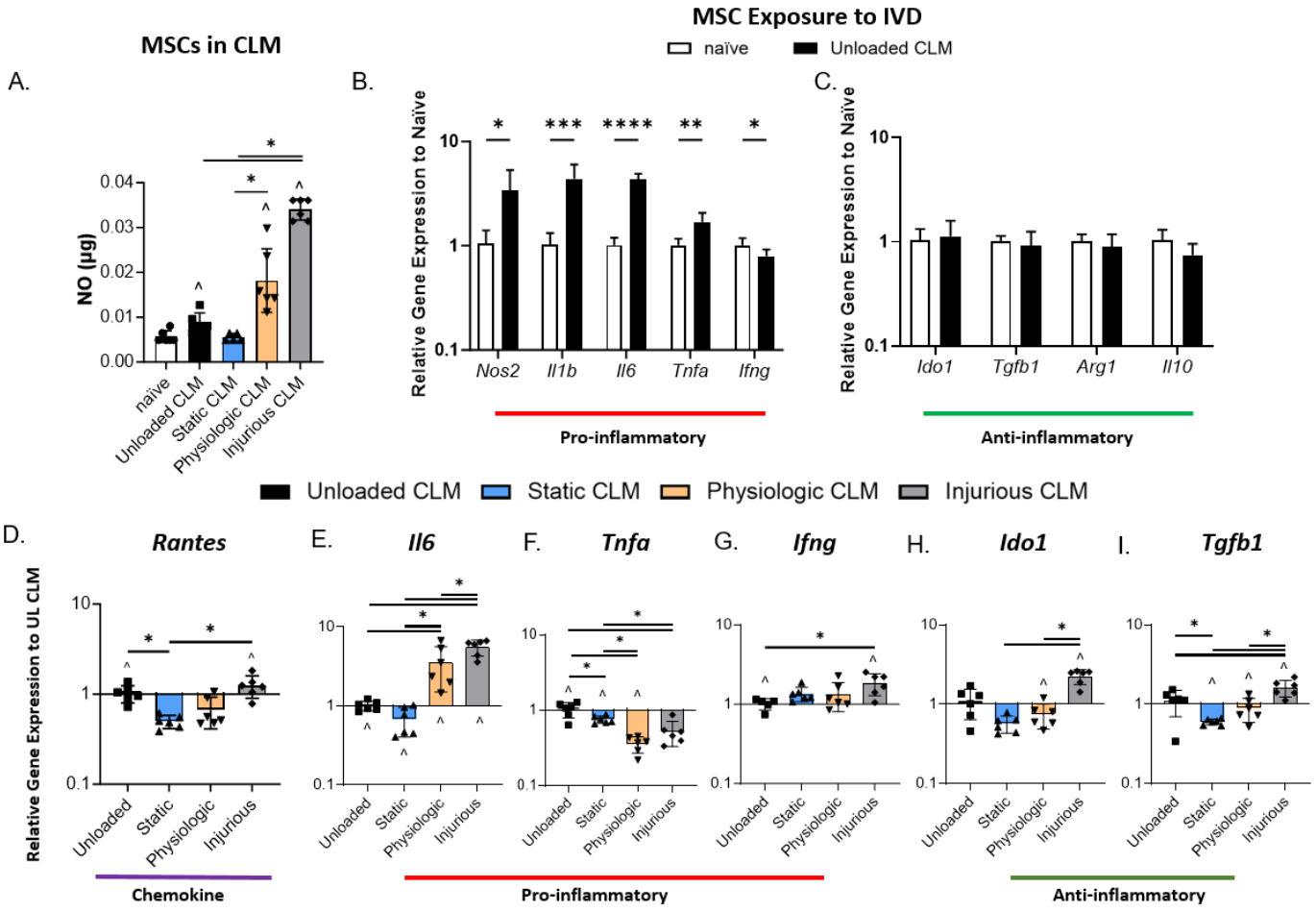

Figure 5.9: NO release into CLM-MSC media and gene expression CLM-MSCs.

A. NO release into CLM-MSC media. **B.** Proinflammatory and **C.** anti-inflammatory gene expression of MSC exposure to IVD CLM. Gene expression of chemokine **D.** *Rantes*, pro-inflammatory cytokines **E.** *Il6*, **F.** *Tnfa*, and **G.** *Ifng* as well as immunomodulatory **H.** *Ido1*, and **I.** *Tgfb1* in CLM-MSCs. (N=5-6) *p<0.05 compared to unloaded CLM; ^p<0.05 compared to naïve MSCs

5.3.8 Injurious CLM-MSCs significantly decreased T-cell proliferation compared to naïve and unloaded-CLM-MSCs

Injuriously primed CLM-MSCs inhibited T-cell proliferation significantly more than naïve MSCs. The division index (calculated as the average number of divisions of all total cells) of spleen T-cells cultured with CLM-MSCs exhibits that injurious CLM-MSCs were able to significantly decrease T-cell proliferation compared to the unloaded CLM-MSCs (p=0.0059) or naïve MSCs alone (p=0.0027) post 72-hour culture (N=3). Additionally, unloaded CLM-MSCs could inhibit T-cell proliferation more than unprimed naïve MSCs alone (p=0.0091, N=3) (**Fig. 5.10**).

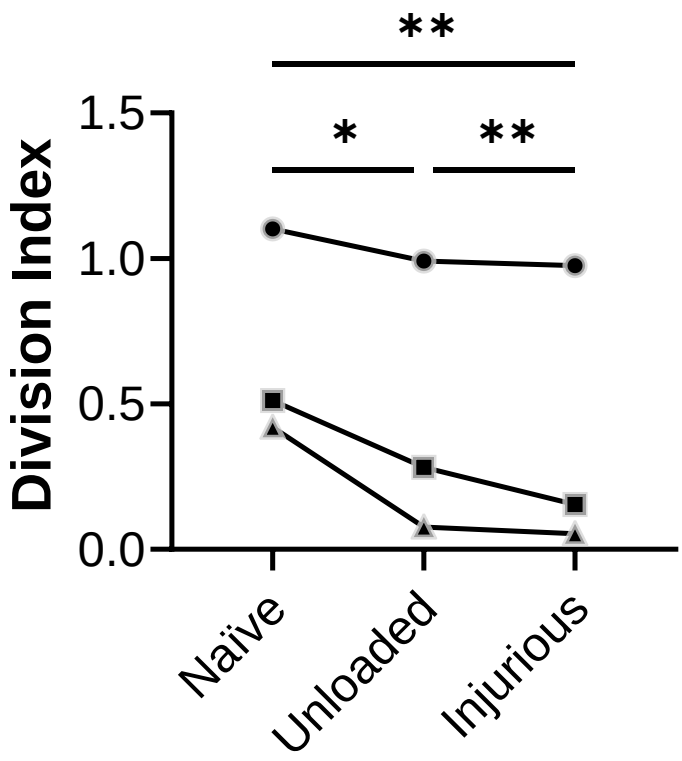

Figure 5.10: Division index of spleen T-cells cultured with CLM-MSCs.

Division index of spleen T-cells cultured with CLM-MSCs. (N=3) *p<0.05, **p<0.01 compared to naïve MSCs

5.3.9 Injurious CLM-MSCs improved immunomodulatory disc response to puncture

During short-term culture post-puncture, there was a slight but insignificant decrease in L-kynurenine/IDO activity of whole motion segments (p=0.066, N=8) (**Fig. 5.11A**). However, treatment group was a significant variable in NO release during puncture, despite no between-group differences (p=0.020, N=8) (**Fig. 5.11B**). Additionally, gene expression of the discs' separated NP and AF regions revealed an increase in *Ido1* post puncture in the NP region compared to control NP (p=0.048, N=4), with no difference observed in the AF (**Fig. 5.11C**). There was no difference in *Nos2* gene expression in both IVD regions across treatment groups (N=4) (**Fig. 5.11D**). Puncture increased NP *Il6* expression compared to control NP (p=0.013), and PCLM NP attenuated it in just 2 days post puncture (p=0.048, N=4) (**Fig. 5.11E**). *Il13ra1* expression was also increased with puncture (p=0.010) yet was significantly decreased in the NP of PM discs (p=0.030, N=4) (**Fig. 5.11F**). However, there is no difference in *Il13* gene expression across treatment groups in both IVD regions (N=3-4) (**Fig. 5.11G**). Additionally, *Cxcl1* gene expression significantly increased with PCLM in NP compared to both punctured (p=0.012) and PM NP groups (p=0.012, N=4) (**Fig. 5.11H**). NP *Cxcl1* gene expression was also significantly higher than control NP (p=0.0015, N=4) (**Fig. 5.11H**). *Il4r* expression also increased in PM NP compared to both puncture (p=0.030) and control NP (p=0.017, N=3-4) (**Fig. 5.11I**). However, PCLM NP was not significantly increased compared to punctured (p=0.39) or control NP (p=0.28, N=3-4) (**Fig. 5.11I**). *Il4* expression, nevertheless, significantly increased in PCLM NP compared to control NP (p=0.032, N=4) (**Fig. 5.11J**).

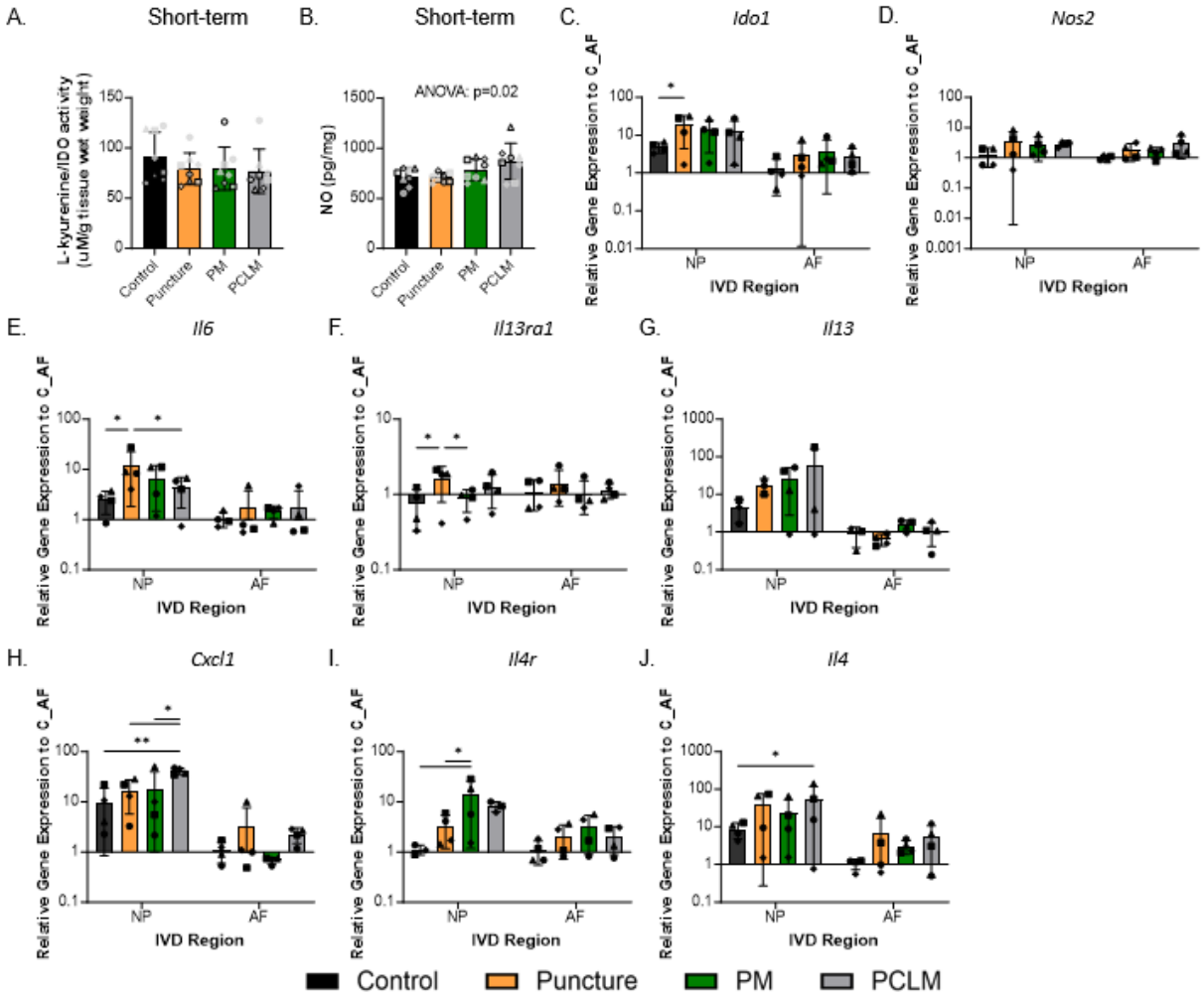

Figure 5.11: IDO, NO, and gene expression of *ex vivo* punctured discs injected with injurious CLM-MSCs and naïve MSCs.

Short-term release of **A.** IDO and **B.** NO in motion segment culture (N=8). Gene expression of **C.** *Ido1*, **D.** *Nos2*, **E.** *Il6*, **F.** *Il13ra1*, **G.** *Il13*, **H.** *Cxcl1*, **I.** *Il4r*, and **J.** *Il4* (N=3-4). **$p<0.01$, *$p<0.05$ compared to respective control IVD region

5.3.10 Injurious CLM-MSCs improved short-term AF ECM response to puncture

There was no difference in *Acan* (N=3-4), *Mmp3* (N=4), or *Adamts4* (N=3-4) gene expression across treatment groups in both IVD regions (**Fig. 5.12A-C**). *Col2a1* gene expression in the puncture group significantly decreased in the AF region compared to control AF (p=0.0088, N=3-4) (**Fig. 5.12D**). Additionally, *Col2a1* gene expression of PM (p=0.010) and PCLM (p=0.025) AF also decreased compared to control AF (N=3-4) (**Fig. 5.12D**). Gene expression of *Col1a1* decreased in punctured AF compared to control AF (p=0.043); however, this significant decrease was not observed in PM (p=0.040) or PCLM AF (p=0.040) compared to control AF (N=3-4) (**Fig. 5.12E**). Meanwhile, GAG loss into the media was decreased in short-term punctured discs compared to control (p=0.048), while PM (p=0.13) and PCLM (p=0.62) groups were not significantly lower than control discs (**Fig. 5.12F**).

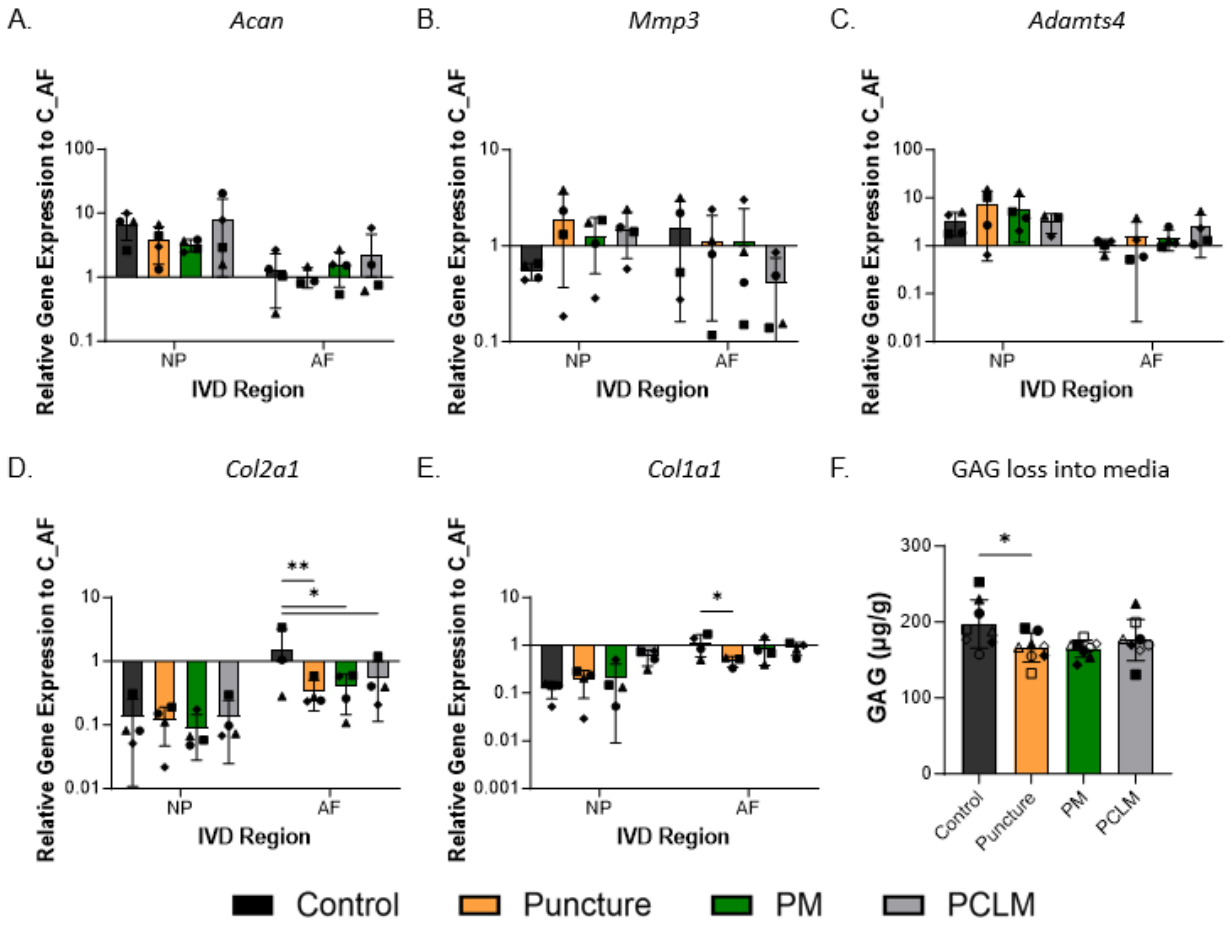

Figure 5.12: ECM gene expression and GAG release of *ex vivo* punctured discs injected with injurious CLM-MSCs and naïve MSCs.

ECM gene expression of **A.** *Acan*, **B.** *Mmp3*, **C.** *Adamts4*, **D.** *Col2a1*, and **E.** *Col1a1* (N=3-4). **p*<0.05, ***p*<0.01 compared to respective control IVD region and **F.** GAG loss into media (N=8). **p*<0.05 compared to control IVD motion segment

5.4 Discussion

This chapter examined the potential of using loaded IVD secretomes from distinct loading profiles to inform new therapeutics. This process was conducted via the generation and characterization of CLM as a potential therapy alone, using CLM for MSC priming, and then assessing the efficacy of primed MSCs in the well-established *ex vivo* puncture model discussed in Chapter 3. Study 1 revealed that the secretome of CLM is dependent on the magnitude and frequency of the loading profile applied to motion segments. Characterizing the presence and number of immunomodulatory cytokines and proteins can inform prospects of CLM as a therapeutic alone. In addition, Study 1 also examined the use of CLM as a priming agent for MSCs and determined that injurious CLM may lead to the most immunomodulatory and regenerative MSC outcomes. Study 2 then evaluated the immunosuppressive functional aspect of injurious CLM-MSCs by conducting a standardized T-cell proliferation assay and deemed the injurious CLM-MSCs to be more immunosuppressive than naïve MSCs. The final study in this chapter assessed the functional aspect of CLM-MSCs in an *ex vivo* puncture model to assess immunomodulation and regeneration, and results were promising as injurious CLM-MSCs were able to attenuate the immunomodulatory response in the punctured NP and improve the ECM gene expression of the AF.

Interestingly, our data agrees with a study in the literature that examined the secretome of healthy, traumatic, or degenerated human IVDs. Wrangler *et al.* used conditioned medium from traumatic/degenerative IVD tissues as well as organ donor human IVDs in an MSC co-culture. When characterizing their traumatic and degenerative media samples, they saw elevated cytokine levels of IL-6, TNFα, IL-1β, IL-13, IL-10, and GM-CSF compared to healthy media as well as decreased levels of MCP-1 and IL-17A in the traumatic and degenerative groups compared to

healthy media. These results correlate with our findings in IVD CLM, where we also saw a significant increase in TNFα, IL-6, IL-1β, IL-10, and GM-CSF and a decrease in MCP-1 and IL-17A in the injurious CLM compared to unloaded control loading media.

In addition to the presence of immune factors in CLM, injurious CLM exhibited a distinct signature for immune system signaling, actomyosin contractility, and extracellular matrix compared to unloaded IVDs. Interestingly, the secretomes of physiologically loaded and statically loaded IVDs were not appreciably different from the unloaded IVD secretome. Although we initially hypothesized that HMGB1 would be a DAMP secreted from loaded IVDs, we found other proteins, specifically glycoproteins and cartilage matrix proteins, released during loading that are more direct in activating the inflammatory response/innate immune system. Findings from injurious loading secretome suggest that the innate immune system is highly implicated during loading events, specifically neutrophil degranulation. The proteins secreted by loaded IVDs suggest that neutrophil mobilization is downregulated to minimize damage to host tissue [211, 212]. Downregulation of neutrophil degranulation has been researched as an effective therapeutic strategy [213]. Thus, findings suggest that decreased neutrophil degranulation through the increased release of PGAM1, FABP6, LGALS3, and MVP leads to increased therapeutic potential, implicating increased anti-microbial and proteolytic properties of the injurious CLM, while the decrease in secondary granules (ex. LYZ1) may differentiate the type of granule mobilization. Additionally, many neutrophil receptors can activate chemokine receptors such as CXCR1; thus, downregulation of CXCL1 may affect eventual signaling through the receptor, CXCR1 [213].

Findings also suggest that injurious loading leads to activation of the Arp2/3 complex through ACTR3 and a decrease in the presence of actin monomer binding protein, PFN2 [214]. Furthermore, the downregulation of the sulfated glycoproteins, NID1 and EFEMP1, suggests that

DAMP signaling is reduced compared to unloaded CLM, and upregulation of cartilage matrix protein CHAD in injurious CLM suggests that with decreased ECM glycoprotein release, the IVD attempts to increase release of proteins that can recover ECM-producing cells, such as chondrocytes, especially since CHAD increases attachment of chondrocytes, fibroblasts, and osteoblasts. CHAD is also an important indicator of matrix homeostasis and is found fragmented in degenerate and adult human discs, potentially due to excessive loading [215, 216]; thus, our results agree with the literature. Furthermore, the downregulation of the EFEMP1 protein suggests that injurious CLM can inhibit cell adhesion and migration while increasing chondrocyte differentiation [217].

Physiologic CLM led to the significant downregulation of CXCL1 compared to unloaded CLM. This observed downregulation suggests that the physiologic CLM alone may be immunosuppressive. Physiologic CLM also exhibited increased immunosuppressive protein release of IDO compared to unloaded CLM. As previously mentioned, IDO1 is an inducible heme-containing enzyme whose upregulation has been seen as essential for immunoregulatory abilities [146]. The production of L-Kyn as IDO breaks down L-Tyrp can lead to the differentiation of effector T cells into Treg cells and the reprogramming of dendritic cells (DCs) towards a long-term immunoregulatory phenotype.

However, CLM alone cannot be used as a therapeutic on its own due to low retention and unstable localization if it were to be injected into an injured disc. The injection of primed cells thus increases retention, improves the localization of treatment, and increases the likelihood of efficacy. It is promising to know that physiologic CLM may have some benefits alone; however, the mechanism in which it acts on MSCs varies from that of injurious CLM on MSCs. Interestingly, while physiologic CLM-MSCs were not significantly different from naïve MSCs, CD163

mediating an anti-inflammatory response, regulation of hmox1 expression and activity, and heme signaling were the most altered pathways in their DESeq2 transcriptome results. Since IDO is an inducible heme-containing enzyme, its increased presence in CLM may explain why physiologic CLM-MSCs also upregulate CD163 and heme signaling compared to naïve MSCs, albeit not significantly based on FDR. However, due to the greater presence of pro-inflammatory cytokines and ECM factors, injurious CLM may be better at priming cells towards a more immunomodulatory phenotype than physiologic CLM. Thus, injurious CLM, or more degenerative conditions, may be better at priming cells to create a promising therapeutic. However, the mechanism at play is distinct from that of physiologic CLM. This study suggests that IVD motion segment protein release in CLM, or the secretome, not only informs loading-induced ECM loss but can also affect the immune system's response through paracrine signaling, which may be optimized for potential therapeutic applications.

This study suggests that IVD paracrine factors released in CLM, or the secretome, can influence the immunomodulatory response of MSCs, which can be optimized for potential therapeutic priming applications. Culturing MSCs in IVD-CLM led to distinct MSC responses dependent on loading magnitude and frequency, as evidenced by the NO release and gene expression, presumably via paracrine factors released from the IVD motion segment. The presence of an unloaded IVD did not alter anti-inflammatory genes; instead, it significantly increased most pro-inflammatory genes investigated compared to naïve MSCs. Previous results from our lab have shown upregulation of *Il6* and *Rantes* in MSCs activated with LPS or poly I:C stimulations (not shown), suggesting that increases in MSC gene expression due to IVD-CLM may represent a form of stem cell activation due to the factors released during IVD loading. Indeed, injurious CLM led to the greatest upregulation of anti-inflammatory-associated genes.

Compared to static CLM, *Rantes*, *Ido1*, and *Tgfb1* levels were significantly greater in injured CLM, suggesting static CLM to be detrimental to anti-inflammatory priming of MSCs. At the same time, injurious CLM led to a higher expression of these genes in MSCs. This observed result suggests that dynamic loading releases certain paracrine factors that can immunomodulate MSCs in a manner that differs from unloaded or static loading. Previous literature co-culturing degenerated and post-traumatic IVD fragments and synovial MSCs had shown an increase in *Tgbf1* and *Il10* gene expression at day 1 compared to baseline [218]. While we did see an increase in the immunomodulatory marker *Tgfb1* in injurious IVD-CLM compared to other conditions, we did not observe a similar increase in *Il10* expression post 24-hour culture with IVD CLM (not shown). This result may be due to differences inherent to rat versus human MSCs, the source of MSCs, or soluble factors released during loading-induced IVD degeneration.

Injurious CLM-MSCs led to the greatest inhibition of T-cell proliferation based on division index compared to both unloaded CLM-MSCs and naïve MSCs. Since inhibition of T-cell proliferation is seen as a critical component of MSC immunomodulatory activity, this suggests that these primed MSCs are more effective than naïve MSCs. This mechanism may be due to the increase in IDO that is present in CLM. While the injurious CLM alone did not have the greatest amount of L-kynurenine, hence IDO activity, the injurious CLM-MSCs exhibited the highest *Ido1* gene expression compared to static and physiologic CLM-MSCs. According to the literature, human MSCs that are strong producers of IDO are more potent inhibitors of T cell proliferation *in vitro* [219]. However, this finding may not hold in rodent MSCs due to disputing results in rodent and human IDO biochemical and structural properties [220].

Nevertheless, injurious CLM-MSCs were the most immunosuppressive potentially through IDO presence or the resultant increase in other cytokines such as TGFβ1, which have also been

shown to be immunosuppressive. At the same time, the injurious CLM-MSCs had the highest *Il6* gene expression, and this cytokine has been known to stimulate T cell proliferation [219, 221]. Furthermore, other cytokines such as TNFα, IL-10, and IL-6 may synergize with each other to increase IDO1 expression [148]. Within the 4 main priming approaches in which one can improve MSC therapeutic efficacy, the use of CLM appears to fall underneath the cytokine or growth factors category due to the release of paracrine factors during loading [141].

Additionally, injurious CLM-MSCs improved disc outcomes post puncture potentially through IL-6, IL-13, and IL-4 signaling. As evidenced by RNA sequencing on the injurious CLM-MSCs, these pathways were upregulated compared to naïve MSCs. Thus, when injected into injured discs, it appears that the MSCs were able to affect each distinct signaling pathway differentially. While NP *Il6* gene expression was directly attenuated with injurious CLM-MSCs post puncture, so was NP *Il13ra* gene expression. Moreover, *Il6* expression is pro-inflammatory, *Il13* has been shown to have regenerative and anti-inflammatory effects. This observed result suggests that while puncture injury will lead to an upregulation of these genes in the NP, the immunomodulatory injurious CLM-MSCs were able to reduce the inflammatory gene expression levels to control NP levels. Our results using injurious CLM-MSCs in an *ex vivo* puncture rat model agree with an *in vivo* study in the literature, where blocking of NF-κB essential modulator (NEMO) occurred via a NEMO binding domain (NDB) injection immediately post puncture injury in rats. Researchers observed attenuation of *Il6* 3 days post puncture compared to uninjured, whole discs [222]. However, while their study observed an increase in whole disc *Mmp3* expression, in our study, punctured NP *Mmp3* expression was not significant compared to control NP, potentially due to our results being separated by IVD region or due to differences in responses to *in vivo* vs. *ex vivo* injury.

Although IL-4 receptor levels were not significantly increased using injurious CLM-MSCs, treatment with naïve MSCs increased IL-4 receptor levels compared to control NP, suggesting that MSCs will increase this expression regardless of priming. *Il4* gene expression was significantly higher in injurious CLM-MSCs, however, compared to control NP suggesting that the injurious priming may affect the signaling pathway, despite not altering receptor levels. Hence, the upregulation of these anti-inflammatory genes, IL-13 and IL-4, is promising for the use of injurious CLM-MSCs as an injectable therapy. Additionally, while the AF was not responsive in an inflammatory manner, collagen gene expression levels were decreased with the puncture injury. Moreover, naïve and injurious CLM-MSCs recovered AF *Col1a1* expression post puncture injury, which is promising for ECM protection with the use of primed or naïve MSCs.

Overall, this chapter addresses a knowledge gap regarding the characterization of IVD paracrine factors released during loading and how to use them to inform and improve potential therapeutics. Whether using CLM alone or through priming MSCs, the knowledge gained from this study can help inform more personalized therapies, hence, personalized medicine. Limitations of this study include the limited *ex vivo* evaluation of CLM-MSCs compared to *in vivo* response. Another limitation was MSC donor variability conducting the T-cell proliferation assay, as each batch of T-cells and MSCs behaved differently. However, comparing multiple batches in paired analyses yielded consistent results supporting decreased division index with CLM-MSCs. Furthermore, localization of the CLM-MSCs injection was not examined but may be pursued by tracking the cells after injection *ex vivo* or *in vivo*.

Chapter 6: Conclusion

The primary focus of this thesis is to evaluate the IVD response to injury, identify the role of TLR4 signaling, and use the IVD inflammatory response during injury to drive cell and molecular therapy development, all in an *ex vivo* organ culture model.

Aim 1 studies in Chapter 3 began by discussing common injury models such as LPS stimulation and puncture injuries *ex vivo*, yet focused in a novel manner on the IVD inflammatory and biochemical regional response to each respective injury. Findings showed that chemical injury using LPS led to a greater inflammatory response in female discs than in male discs in the short-term study, yet this difference in response is lost when looking at the long-term results. In contrast, a greater inflammatory response was seen in males compared to females in the long-term study after puncture injury. The findings of the current study extend earlier findings on sex-effects in rat IVDs. Mosley *et al.* identified some baseline distinct sex differences in IVD height where males had greater baseline IVD height than females. Similarly, additional sex-based differences were reported due to an *in vivo* 3x puncture injury [171]. These findings suggest that the IVD inflammatory response to injury is sex- and time-dependent. One advantage of using this *ex vivo* approach was that it isolated sex-based differences specific to the IVD motion segment and set the stage for the rest of the thesis chapters.

Furthermore, the role of TLR4/HMGB1 signaling was also discussed using the LPS and puncture injury modalities in Aim 1 studies. HMGB1 release was increased in punctured discs, with no sex-based effect, suggesting that cell necrosis due to puncture injury may be contributing to HMGB1 release [173]. Stratifying by sex further magnified injury effects on HMGB1 release. Interestingly, LPS stimulation did not induce significant HMGB1 release, differing from prior

findings on LPS injured human NP cells [11], indicating that the presence of complex ECM may be regulating HMGB1 responses. Thus, HMGB1 release appears to be dependent on disc injury.

Surprisingly, TAK-242 was more effective at improving the punctured discs' structural and functional properties than LPS-stimulated discs. Since HMGB1 can serve as an agonist of TLR4 and lead to downstream NF-κβ activation, the greater effectiveness on punctured IVDs may be due to the drug's blocking of TLR4 signaling through the HMGB1 ligand. Direct LPS stimulation may have overpowered the potential protective effects of TAK-242. Additionally, the puncture injury may have facilitated better diffusion of the TAK-242 drug into the motion segment, whereas the structural integrity of LPS injured discs was maintained, thus limiting diffusion of TAK-242 throughout the motion segment. TAK-242 appeared to improve the dynamic modulus of female punctured but not male discs, which may be evidenced by greater levels of COL/DW (albeit not significant) in female NP and AF compared to punctured-only discs. This study also supports the notion for future preclinical research to consider separate male and female cohorts, as there are baseline differences in the IVD, as well as distinct sex-dependent responses to physical and chemical injury.

In Aim 2 studies (Chapter 4), the role of physiological and detrimental mechanical loading on the IVD regarding its inflammatory response was investigated using various loading profiles via the *ex vivo* IVD motion segment model. The catabolic IVD tissue response to static and high-dynamic loading suggests that non-physiological loading elicits a similar molecular profile, including significant increases in TNFα and IL-1β expression. TNFα and IL-1β are key pro-inflammatory cytokines elevated in human degenerated disc samples [190]. Though IL-6 is also associated with advanced degeneration [134, 191, 192], we did not see significant increases in either short- or long-term loading protocol (**Fig. 4.8,4.9**). TNFα also promotes IL-10 secretion,

which serves as negative feedback to pro-inflammatory cytokines to mitigate damage [193-195]. Indeed, we observed TNFα upregulation along with IL-10 upregulation in injurious loading conditions.

Furthermore, the role of TLR4/HMGB1 signaling was also discussed, as TLR4 was upregulated in static and high-dynamic loading versus unloaded discs. Activation of TLR4 can enhance the production of mediators such as HMGB1, which can also augment the inflammatory response [7, 174]. High HMGB1 levels can promote GAG loss in discs, which may contribute to the GAG loss observed in the histological analyses of static and high-dynamic loading [186]. In addition, the role of TLR4 signaling in loading was studied via TLR4 inhibition. While co-treatment with TAK-242 post-injury significantly decreased NO release in unloaded discs, its effects on loaded IVD motion segments differed by loading profiles. TAK-242 co-treatment decreased pro-inflammatory expression in unloaded and static, but not dynamic loaded groups, suggesting that TLR4 plays a direct role in mediating inflammatory responses of IVD to static loading. There was a slight qualitative difference in the representative histology of +TAK static loaded discs in which the ECM was better conserved than the -TAK counterpart. This observed result is consistent with gene expression results where TAK-242 mitigated the effects of static loading. However, during loading, NO release was not affected by TAK-242. Thus, TLR4 may mediate post-injury rather than during-injury inflammatory responses. Some possible reasons for this may be that the loading period is too short for the drug to penetrate and influence cells within a compacted ECM during compression.

Limitations of this study include discs being exposed to different loading profiles and orientations compared to an *in vivo* setting due to soft tissue removal during dissection and an absence of systemic circulation *in vitro*. Furthermore, gene expression reported in this study

represents contributions of heterogeneous IVD tissue, including NP, AF, and CEPs, with media analyses including contributions of surrounding vertebral bone. Future studies will look at separated NP and AF compartments to stratify which IVD region contributes to the inflammatory and biochemical response.

Aim 3 studies (Chapter 5) delved into characterizing the secretome of a loaded IVD using the aforementioned mechanical loading profiles and the potential of using the secreted CLM as a form of cell therapy with MSCs. Study 1 revealed that the secretome of CLM is dependent on the magnitude and frequency of the loading profile applied to motion segments, as seen in the various proteins released and measured via multi-plex assay and proteomics analysis. This study is a promising contribution to the field as characterization of the presence and number of immunomodulatory cytokines and proteins can inform prospects of CLM as a therapeutic alone.

In addition, Aim 3 Study 1 also examined the use of CLM as a priming agent for MSCs and determined that injurious CLM may lead to the most immunomodulatory and regenerative MSC outcomes despite physiologic CLM alone exhibiting high IDO activity. Based on the upregulated pathways, injurious CLM holds the most potential for motivating *in vivo* studies to begin looking at degenerated back/spines to inform future therapeutics.

Aim 3 Study 2 then assessed the immunosuppressive functional aspect of injurious CLM-MSCs by conducting a standardized T-cell proliferation assay and deemed the injurious CLM-MSCs more immunosuppressive than naïve MSCs. The final study of this Aim evaluated the functional aspect of CLM-MSCs in an *ex vivo* puncture model to assess immunomodulation and regeneration, and results were deemed promising since injurious CLM-MSCs were able to attenuate the immunomodulatory response in the punctured NP and improve the ECM gene expression of the AF. While it is still unclear which immunomodulatory factors are the most

important, we know that there are distinct differences in the loading profiles applied. While physiologic loading promotes the production of IDO, other CLMs mitigate inflammatory cytokines in a more specific manner. Between IFNγ, IL-6, and IL-13Ra, we have still not systematically determined which one of these factors is the most important to lead to the best stem cell response and IVD therapeutic response. Nevertheless, the combination appears to be a promising approach for promoting IVD-specific immunomodulation. Moreover, differences in CLMs may be utilized in more personalized medicine approaches to address patient-specific phenotypes or sub-phenotypes of disc degeneration, based on molecular diagnostics.

6.1 Future Directions

Based on the findings of this thesis and the conclusions discussed in this chapter, the following are suggestions as to the future directions related to this thesis:

The IVD injury response is sex- and region-dependent.

The findings of this study provide more motivation to analyze outcomes in dedicated male and female cohorts in future experiments. Additionally, it is essential to separate the IVD by region, as the NP and the AF will have different responses to injury and therapy. It may be that the NP is more responsive than the AF; however, one would have to design an experiment to evaluate that hypothesis.

In addition to LPS stimulation, puncture injury, and both static and dynamic loading profiles activate TLR4 signaling.

As evidenced by the release of HMGB1 into the media, and increased TLR4 and HMGB1 gene expression from loaded discs, TLR4 signaling plays a role in the IVD response to injury and loading modalities. These results can inform future therapeutics as one now knows that the TLR4 signaling pathway is present in the IVD response. Figuring out what can activate TLR4 from the proteomics results could inform targets to mitigate and attenuate in future studies. Additionally, the *in vivo* loading model to investigate TLR4 signaling would be highly informative once the mechanical loader is functional. By understanding the *in vivo* response to loading and comparing it to the *in vitro* results, translation of therapeutics becomes more facilitated.

TAK-242 or inhibition of TLR4 could help treat long-term static loads but not dynamic loads.

TLR4 signaling was attenuated with the use of TAK-242 when the load induced was an injurious static 3-hour load. However, injurious dynamic loading may be too intense for a drug like TAK-242 to be able to have an effect. This loading profile may have resulted in matrix compaction affecting tissue permeability and drug accessibility. Additionally, the drug was successful with a 1-hour pre-treatment time. Future directions could investigate other drugs that can inhibit TLR4 but in a mechanism of action different from TAK-242. Previously, O-vanillin was investigated and determined more suitable for RAGE signaling[11]. Different delivery methods could also be investigated instead of exogenous distribution in the culture media. An *in situ* delivery method could be considered.

CLM may be an up-and-coming direction for personalized medicine.

Personalized medicine is critical. Not only do we have to take sex in account when understanding injury response or even attempting to treat patients, but we also must consider the different factors that are released from our bodies and how they can be leveraged as therapies. Whereas CLM having greater IDO levels may be beneficial in one case, priming MSCs and eventually leading to a slow increase of *Ido1* may be more beneficial in another case. Our lab has previously injected naïve MSCs in punctured caudal disc segments and evaluated the impact of varying the therapeutic window on the efficacy and fate of an MSC injection *in vivo*, observing that an MSC injection 3-days post injury was crucial in maintaining MSC signal intensity, as well as improving GAG content in injured discs. Given that a major function of MSCs in tissue repair is their anti-inflammatory ability to modulate disease microenvironments through immune cell modulation, ex. macrophage and T-cell proliferation, we can try to understand this potential response *in vivo*. Future directions for this study include conducting an *in vivo* puncture study followed by injection of injuriously primed CLM-MSCs in rats to evaluate the functional aspect of CLM-MSCs *in vivo* via resultant disc structure and function and through the presence of immune cells population (T-cells and macrophages) in the punctured disc. Primed MSC functionality can be evaluated using MRI/T2, biomechanical, biochemical, and histological properties of the discs at 1, 2, and 4 weeks post injury in addition to determining the immune cell composition (focusing on T-cell and macrophage populations) of the NP and AF regions of uninjured and punctured rat discs.

Clinical trials of stem cell treatment for disc degeneration find large numbers of non-responder subjects. This observation suggests that one therapy may not apply to all facets of disc degeneration. Theoretically, one can optimize CLM or prime MSCs using individualized CLM to tailor the treatment to improve outcomes depending on individual patient factors or if cytokines

are elevated or decreased based on specific mechanisms of action that differ from patient to patient.

Bibliography

1. Wu, A., et al., *Global low back pain prevalence and years lived with disability from 1990 to 2017: estimates from the Global Burden of Disease Study 2017.* Ann Transl Med, 2020. **8**(6): p. 299.
2. Frymoyer, J.W. and W.L. Cats-Baril, *An overview of the incidences and costs of low back pain.* The Orthopedic clinics of North America, 1991. **22**(2): p. 263-271.
3. Warburton, A., et al., *Biomaterials in Spinal Implants: A Review.* Neurospine, 2020. **17**(1): p. 101-110.
4. Klawitter, M., et al., *Expression and regulation of toll-like receptors (TLRs) in human intervertebral disc cells.* European Spine Journal, 2014. **23**(9): p. 1878-1891.
5. Quero, L., et al., *Hyaluronic acid fragments enhance the inflammatory and catabolic response in human intervertebral disc cells through modulation of toll-like receptor 2 signalling pathways.* Arthritis Research & Therapy, 2013. **15**(4): p. R94.
6. Gomez, R., et al., *TLR4 signalling in osteoarthritis--finding targets for candidate DMOADs.* Nat Rev Rheumatol, 2015. **11**(3): p. 159-70.
7. Rajan, N.E., et al., *Toll-Like Receptor 4 (TLR4) Expression and Stimulation in a Model of Intervertebral Disc Inflammation and Degeneration:.* Spine, 2013. **38**(16): p. 1343-1351.
8. Maidhof, R., et al., *Inflammation induces irreversible biophysical changes in isolated nucleus pulposus cells.* PloS One, 2014. **9**(6): p. e99621.
9. Shamji, M.F., et al., *Proinflammatory cytokine expression profile in degenerated and herniated human intervertebral disc tissues.* Arthritis and Rheumatism, 2010. **62**(7): p. 1974-1982.
10. Krock, E., et al., *Toll-like Receptor Activation Induces Degeneration of Human Intervertebral Discs.* Scientific Reports, 2017. **7**(1): p. 17184.
11. Shah, B.S., et al., *High mobility group box-1 induces pro-inflammatory signaling in human nucleus pulposus cells via toll-like receptor 4-dependent pathway.* Journal of Orthopaedic Research, 2019. **37**(1): p. 220-231.
12. Fang, F. and D. Jiang, *IL-1β/HMGB1 signalling promotes the inflammatory cytokines release via TLR signalling in human intervertebral disc cells.* Bioscience Reports, 2016. **36**(5).
13. Wilke, H.-J., et al., *New In Vivo Measurements of Pressures in the Intervertebral Disc in Daily Life.* Spine, 1999. **24**(8): p. 755–762.
14. Nachemson, A.L., *Disc pressure measurements.* Spine, 1981. **6**(1): p. 93-97.
15. Baer, A.E., et al., *The micromechanical environment of intervertebral disc cells determined by a finite deformation, anisotropic, and biphasic finite element model.* Journal of Biomechanical Engineering, 2003. **125**(1): p. 1-11.
16. Best, B.A., et al., *Compressive mechanical properties of the human anulus fibrosus and their relationship to biochemical composition.* Spine, 1994. **19**(2): p. 212-221.
17. Gu, W.Y. and H. Yao, *Effects of hydration and fixed charge density on fluid transport in charged hydrated soft tissues.* Annals of Biomedical Engineering, 2003. **31**(10): p. 1162-1170.
18. Iatridis, J.C., et al., *Degeneration affects the anisotropic and nonlinear behaviors of human anulus fibrosus in compression.* Journal of Biomechanics, 1998. **31**(6): p. 535-544.

19. O'Connell, G.D., et al., *Human internal disc strains in axial compression measured noninvasively using magnetic resonance imaging.* Spine, 2007. **32**(25): p. 2860-2868.
20. O'Connell, G.D., E.J. Vresilovic, and D.M. Elliott, *Human intervertebral disc internal strain in compression: The effect of disc region, loading position, and degeneration.* Journal of Orthopaedic Research, 2011. **29**(4): p. 547-555.
21. Schultz, A.B., et al., *Mechanical Properties of Human Lumbar Spine Motion Segments—Part I: Responses in Flexion, Extension, Lateral Bending, and Torsion.* Journal of Biomechanical Engineering, 1979. **101**(1): p. 46-52.
22. MacLean, J.J., et al., *Anabolic and catabolic mRNA levels of the intervertebral disc vary with the magnitude and frequency of in vivo dynamic compression.* Journal of Orthopaedic Research, 2004. **22**(6): p. 1193-1200.
23. Wuertz, K., et al., *In vivo remodeling of intervertebral discs in response to short- and long-term dynamic compression.* Journal of Orthopaedic Research, 2009. **27**(9): p. 1235-1242.
24. Maclean, J.J., et al., *The effects of short-term load duration on anabolic and catabolic gene expression in the rat tail intervertebral disc.* Journal of Orthopaedic Research, 2005. **23**(5): p. 1120-1127.
25. Walsh, A.J.L. and J.C. Lotz, *Biological response of the intervertebral disc to dynamic loading.* Journal of Biomechanics, 2004. **37**(3): p. 329-337.
26. Sandover, J., *Dynamic Loading as a Possible Source of Low-Back Disorders:*. Spine, 1983. **8**(6): p. 652-658.
27. Wilder, D. and M. Pope, *Epidemiological and aetiological aspects of low back pain in vibration environments—an update.* Clinical Biomechanics, 1996. **11**(2): p. 61-73.
28. Healy, G.N., et al., *Sedentary time and cardio-metabolic biomarkers in US adults: NHANES 2003–06.* European Heart Journal, 2011. **32**(5): p. 590-597.
29. Matthews, C.E., et al., *Amount of Time Spent in Sedentary Behaviors in the United States, 2003-2004.* American Journal of Epidemiology, 2008. **167**(7): p. 875-881.
30. Dunstan, D.W., et al., *Too much sitting – A health hazard.* Diabetes Research and Clinical Practice, 2012. **97**(3): p. 368-376.
31. Pope, M.H., M. Magnusson, and D.G. Wilder, *Low Back Pain and Whole Body Vibration:*. Clinical Orthopaedics and Related Research, 1998. **354**: p. 241-248.
32. Magnusson, M., *Measurement of Height Loss During Whole Body Vibrations*. 1992, Journal of Spinal Disorders.
33. Christ, W. and H. Dupuis, *[On the stressing of the spine under the effect of sinusoidal and stochastic vibrations].* Int Z Angew Physiol, 1966. **22**(3): p. 258-78.
34. Hickey, D.S. and D.W. Hukins, *Relation between the structure of the annulus fibrosus and the function and failure of the intervertebral disc.* Spine (Phila Pa 1976), 1980. **5**(2): p. 106-16.
35. Urban, J. and A. Maroudas, *The Chemistry of the Intervertebral-Disk in Relation to Its Physiological-Function and Requirements.* Clinics in Rheumatic Diseases, 1980. **6**(1): p. 51-76.
36. Lundon, K. and K. Bolton, *Structure and function of the lumbar intervertebral disk in health, aging, and pathologic conditions.* J Orthop Sports Phys Ther, 2001. **31**(6): p. 291-303; discussion 304-6.
37. Marchand, F. and A.M. Ahmed, *Investigation of the laminate structure of lumbar disc anulus fibrosus.* Spine (Phila Pa 1976), 1990. **15**(5): p. 402-10.

38. Choi, Y.-S., *Pathophysiology of degenerative disc disease.* Asian spine journal, 2009. **3**(1): p. 39-44.
39. Balka, K.R. and D. De Nardo, *Understanding early TLR signaling through the Myddosome.* Journal of Leukocyte Biology, 2019. **105**(2): p. 339-351.
40. Guerrero, A.T.G., et al., *Toll-like receptor 2/MyD88 signaling mediates zymosan-induced joint hypernociception in mice: Participation of TNF-α, IL-1β and CXCL1/KC.* European Journal of Pharmacology, 2012. **674**(1): p. 51-57.
41. Christianson, C.A., et al., *Spinal TLR4 mediates the transition to a persistent mechanical hypersensitivity after the resolution of inflammation in serum-transferred arthritis.* Pain, 2011. **152**(12): p. 2881-2891.
42. Wang, P., et al., *Response of chondrocytes to shear stress: antagonistic effects of the binding partners Toll-like receptor 4 and caveolin-1.* FASEB journal : official publication of the Federation of American Societies for Experimental Biology, 2011. **25**(10): p. 3401-3415.
43. Takeda, K. and S. Akira, *TLR signaling pathways.* Toll Receptor Families Structure and Function, 2004. **16**(1): p. 3-9.
44. Walter, B.A., et al., *TNFα transport induced by dynamic loading alters biomechanics of intact intervertebral discs.* PloS one, 2015. **10**(3): p. e0118358-e0118358.
45. Li, K., et al., *Sesamin inhibits lipopolysaccharide-induced inflammation and extracellular matrix catabolism in rat intervertebral disc.* Connective Tissue Research, 2016. **57**(5): p. 347-359.
46. Gawri, R., et al., *Physiological loading can restore the proteoglycan content in a model of early IVD degeneration.* PLoS One, 2014. **9**(7): p. e101233.
47. Palsson-McDermott, E.M. and L.A. O'Neill, *Signal transduction by the lipopolysaccharide receptor, Toll-like receptor-4.* Immunology, 2004. **113**(2): p. 153-62.
48. Kumar, H., T. Kawai, and S. Akira, *Toll-like receptors and innate immunity.* Biochem Biophys Res Commun, 2009. **388**(4): p. 621-5.
49. Aota, Y., et al., *Comparison of cellular response in bovine intervertebral disc cells and articular chondrocytes: effects of lipopolysaccharide on proteoglycan metabolism.* Cell and Tissue Research, 2006. **326**(3): p. 787-793.
50. Gu, R.H., et al., *Moracin attenuates LPS-induced inflammation in nucleus pulposus cells via Nrf2/HO-1 and NF-κB/TGF-β pathway.* Bioscience Reports, 2019. **39**.
51. Du, M., et al., *The LPS-inducible lncRNA Mirt2 is a negative regulator of inflammation.* Nature Communications, 2017. **8**.
52. Du, K.T., X.G. He, and J.Q. Deng, *MicroRNA-16 inhibits the lipopolysaccharide-induced inflammatory response in nucleus pulposus cells of the intervertebral disc by targeting.* Archives of Medical Science, 2021. **17**(2): p. 500-513.
53. Li, Y., et al., *Cordycepin inhibits LPS-induced inflammatory and matrix degradation in the intervertebral disc.* PeerJ, 2016. **4**: p. e1992.
54. Jacobsen, T.D., P.A. Hernandez, and N.O. Chahine, *Inhibition of toll-like receptor 4 protects against inflammation-induced mechanobiological alterations to intervertebral disc cells.* Eur Cell Mater, 2021. **41**: p. 576-591.
55. Han, Y.C., et al., *Metformin decreases LPS-induced inflammatory response in rabbit annulus fibrosus stem/progenitor cells by blocking HMGB1 release.* Aging-Us, 2019. **11**(22): p. 10252-10265.

56. Molladavoodi, S., S.J. DeWitte-Orr, and D.E. Gregory, *An in vitro 3D annulus fibrosus cell culture model with type I collagen: An examination of cell-matrix interactions.* Jor Spine, 2022. **5**(1).
57. Sobajima, S., et al., *Quantitative analysis of gene expression in a rabbit model of intervertebral disc degeneration by real-time polymerase chain reaction.* Spine J, 2005. **5**(1): p. 14-23.
58. Gullbrand, S.E., et al., *A large animal model that recapitulates the spectrum of human intervertebral disc degeneration.* Osteoarthritis Cartilage, 2017. **25**(1): p. 146-156.
59. Willems, N., et al., *Safety of intradiscal injection and biocompatibility of polyester amide microspheres in a canine model predisposed to intervertebral disc degeneration.* J Biomed Mater Res B Appl Biomater, 2017. **105**(4): p. 707-714.
60. Korecki, C.L., J.J. Costi, and J.C. Iatridis, *Needle puncture injury affects intervertebral disc mechanics and biology in an organ culture model.* Spine, 2008. **33**(3): p. 235-241.
61. Michalek, A.J., K.L. Funabashi, and J.C. Iatridis, *Needle puncture injury of the rat intervertebral disc affects torsional and compressive biomechanics differently (vol 19, pg 2110, 2010).* European Spine Journal, 2011. **20**(4): p. 667-667.
62. Hu, M.H., et al., *Optimization of puncture injury to rat caudal disc for mimicking early degeneration of intervertebral disc.* Journal of Orthopaedic Research, 2018. **36**(1): p. 202-211.
63. Zhang, H.N., et al., *Developing consistently reproducible intervertebral disc degeneration at rat caudal spine by using needle puncture Laboratory investigation.* Journal of Neurosurgery-Spine, 2009. **10**(6): p. 522-530.
64. Tian, T., et al., *Intervertebral Disc Degeneration Induced by Needle Puncture and Ovariectomy: A Rat Coccygeal Model.* Biomed Research International, 2021. **2021**.
65. Shang, P., et al., *Procyanidin B3 alleviates intervertebral disc degeneration via interaction with the TLR4/MD-2 complex.* Journal of Cellular and Molecular Medicine, 2020. **24**(6): p. 3701-3711.
66. Adams, M.A., et al., *Sustained loading generates stress concentrations in lumbar intervertebral discs.* Spine, 1996. **21**(4): p. 434-438.
67. Adams, M.A., D.S. McNally, and P. Dolan, *'Stress' distributions inside intervertebral discs. The effects of age and degeneration.* The Journal of bone and joint surgery. British volume, 1996. **78**(6): p. 965-972.
68. Fearing, B.V., et al., *Mechanotransduction and cell biomechanics of the intervertebral disc.* JOR spine, 2018. **1**(3): p. e1026.
69. Lang, G., et al., *An intervertebral disc whole organ culture system to investigate proinflammatory and degenerative disc disease condition.* Journal of Tissue Engineering and Regenerative Medicine, 2018. **12**(4): p. e2051-e2061.
70. MacLean, J.J., et al., *Effects of Immobilization and Dynamic Compression on Intervertebral Disc Cell Gene Expression In Vivo:.* Spine, 2003. **28**(10): p. 973-981.
71. Gilbert, H.T., J.A. Hoyland, and S.J. Millward-Sadler, *The response of human anulus fibrosus cells to cyclic tensile strain is frequency-dependent and altered with disc degeneration.* Arthritis Rheum, 2010. **62**(11): p. 3385-94.
72. Belavý, D.L., et al., *Can Exercise Positively Influence the Intervertebral Disc?* Sports Medicine, 2016. **46**(4): p. 473-485.
73. Belavý, D.L., et al., *Running exercise strengthens the intervertebral disc.* Scientific Reports, 2017. **7**(1): p. 45975.

74. Rohlmann, A., et al., *In vivo measurements of the effect of whole body vibration on spinal loads.* Eur Spine J, 2014. **23**(3): p. 666-72.
75. Chan, S.C.W., S.J. Ferguson, and B. Gantenbein-Ritter, *The effects of dynamic loading on the intervertebral disc.* European Spine Journal, 2011. **20**(11): p. 1796-1812.
76. Korecki, C.L., et al., *Intervertebral disc cell response to dynamic compression is age and frequency dependent.* Journal of Orthopaedic Research, 2009. **27**(6): p. 800-806.
77. Wang, D.-L., S.-D. Jiang, and L.-Y. Dai, *Biologic response of the intervertebral disc to static and dynamic compression in vitro.* Spine, 2007. **32**(23): p. 2521-2528.
78. Dou, Y., et al., *Intervertebral Disk Degeneration: The Microenvironment and Tissue Engineering Strategies.* Front Bioeng Biotechnol, 2021. **9**: p. 592118.
79. Uceyler, N., et al., *Differential expression of cytokines in painful and painless neuropathies.* Neurology, 2007. **69**(1): p. 42-9.
80. Khan, A.N., et al., *Inflammatory biomarkers of low back pain and disc degeneration: a review.* Annals of the New York Academy of Sciences, 2017. **1410**(1): p. 68-84.
81. Licciardone, J.C., et al., *Associations of cytokine concentrations with key osteopathic lesions and clinical outcomes in patients with nonspecific chronic low back pain: results from the OSTEOPATHIC Trial.* J Am Osteopath Assoc, 2012. **112**(9): p. 596-605.
82. De Luca, P., et al., *INTERVERTEBRAL DISC AND ENDPLATE CELLS RESPONSE TO IL-1β INFLAMMATORY CELL PRIMING AND IDENTIFICATION OF MOLECULAR TARGETS OF TISSUE DEGENERATION.* European Cells & Materials, 2020. **39**: p. 227-248.
83. Navone, S.E., et al., *Mechanical loading of intervertebral disc modulates microglia proliferation, activation, and chemotaxis.* Osteoarthritis and Cartilage, 2018. **26**(7): p. 978-987.
84. Pattappa, G., et al., *Ccl5/Rantes Is a Key Chemoattractant Released by Degenerative Intervertebral Discs in Organ Culture.* European Cells & Materials, 2014. **27**: p. 124-136.
85. Hansen, H.J., *A pathologic-anatomical study on disc degeneration in dog, with special reference to the so-called enchondrosis intervertebralis.* Acta Orthop Scand Suppl, 1952. **11**: p. 1-117.
86. Smolders, L.A., et al., *Intervertebral disc degeneration in the dog. Part 2: Chondrodystrophic and non-chondrodystrophic breeds.* Veterinary Journal, 2013. **195**(3): p. 292-299.
87. Erwin, W.M., et al., *The biological basis of degenerative disc disease: proteomic and biomechanical analysis of the canine intervertebral disc.* Arthritis Research & Therapy, 2015. **17**.
88. Matta, A., et al., *Molecular Therapy for Degenerative Disc Disease: Clues from Secretome Analysis of the Notochordal CellRich Nucleus Pulposus.* Scientific Reports, 2017. **7**.
89. Malham, G.M., et al., *Anterior lumbar interbody fusion using recombinant human bone morphogenetic protein-2: a prospective study of complications.* Journal of Neurosurgery-Spine, 2014. **21**(6): p. 851-860.
90. Carreon, L.Y., et al., *RhBMP-2*

Iliac Crest Bone Graft for Lumbar Spine Fusion in Patients Over 60 Years of Age A Cost-Utility Study. Spine, 2009. **34**(3): p. 238-243.

91. Goupille, P., D. Mulleman, and X. Chevalier, *Is interleukin-1 a good target for therapeutic intervention in intervertebral disc degeneration: lessons from the osteoarthritic experience.* Arthritis Research & Therapy, 2007. **9**(6).
92. Sinclair, S.M., et al., *Attenuation of Inflammatory Events in Human Intervertebral Disc Cells With a Tumor Necrosis Factor Antagonist.* Spine, 2011. **36**(15): p. 1190-1196.
93. Fernandez-Botran, R., F.A. Crespo, and X.C. Sun, *Soluble cytokine receptors in biological therapy.* Expert Opinion on Biological Therapy, 2002. **2**(6): p. 585-605.
94. Clarke, L.E., S.M. Richardson, and J.A. Hoyland, *Harnessing the Potential of Mesenchymal Stem Cells for IVD Regeneration.* Current Stem Cell Research & Therapy, 2015. **10**(4): p. 296-306.
95. Hoffman, A.M. and S.W. Dow, *Concise Review: Stem Cell Trials Using Companion Animal Disease Models.* Stem Cells (Dayton, Ohio), 2016. **34**(7): p. 1709-1729.
96. Richardson, S.M., et al., *Mesenchymal stem cells in regenerative medicine: Focus on articular cartilage and intervertebral disc regeneration.* Methods (San Diego, Calif.), 2016. **99**: p. 69-80.
97. Smith, L.J., et al., *Advancing cell therapies for intervertebral disc regeneration from the lab to the clinic: Recommendations of the ORS spine section.* JOR spine, 2018. **1**(4): p. e1036.
98. Crevensten, G., et al., *Intervertebral disc cell therapy for regeneration: mesenchymal stem cell implantation in rat intervertebral discs.* Annals of Biomedical Engineering, 2004. **32**(3): p. 430-434.
99. Lin, X., et al., *Decellularized allogeneic intervertebral disc: natural biomaterials for regenerating disc degeneration.* Oncotarget, 2016. **7**(11): p. 12121-12136.
100. Peng, Y., et al., *Decellularized Disc Hydrogels for hBMSCs tissue-specific differentiation and tissue regeneration.* Bioactive Materials, 2021. **6**(10): p. 3541-3556.
101. Sakai, D., et al., *Transplantation of mesenchymal stem cells embedded in Atelocollagen gel to the intervertebral disc: a potential therapeutic model for disc degeneration.* Biomaterials, 2003. **24**(20): p. 3531-3541.
102. Sakai, D., et al., *Differentiation of Mesenchymal Stem Cells Transplanted to a Rabbit Degenerative Disc Model: Potential and Limitations for Stem Cell Therapy in Disc Regeneration.* Spine, 2005. **30**(21): p. 2379–2387.
103. Hiyama, A., et al., *Transplantation of mesenchymal stem cells in a canine disc degeneration model.* Journal of Orthopaedic Research: Official Publication of the Orthopaedic Research Society, 2008. **26**(5): p. 589-600.
104. Ho, G., et al., *Effect of severity of intervertebral disc injury on mesenchymal stem cell-based regeneration.* Connective Tissue Research, 2008. **49**(1): p. 15-21.
105. Le Maitre, C.L., et al., *An in vitro study investigating the survival and phenotype of mesenchymal stem cells following injection into nucleus pulposus tissue.* Arthritis Research & Therapy, 2009. **11**(1): p. R20.
106. Paesold, G., A.G. Nerlich, and N. Boos, *Biological treatment strategies for disc degeneration: potentials and shortcomings.* European Spine Journal, 2007. **16**(4): p. 447-468.
107. Sakai, D. and G.B.J. Andersson, *Stem cell therapy for intervertebral disc regeneration: obstacles and solutions.* Nature Reviews. Rheumatology, 2015. **11**(4): p. 243-256.

108. Yim, R.L.-H., et al., *A Systematic Review of the Safety and Efficacy of Mesenchymal Stem Cells for Disc Degeneration: Insights and Future Directions for Regenerative Therapeutics.* Stem Cells and Development, 2014. **23**(21): p. 2553-2567.
109. Erwin, W.M., et al., *Intervertebral disc-derived stem cells: implications for regenerative medicine and neural repair.* Spine, 2013. **38**(3): p. 211-216.
110. Huang, Y.C., et al., *The effects of microenvironment in mesenchymal stem cell-based regeneration of intervertebral disc.* Spine Journal, 2013. **13**(3): p. 352-362.
111. Gan, Y., et al., *Spatially defined single-cell transcriptional profiling characterizes diverse chondrocyte subtypes and nucleus pulposus progenitors in human intervertebral discs.* Bone Research, 2021. **9**(1): p. 37.
112. Risbud, M.V., et al., *Evidence for skeletal progenitor cells in the degenerate human intervertebral disc.* Spine, 2007. **32**(23): p. 2537-2544.
113. Lee, C.K., et al., *Advances in Tissue Engineering for Disc Repair.* Applied Sciences, 2021. **11**(4): p. 1919.
114. Krock, E., D.H. Rosenzweig, and L. Haglund, *The Inflammatory Milieu of the Degenerate Disc: Is Mesenchymal Stem Cell-based Therapy for Intervertebral Disc Repair a Feasible Approach?* Current Stem Cell Research & Therapy, 2015. **10**(4): p. 317-328.
115. Karp, J.M. and G.S.L. Teol, *Mesenchymal Stem Cell Homing: The Devil Is in the Details.* Cell Stem Cell, 2009. **4**(3): p. 206-216.
116. Fong, E.L.S., C.K. Chan, and S.B. Goodman, *Stem cell homing in musculoskeletal injury.* Biomaterials, 2011. **32**(2): p. 395-409.
117. Honczarenko, M., et al., *Human bone marrow stromal cells express a distinct set of biologically functional chemokine receptors.* Stem Cells, 2006. **24**(4): p. 1030-1041.
118. Ozaki, Y., et al., *Comprehensive analysis of chemotactic factors for bone marrow mesenchymal stem cells.* Stem Cells and Development, 2007. **16**(1): p. 119-129.
119. Henriksson, H.B., et al., *Transplantation of human mesenchymal stems cells into intervertebral discs in a xenogeneic porcine model.* Spine, 2009. **34**(2): p. 141-148.
120. Zhang, Y.G., et al., *Bone mesenchymal stem cells transplanted into rabbit intervertebral discs can increase proteoglycans.* Clinical Orthopaedics and Related Research, 2005(430): p. 219-226.
121. Yang, F., et al., *Mesenchymal Stem Cells Arrest Intervertebral Disc Degeneration Through Chondrocytic Differentiation and Stimulation of Endogenous Cells.* Molecular Therapy, 2009. **17**(11): p. 1959-1966.
122. Sivan, S.S., et al., *Encapsulation of Human-Bone-Marrow-Derived Mesenchymal Stem Cells in Small Alginate Beads Using One-Step Emulsification by Internal Gelation: In Vitro, and In Vivo Evaluation in Degenerate Intervertebral Disc Model.* Pharmaceutics, 2022. **14**(6).
123. Kumar, H., et al., *Safety and tolerability of intradiscal implantation of combined autologous adipose-derived mesenchymal stem cells and hyaluronic acid in patients with chronic discogenic low back pain: 1-year follow-up of a phase I study.* Stem Cell Research & Therapy, 2017. **8**.
124. Mochida, J., et al., *Intervertebral Disc Repair with Activated Nucleus Pulposus Cell Transplantation: A Three-Year, Prospective Clinical Study of Its Safety.* European Cells & Materials, 2015. **29**: p. 202-212.

125. Soufi, K.H., et al., *Potential Role for Stem Cell Regenerative Therapy as a Treatment for Degenerative Disc Disease and Low Back Pain: A Systematic Review.* International Journal of Molecular Sciences, 2023. **24**(10).
126. Neidlinger-Wilke, C., et al., *Mesenchymal Stem Cell Secretome Decreases the Inflammatory Response in Annulus Fibrosus Organ Cultures.* European Cells & Materials, 2021. **42**: p. 1-19.
127. Tilotta, V., et al., *Mesenchymal stem cell-derived secretome enhances nucleus pulposus cell metabolism and modulates extracellular matrix gene expression.* Frontiers in Bioengineering and Biotechnology, 2023. **11**.
128. Gonzalez-Cubero, E., et al., *Extracellular vesicle and soluble fractions of adipose tissue-derived mesenchymal stem cells secretome induce inflammatory cytokines modulation in an in vitro model of discogenic pain.* Spine Journal, 2022. **22**(7): p. 1222-1234.
129. Ferreira, J., et al., *IL-1β-PRE-CONDITIONED MESENCHYMAL STEM/STROMAL CELLS' SECRETOME MODuLA TES THE INFLAMMATORY RESPONSE AND AGGRECAN DEPOSITION IN THE INTERVERTEBRAL DISC.* European Cells & Materials, 2021. **41**: p. 431-453.
130. Gan, Y., et al., *A Controlled Release Codelivery System of MSCs Encapsulated in Dextran/Gelatin Hydrogel with TGF-beta3-Loaded Nanoparticles for Nucleus Pulposus Regeneration.* Stem Cells Int, 2016. **2016**: p. 9042019.
131. Ahn, J., et al., *Transplantation of human Wharton's jelly-derived mesenchymal stem cells highly expressing TGFbeta receptors in a rabbit model of disc degeneration.* Stem Cell Res Ther, 2015. **6**: p. 190.
132. Gay, M.H.P., et al., *Nose to Back: Compatibility of Nasal Chondrocytes with Environmental Conditions Mimicking a Degenerated Intervertebral Disc.* European Cells & Materials, 2019. **37**: p. 214-232.
133. Urban, J.P.G., *The role of the physicochemical environment in determining disc cell behaviour.* Biochemical Society Transactions, 2002. **30**: p. 858-864.
134. Risbud, M.V. and I.M. Shapiro, *Role of cytokines in intervertebral disc degeneration: pain and disc content.* Nature Reviews. Rheumatology, 2014. **10**(1): p. 44-56.
135. Vadala, G., et al., *Interaction between Mesenchymal Stem Cells and Intervertebral Disc Microenvironment: From Cell Therapy to Tissue Engineering.* Stem Cells Int, 2019. **2019**: p. 2376172.
136. Waterman, R.S., et al., *A new mesenchymal stem cell (MSC) paradigm: polarization into a pro-inflammatory MSC1 or an Immunosuppressive MSC2 phenotype.* PLoS One, 2010. **5**(4): p. e10088.
137. Goncalves, R.M., et al., *Interleukin-1beta More Than Mechanical Loading Induces a Degenerative Phenotype in Human Annulus Fibrosus Cells, Partially Impaired by Anti-Proteolytic Activity of Mesenchymal Stem Cell Secretome.* Front Bioeng Biotechnol, 2021. **9**: p. 802789.
138. Wangler, S., et al., *Uncovering the secretome of mesenchymal stromal cells exposed to healthy, traumatic, and degenerative intervertebral discs: a proteomic analysis.* Stem Cell Res Ther, 2021. **12**(1): p. 11.
139. Cassano, J.M., et al., *Inflammatory licensed equine MSCs are chondroprotective and exhibit enhanced immunomodulation in an inflammatory environment.* Stem Cell Res Ther, 2018. **9**(1): p. 82.

140. Teixeira, G.Q., et al., *A Degenerative/Proinflammatory Intervertebral Disc Organ Culture: An Ex Vivo Model for Anti-inflammatory Drug and Cell Therapy.* Tissue Engineering Part C: Methods; New Rochelle, 2016. **22**(1): p. 8-19.
141. Noronha, N.D., et al., *Priming approaches to improve the efficacy of mesenchymal stromal cell-based therapies (vol 10, 131, 2019).* Stem Cell Research & Therapy, 2019. **10**.
142. Mohyeldin, A., T. Garzón-Muvdi, and A. Quiñones-Hinojosa, *Oxygen in Stem Cell Biology: A Critical Component of the Stem Cell Niche.* Cell Stem Cell, 2010. **7**(2): p. 150-161.
143. Krampera, M., et al., *Immunological Characterization of Multipotent Mesenchymal Stromal Cells. The International Society for Cellular Therapy (Isct) Working Proposal.* Cytotherapy, 2014. **16**(4): p. S81-S81.
144. François, M. and J. Galipeau, *New insights on translational development of mesenchymal stromal cells for suppressor therapy.* Journal of Cellular Physiology, 2012. **227**(11): p. 3535-3538.
145. Carmen, J., et al., *Developing assays to address identity, potency, purity and safety: cell characterization in cell therapy process development.* Regenerative Medicine, 2012. **7**(1): p. 85-100.
146. Pallotta, M.T., et al., *Indoleamine 2,3-dioxygenase 1 (IDO1): an up-to-date overview of an eclectic immunoregulatory enzyme.* Febs Journal, 2022. **289**(20): p. 6099-6118.
147. Munn, D.H., et al., *GCN2 kinase in T cells mediates proliferative arrest and anergy induction in response to indoleamine 2,3-dioxygenase.* Immunity, 2005. **22**(5): p. 633-42.
148. Zhai, L.J., et al., *Molecular Pathways: Targeting IDO1 and Other Tryptophan Dioxygenases for Cancer Immunotherapy.* Clinical Cancer Research, 2015. **21**(24): p. 5427-5433.
149. (IHME), I.f.H.M.a.E., *Global Burden of Disease Study 2019 (GBD 2019) Results*, G.B.o.D.C. Network, Editor. 2020: Seattle, United States.
150. Carmona, L., *The burden of musculoskeletal diseases in the general population of Spain: results from a national survey.* Annals of the Rheumatic Diseases, 2001. **60**(11): p. 1040-1045.
151. Manson, N.A., E.J. Goldberg, and G.B. Andersson, *Sexual dimorphism in degenerative disorders of the spine.* Orthop Clin North Am, 2006. **37**(4): p. 549-53.
152. Borg-Stein, J., S.A. Dugan, and J. Gruber, *Musculoskeletal aspects of pregnancy.* Am J Phys Med Rehabil, 2005. **84**(3): p. 180-92.
153. Fillingim, R.B., et al., *Sex, Gender, and Pain: A Review of Recent Clinical and Experimental Findings.* The Journal of Pain, 2009. **10**(5): p. 447-485.
154. Gautschi, O.P., et al., *Sex differences in lumbar degenerative disc disease.* Clinical Neurology and Neurosurgery, 2016. **145**: p. 52-57.
155. Wang, Y.X.J., *Postmenopausal Chinese women show accelerated lumbar disc degeneration compared with Chinese men.* J Orthop Translat, 2015. **3**(4): p. 205-211.
156. Miller, J.A., C. Schmatz, and A.B. Schultz, *Lumbar disc degeneration: correlation with age, sex, and spine level in 600 autopsy specimens.* Spine (Phila Pa 1976), 1988. **13**(2): p. 173-8.
157. Lebkowski, W.J., *[Autopsy evaluation of the extent of degeneration of the lumbar intervertebral discs].* Pol Merkur Lekarski, 2002. **13**(75): p. 188-90.

158. Wang, Y.-X.J., et al., *Prevalence and Sex Difference of Lumbar Disc Space Narrowing in Elderly Chinese Men and Women: Osteoporotic Fractures in Men (Hong Kong) and Osteoporotic Fractures in Women (Hong Kong) Studies: Radiographic Lumbar Disc Space Narrowing in Elderly Chinese.* Arthritis & Rheumatism, 2013. **65**(4): p. 1004-1010.
159. Fujiwara, A., et al., *The effect of disc degeneration and facet joint osteoarthritis on the segmental flexibility of the lumbar spine.* Spine (Phila Pa 1976), 2000. **25**(23): p. 3036-44.
160. Bonnheim, N.B., et al., *ISSLS Prize in Bioengineering Science 2023: Age- and sex-related differences in lumbar intervertebral disc degeneration between patients with chronic low back pain and asymptomatic controls.* Eur Spine J, 2023.
161. Reiser, K.M., et al., *Quantitative analysis of structural disorder in intervertebral disks using second harmonic generation imaging: comparison with morphometric analysis.* J Biomed Opt, 2007. **12**(6): p. 064019.
162. Mosley, G.E., *Males and females exhibit distinct relationships between intervertebral disc degeneration and pain in a rat model.* Scientific Reports, 2020: p. 14.
163. Krishnamoorthy, D., et al., *Dietary advanced glycation end-product consumption leads to mechanical stiffening of murine intervertebral discs.* Disease Models & Mechanisms, 2018: p. dmm.036012.
164. Lee, S., et al., *Voluntary running attenuates behavioural signs of low back pain: dimorphic regulation of intervertebral disc inflammation in male and female SPARC-null mice.* Osteoarthritis Cartilage, 2022. **30**(1): p. 110-123.
165. Keil, K.P., et al., *In vivo and in vitro sex differences in the dendritic morphology of developing murine hippocampal and cortical neurons.* Sci Rep, 2017. **7**(1): p. 8486.
166. Hu, Y.T., et al., *Sex differences in hippocampal beta-amyloid accumulation in the triple-transgenic mouse model of Alzheimer's disease and the potential role of local estrogens.* Front Neurosci, 2023. **17**: p. 1117584.
167. Kelly, T.-A.N., et al., *Low-Serum Media and Dynamic Deformational Loading in Tissue Engineering of Articular Cartilage.* Annals of Biomedical Engineering, 2008. **36**(5): p. 769-779.
168. Schneider, C.A., W.S. Rasband, and K.W. Eliceiri, *NIH Image to ImageJ: 25 years of image analysis.* Nature Methods, 2012. **9**(7): p. 671-675.
169. Stegemann, H. and K. Stalder, *Determination of hydroxyproline.* Clin Chim Acta, 1967. **18**(2): p. 267-73.
170. Lai, A., et al., *Development of a standardized histopathology scoring system for intervertebral disc degeneration in rat models: An initiative of the ORS spine section.* JOR Spine, 2021. **4**(2): p. e1150.
171. Mosley, G.E., et al., *Sex Differences in Rat Intervertebral Disc Structure and Function Following Annular Puncture Injury.* Spine, 2019. **44**(18): p. 1257–1269.
172. Kelm, M., *Nitric oxide metabolism and breakdown.* Biochimica Et Biophysica Acta-Bioenergetics, 1999. **1411**(2-3): p. 273-289.
173. Scaffidi, P., T. Misteli, and M.E. Bianchi, *Release of chromatin protein HMGB1 by necrotic cells triggers inflammation.* Nature, 2002. **418**(6894): p. 191-5.
174. He, M., et al., *Exploring the biological functional mechanism of the HMGB1/TLR4/MD-2 complex by surface plasmon resonance.* Molecular Medicine, 2018. **24**(1): p. 21.

175. Korecki, C.L., J.J. Costi, and J.C. Iatridis, *Needle Puncture Injury Affects Intervertebral Disc Mechanics and Biology in an Organ Culture Model:*. Spine, 2008. **33**(3): p. 235-241.
176. Raub, C.B., et al., *Predicting bulk mechanical properties of cellularized collagen gels using multiphoton microscopy.* Acta Biomater, 2010. **6**(12): p. 4657-65.
177. Bancelin, S., et al., *Determination of collagen fibril size via absolute measurements of second-harmonic generation signals.* Nat Commun, 2014. **5**: p. 4920.
178. Matsunaga, N., et al., *TAK-242 (Resatorvid), a Small-Molecule Inhibitor of Toll-Like Receptor (TLR) 4 Signaling, Binds Selectively to TLR4 and Interferes with Interactions between TLR4 and Its Adaptor Molecules.* Molecular Pharmacology, 2011. **79**(1): p. 34-41.
179. Huang, C.Y. and W.Y. Gu, *Effects of mechanical compression on metabolism and distribution of oxygen and lactate in intervertebral disc.* J Biomech, 2008. **41**(6): p. 1184-96.
180. Le Maitre, C.L., et al., *Human cells derived from degenerate intervertebral discs respond differently to those derived from non-degenerate intervertebral discs following application of dynamic hydrostatic pressure.* Biorheology, 2008. **45**(5): p. 563-575.
181. Le Maitre, C.L., et al., *Altered integrin mechanotransduction in human nucleus pulposus cells derived from degenerated discs.* Arthritis and Rheumatism, 2009. **60**(2): p. 460-469.
182. Salvatierra, J.C., et al., *Difference in Energy Metabolism of Annulus Fibrosus and Nucleus Pulposus Cells of the Intervertebral Disc.* Cellular and molecular bioengineering, 2011. **4**(2): p. 302-310.
183. Setton, L.A. and J. Chen, *Mechanobiology of the intervertebral disc and relevance to disc degeneration.* The Journal of Bone and Joint Surgery. American Volume, 2006. **88 Suppl 2**: p. 52-57.
184. Yao, H. and W.Y. Gu, *Physical signals and solute transport in human intervertebral disc during compressive stress relaxation: 3D finite element analysis.* Biorheology, 2006. **43**(3,4): p. 323-335.
185. Zhou, M., S. Lim, and G.D. O'Connell, *A Robust Multiscale and Multiphasic Structure-Based Modeling Framework for the Intervertebral Disc.* Front Bioeng Biotechnol, 2021. **9**: p. 685799.
186. Shah, B.S. and N.O. Chahine, *Dynamic Hydrostatic Pressure Regulates Nucleus Pulposus Phenotypic Expression and Metabolism in a Cell Density-Dependent Manner.* Journal of Biomechanical Engineering, 2018. **140**(2): p. 021003.
187. Ellman, M.B., et al., *Toll-like receptor adaptor signaling molecule MyD88 on intervertebral disk homeostasis: In vitro, ex vivo studies.* Gene, 2012. **505**(2): p. 283-290.
188. Johannessen, W., et al., *Intervertebral Disc Mechanics Are Restored Following Cyclic Loading and Unloaded Recovery.* Annals of Biomedical Engineering, 2004. **32**(1): p. 70-76.
189. Evans, R.C. and T.M. Quinn, *Dynamic Compression Augments Interstitial Transport of a Glucose-Like Solute in Articular Cartilage.* Biophysical Journal, 2006. **91**(4): p. 1541-1547.
190. Le Maitre, C.L., J.A. Hoyland, and A.J. Freemont, *Catabolic cytokine expression in degenerate and herniated human intervertebral discs: IL-1β and TNFα expression profile.* Arthritis Research & Therapy, 2007. **9**(4): p. R77.

191. Svensson, C.I., *Interleukin-6: a local pain trigger?* Arthritis Research & Therapy, 2010. **12**(5): p. 145, ar3138.
192. Capossela, S., et al., *Degenerated human intervertebral discs contain autoantibodies against extracellular matrix proteins.* Eur Cell Mater, 2014. **27**: p. 251-63; discussion 263.
193. Wanidworanun, C. and W. Strober, *Predominant role of tumor necrosis factor-alpha in human monocyte IL-10 synthesis.* The Journal of Immunology, 1993. **151**(12): p. 6853-6861.
194. Ouyang, W., et al., *Regulation and functions of the IL-10 family of cytokines in inflammation and disease.* Annual Review of Immunology, 2011. **29**: p. 71-109.
195. de Waal Malefyt, R., et al., *Interleukin 10(IL-10) inhibits cytokine synthesis by human monocytes: an autoregulatory role of IL-10 produced by monocytes.* Journal of Experimental Medicine, 1991. **174**(5): p. 1209-1220.
196. Brierley, M.M. and E.N. Fish, *Review: IFN-alpha/beta receptor interactions to biologic outcomes: understanding the circuitry.* Journal of Interferon & Cytokine Research: The Official Journal of the International Society for Interferon and Cytokine Research, 2002. **22**(8): p. 835-845.
197. Paul, C.P.L., et al., *Dynamic and Static Overloading Induce Early Degenerative Processes in Caprine Lumbar Intervertebral Discs.* PLoS ONE, 2013. **8**(4): p. e62411.
198. Paul, C.P.L., et al., *Static axial overloading primes lumbar caprine intervertebral discs for posterior herniation.* PLOS ONE, 2017. **12**(4): p. e0174278.
199. Feng, Y., et al., *Neuroprotective Effects of Resatorvid Against Traumatic Brain Injury in Rat: Involvement of Neuronal Autophagy and TLR4 Signaling Pathway.* Cellular and Molecular Neurobiology, 2017. **37**(1): p. 155-168.
200. Adhikari, A., M. Xu, and Z.J. Chen, *Ubiquitin-mediated activation of TAK1 and IKK.* Oncogene, 2007. **26**(22): p. 3214-3226.
201. Kang, J.D., et al., *Herniated lumbar intervertebral discs spontaneously produce matrix metalloproteinases, nitric oxide, interleukin-6, and prostaglandin E2.* Spine, 1996. **21**(3): p. 271-277.
202. Lambert, C., et al., *The Damage-Associated Molecular Patterns (DAMPs) as Potential Targets to Treat Osteoarthritis: Perspectives From a Review of the Literature.* Frontiers in Medicine, 2021. **7**.
203. Krampera, M., et al., *Immunological characterization of multipotent mesenchymal stromal cells--The International Society for Cellular Therapy (ISCT) working proposal.* Cytotherapy, 2013. **15**(9): p. 1054-61.
204. Maidhof, R., et al., *Timing of mesenchymal stem cell delivery impacts the fate and therapeutic potential in intervertebral disc repair.* Journal of Orthopaedic Research: Official Publication of the Orthopaedic Research Society, 2017. **35**(1): p. 32-40.
205. Daubener, W., et al., *A New, Simple, Bioassay for Human Ifn-Gamma.* Journal of Immunological Methods, 1994. **168**(1): p. 39-47.
206. Littlejohn, T.K., et al., *Asp*
and His
are essential for heme binding and catalytic function of human indoleamine 2,3-dioxygenase. Journal of Biological Chemistry, 2003. **278**(32): p. 29525-29531.
207. Takikawa, O., et al., *Mechanism of Interferon-Gamma Action - Characterization of Indoleamine 2,3-Dioxygenase in Cultured Human-Cells Induced by Interferon-Gamma*

and Evaluation of the Enzyme-Mediated Tryptophan Degradation in Its Anticellular Activity. Journal of Biological Chemistry, 1988. **263**(4): p. 2041-2048.
208. Kleifeld, O., et al., *Isotopic labeling of terminal amines in complex samples identifies protein N-termini and protease cleavage products.* Nature Biotechnology, 2010. **28**(3): p. 281-U144.
209. Zappasodi, R., et al., *In vitro assays for effector T cell functions and activity of immunomodulatory antibodies.* Tumor Immunology and Immunotherapy - Cellular Methods, Pt A, 2020. **631**: p. 43-59.
210. Jassal, B., et al., *The reactome pathway knowledgebase.* Nucleic Acids Research, 2019: p. gkz1031.
211. Eichelberger, K.R. and W.E. Goldman, *Manipulating neutrophil degranulation as a bacterial virulence strategy.* Plos Pathogens, 2020. **16**(12).
212. Sengelov, H., et al., *Mobilization of Granules and Secretory Vesicles during in-Vivo Exudation of Human Neutrophils.* Journal of Immunology, 1995. **154**(8): p. 4157-4165.
213. Lacy, P., *Mechanisms of degranulation in neutrophils.* Allergy Asthma Clin Immunol, 2006. **2**(3): p. 98-108.
214. Mullins, R.D., et al., *Arp2/3 complex from Acanthamoeba binds profilin and cross-links actin filaments.* Mol Biol Cell, 1998. **9**(4): p. 841-52.
215. Haglund, L., J. Ouellet, and P. Roughley, *Variation in Chondroadherin Abundance and Fragmentation in the Human Scoliotic Disc.* Spine, 2009. **34**(14): p. 1513-1518.
216. Akhatib, B., et al., *Chondroadherin Fragmentation Mediated by the Protease HTRA1 Distinguishes Human Intervertebral Disc Degeneration from Normal Aging.* Journal of Biological Chemistry, 2013. **288**(26): p. 19280-19287.
217. Wakabayashi, T., et al., *Fibulin-3 negatively regulates chondrocyte differentiation.* Biochemical and Biophysical Research Communications, 2010. **391**(1): p. 1116-1121.
218. Bertolo, A., et al., *Human mesenchymal stem cell co-culture modulates the immunological properties of human intervertebral disc tissue fragments in vitro.* Eur Spine J, 2011. **20**(4): p. 592-603.
219. Francois, M., et al., *Human MSC suppression correlates with cytokine induction of indoleamine 2,3-dioxygenase and bystander M2 macrophage differentiation.* Mol Ther, 2012. **20**(1): p. 187-95.
220. Austin, C.J., et al., *Mouse and human indoleamine 2,3-dioxygenase display some distinct biochemical and structural properties.* Amino Acids, 2009. **36**(1): p. 99-106.
221. Garman, R.D., et al., *B-cell-stimulatory factor 2 (beta 2 interferon) functions as a second signal for interleukin 2 production by mature murine T cells.* Proc Natl Acad Sci U S A, 1987. **84**(21): p. 7629-33.
222. Glaeser, J.D., et al., *NF-κB inhibitor, NEMO-binding domain peptide attenuates intervertebral disc degeneration.* Spine Journal, 2020. **20**(9): p. 1480-1491.
223. Yang, H., et al., *The many faces of HMGB1: molecular structure-functional activity in inflammation, apoptosis, and chemotaxis.* J Leukoc Biol, 2013. **93**(6): p. 865-73.
224. Hou, W., et al., *Strange attractors: DAMPs and autophagy link tumor cell death and immunity.* Cell death & disease, 2013. **4**: p. e966.
225. Ferrara, M., et al., *Oxidation of HMGB1 Is a Dynamically Regulated Process in Physiological and Pathological Conditions.* Front Immunol, 2020. **11**: p. 1122.

226. Lee, G., et al., *Fully reduced HMGB1 accelerates the regeneration of multiple tissues by transitioning stem cells to GAlert.* Proc Natl Acad Sci U S A, 2018. **115**(19): p. E4463-E4472.
227. Andersson, U., et al., *High mobility group 1 protein (HMG-1) stimulates proinflammatory cytokine synthesis in human monocytes.* Journal of Experimental Medicine, 2000. **192**(4): p. 565-570.
228. Gacaferi, H., et al., *The potential roles of high mobility group box 1 (HMGB1) in musculoskeletal disease: A systematic review.* Translational Sports Medicine, 2020. **3**(6): p. 536-564.
229. Venereau, E., et al., *Mutually exclusive redox forms of HMGB1 promote cell recruitment or proinflammatory cytokine release.* Journal of Experimental Medicine, 2012. **209**(9): p. 1519-1528.
230. Bianchi, M.E. and A.A. Manfredi, *High-mobility group box 1 (HMGB1) protein at the crossroads between innate and adaptive immunity.* Immunological Reviews, 2007. **220**: p. 35-46.
231. Yang, H., et al., *The cytokine activity of HMGB1.* Journal of Leukocyte Biology, 2005. **78**(1): p. 1-8.
232. Schiraldi, M., et al., *HMGB1 promotes recruitment of inflammatory cells to damaged tissues by forming a complex with CXCL12 and signaling via CXCR4.* Journal of Experimental Medicine, 2012. **209**(3): p. 551-563.
233. Harris, H.E., U. Andersson, and D.S. Pisetsky, *HMGB1: A multifunctional alarmin driving autoimmune and inflammatory disease.* Nature Reviews Rheumatology, 2012. **8**(4): p. 195-202.
234. Yang, H., C.J. Czura, and K.J. Tracey, *HMGB1 as a late mediator and therapeutic target in sepsis.* Shock, 2004. **21**: p. 124-124.
235. Scaffidi, P., T. Misteli, and M.E. Bianchi, *Release of chromatin protein HMGB1 by necrotic cells triggers inflammation.* Nature, 2002. **418**(6894): p. 191-195.
236. Yang, H., et al., *Redox modification of cysteine residues regulates the cytokine activity of high mobility group box-1 (HMGB1).* Mol Med, 2012. **18**: p. 250-9.
237. Kazama, H., et al., *Induction of immunological tolerance by apoptotic cells requires caspase-dependent oxidation of high-mobility group box-1 protein.* Immunity, 2008. **29**(1): p. 21-32.
238. Yang, H.A., et al., *A critical cysteine is required for HMGB1 binding to Toll-like receptor 4 and activation of macrophage cytokine release.* Proceedings of the National Academy of Sciences of the United States of America, 2010. **107**(26): p. 11942-11947.
239. Salo, H., et al., *Disulfide and Fully Reduced HMGB1 Induce Different Macrophage Polarization and Migration Patterns.* Biomolecules, 2021. **11**(6).

Appendix A. HMGB1 isoforms lead to a differential inflammatory response

A.1 Introduction

HMGB1 and its Distinct Isoforms: HMGB1 is a ubiquitous nuclear non-histone protein in all cell types that regulates many processes in the nucleus, from DNA repair to nucleosome dynamics. While it has both intracellular and extracellular functions, it mediates activation of the innate immune response, leading to chemotaxis and cytokine release [223-228]. Specifically, HMGB1 is a known DAMP that can activate TLR4 signaling. The B-box domain has 2 binding sites for TLR4 (amino acid residues 89-108) and RAGE (amino acid residues 150-183), which are receptors that regulate the release of pro-inflammatory cytokines [223]. HMBG1 signals tissue damage when released into an extracellular medium [229, 230]. For extracellular HMGB1, its oxidation state determines its bioactivity for mediating inflammation and the innate immune response [223]. HMGB1 redox states give the protein contrasting functions and have been detected *ex vivo* in injured muscle [223, 224, 229]. Furthermore, HMGB1 can switch between mutually exclusive redox states [229]. There are 4 main types of known HMGB1 isoforms: disulfide, fully reduced, terminally oxidized, and non-oxidizable.

Oxidation of HMGB1: When released into an extracellular space, HMGB1 is initially in a fully reduced state [223]. It transitions to the disulfide state when it enters an oxidative environment. If exposed to a large amount of reactive oxygen species (ROS) from activated leukocytes, for example, it will become sulfonated HMGB1 or terminally oxidized [223]. Fully reduced HMGB1 binds to CXC motif ligand (CXCL)12 and stimulates chemoattraction via CXCR4 [223, 231, 232]. Usually, most intracellular HMGB1 is fully reduced, allowing for structural integrity and protection against terminal oxidation by ROS [223, 233]. Reduced cysteine

residues, or all-thiol HMGB1, also allow HMGB1 to become a chemoattractant [229] that can recruit leukocytes and promote tissue regeneration [223, 227, 234] as it synergizes with CXCL12 to induce human monocyte migration [232] while disulfide HMGB1 does not [229]. However, disulfide HMGB1 does not compete with all-thiol-HMGB1 [229]. Disulfide HMGB1 has a disulfide bond between cysteine 23 and cysteine 45, allowing it to elicit an inflammatory response and cytokine-inducing activity through TLR4/MD2 35 [223, 229]. Terminally oxidized HMGB1 exists when cysteines are fully oxidized, or C-106 is oxidized. This occurrence leads to the HMGB1 state having no cytokine or chemotactic activity [223]. It can be involved in the resolution of inflammation in highly acidic conditions [223, 235]. ROS can block pro-inflammatory activity of HMGB1 by terminally oxidizing the cysteines to sulfonates [236, 237]. Non-oxidizable HMGB1 occurs when all three cysteines are replaced with serines. This phenomenon prevents cytokine-stimulating activity and eventual inactivation but can preserve chemoattractive activity [229].

While the chemoattractant function of HMGB1 requires CXCR4, the cytokine-stimulating function of HMGB1 requires TLR4 [232, 238]. HMGB1's ability to restrict the interactions of fully reduced (all-thiol) and disulfide HMGB1 to CXCL12 and TLR4 must be investigated [229]. It is suggested that the location and release of the redox status of HMGB1 influences its extracellular activity involving immunity and inflammation [223, 229].

HMGB1 Isoform Co-Culture with Other Cell Types or Discs: HMGB1 release from macrophages, monocytes, and MSCs has been studied and documented in the literature [223, 226]. Salo *et al.* investigated the inflammatory response of murine macrophages with HMGB1 isoform supplementation and saw distinct responses between disulfide and fully reduced treated macrophage cultures. While both disulfide and fully reduced HMGB1 isoforms induced

macrophage migration, disulfide HMGB1 led to cytokine secretion and cellular motility through TLR4 signaling [239]. Venereau *et al.* found disulfide HMGB1 induces activation of the NF-κB pathway and cytokine chemokine expression by macrophages, while all-thiol HMGB1 does not [229]. However, how HMGB1 isoforms can affect the inflammatory response of the IVD remains uninvestigated.

Furthermore, DAMPS, such as HMGB1 or fibronectin fragments, have been shown to have degenerative effects in disc cells including increased expression of inflammatory cytokines and matrix degrading enzymes by signaling through TLRs [9, 10, 186]. HMGB1 signaling increases the expression of TLR4, suggesting a possible potentiation of signaling or feedback through TLRs [12]. Thus, examining HMGB1 release due to puncture and LPS stimulation into culture may provide insight into whether this DAMP is leading to a feedback loop effect in the inflammatory cascade of degenerative disc disease.

A.2 Material and Methods

A.2.1 Study Design

Using the *ex vivo* IVD culture model described in Chapters 3-5, motion segments were co-cultured with exogenous HMGB1 isoforms in the media for 6 days. Supernatants were collected to analyze pro-inflammatory cytokine release (ex. NO, IL-1β, and TNFα), and gene expression of separated NP and AF was analyzed to observe TLR4 or HMGB1 signaling changes.

A.2.2 Culture and treatment of exogenous HMGB1 isoforms

Harvest and Culture of IVD Motion Segments: Caudal motion segments were dissected from 3 skeletally mature male 300 g Sprague-Dawley rats and cultured in CM as described above with an added 4 mM concentration of 3:1 Glutamax:Glutamine.

HMGB1 Treatment of IVD Motion Segments: 24 hrs after dissection, discs were split into four groups: untreated (CM alone), 1 µg/mL terminally oxidized HMGB1 in CM, 1 µg/mL disulfide HMGB1 in CM, or 1 µg/mL fully reduced HMGB1 in CM.

A.2.3 Supernatant ELISAs exogenous HMGB1 isoforms

Media was collected every other day for a 6-day culture period. The supernatant was then analyzed for levels of NO, GAG, TNFα, IL-1β, and LDH release into the media. Supernatant levels were normalized to motion segment wet weight (**Fig. A.1A**).

A.2.4 RNA extraction of separated discs for exogenous HMGB1 isoforms

The tissue was prepped for RNA isolation at the end of the 6-day culture. NP and AF compartments were dissected and then stored at -80°C for long-term storage. Samples were thawed in RNAlaterICE overnight prior to homogenization. Samples were then dipped in microcentrifuge tubes with 100µL of ice-cold RNAlater, transferred to a 3mL round bottom tube with ice-cold Trizol, and pulverized in Trizol using a stick homogenizer (IKA) followed by phase-lock

separation. Total RNA was retrieved using a high salt solution with isopropanol precipitation and the RNeasy Mini Kit (Qiagen). cDNA was synthesized using the iScript cDNA Synthesis Kit. Gene specific master mixes were prepared using designed primers (**Table A.1**) and iTaq Universal SYBR Green Supermix. RT-qPCR was run on a QuantStudio™ 6 Flex Real-Time PCR System. *Gapdh* was used as the housekeeping gene.

Table A.1

Gene	**FWD Primer Sequence**	**REV Primer Sequence**
Gapdh	GCA AGG ATA CTG AGA GCA AGA G	GGA TGG AAT TGT GAG GGA GAT G
Arg1	GAT TAT CGG AGC GCC TTT CT	CGT GGT CTC TCA CAT TGT ACT C
Hmgb1	TCG GCC TTC TTC TTG TTC TG	GTT GTT CCA CAT CTC TCC TAG TT
Il1b	TCT GAC AGG CAA CCA CTT AC	CAT CCC ATA CAC ACG GAC AA
Il6	GAA GTT AGA GTC ACA GAA GGA GTG	GTT TGC CGA GTA GAC CTC ATA G
Nos2	AAC CCA AGG TCT ACG TTC AAG	GCA CAT CGC CAC AAA CAT AAA
Tlr4	CAG AGC CGT TGG TGT ATC TT	AGC AAG GAC TTC TCC ACT TTC
Tnfa	CCC AAT CTG TGT CCT TCT AAC T	CAG CGT CTC GTG TGT TTC T

A.2.5 Statistical analysis

Two-way ANOVAs with Holm-Sidak post-hoc tests were conducted for NO, GAG, TNFα, IL-1β, and LDH release into culture media. Student t-tests were conducted on the gene expression of HMGB1 isoform treated NP or AF versus the respective untreated NP or AF group. Mixed-effects analysis and Mann-Whitney non-parametric tests were used with non-normal data as indicated by the Shapiro-Wilk test. Outliers were excluded from analysis as determined by ROUT(Q=10%). Statistical significance was set at $*p<0.05$ where $\alpha=0.05$ using GraphPad Prism 10.1.2.

A.3 Results

A.3.1 Exogenous HMGB1 isoform treatment does not modulate inflammation

HMGB1 isoform treatment does not appear to modulate inflammation of the IVD motion segment based on the supernatant of the disc organ culture (**Fig. A.1**). There was no difference in NO (p=0.32), IL-1β (p=0.28), TNFα (p=0.24), or GAG (p=0.28) released into the media among HMGB1 isoform groups when normalized to disc wet weight (N=3-4) (**Fig. A.1B-E**). LDH release was significantly higher into the media across all time-pints for disulfide (p<0.05) and fully reduced (p<0.05) treated discs compared to control and terminally oxidized treated discs (N=3-4) (**Fig. A.1F**).

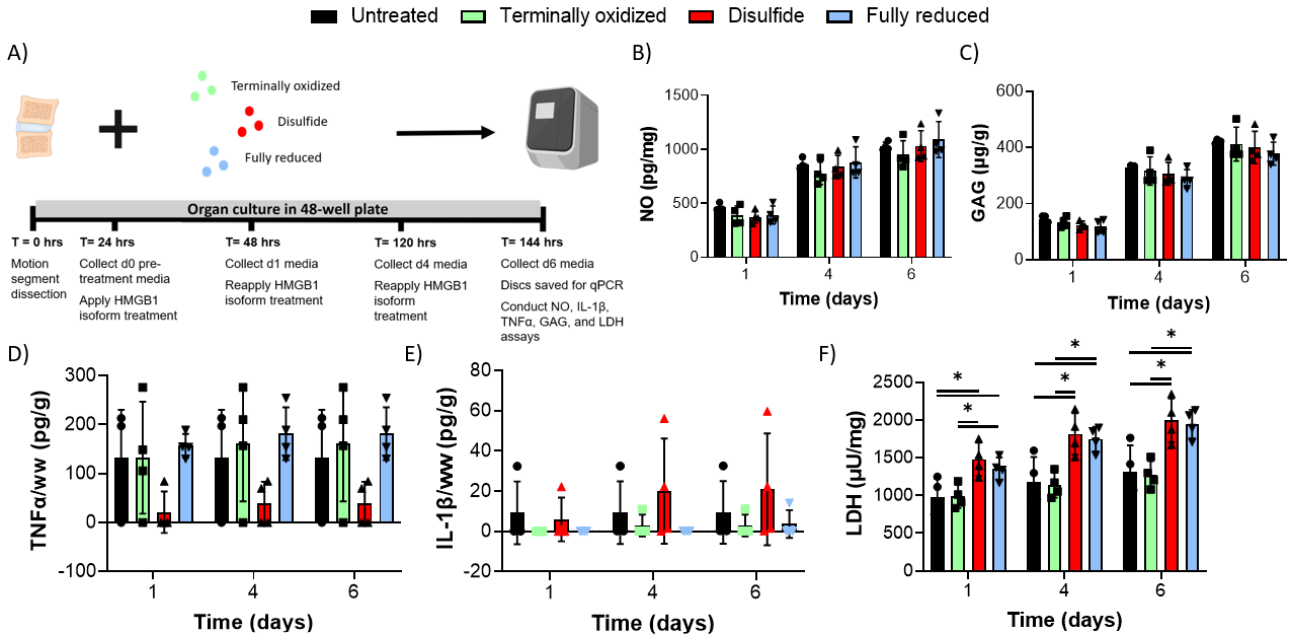

Figure A.1: 6-day experimental plan and supernatant results of HMGB1 isoform supplementation using an *ex vivo* IVD motion segment model.

A) Experimental plan of HMGB1 isoform supplementation in a 6-day IVD motion segment organ culture which led to cumulative **B)** NO, **C)** GAG, **D)** TNFα, **E)** IL-1β, and **F)** LDH release into the media. (N=4) *p<0.05

A.3.2 Fully reduced HMGB1 treatment increases Tlr4 and Il6 expression in the AF

When looking at gene expression of the 6-day HMGB1 treated NP region, there is significant upregulation of *Tlr4* (p=0.0047) expression in the fully reduced group compared to untreated NP (N=3-4). *Tlr4* gene expression (p=0.048) was also significantly upregulated in the fully reduced AF compared to the untreated AF (**Fig. A.2A**). *Il6* gene expression (p=0.042) was also significantly upregulated in the fully reduced AF compared to the untreated AF (**Fig. A.2D**). However, there were no significant differences in *Hmgb1*, *Nos2*, *Il6*, *Tnfa*, *Il1b*, and *Arg1* for disulfide and terminally oxidized treated IVD regions compared to respective untreated IVD regions (**Fig. A.2**).

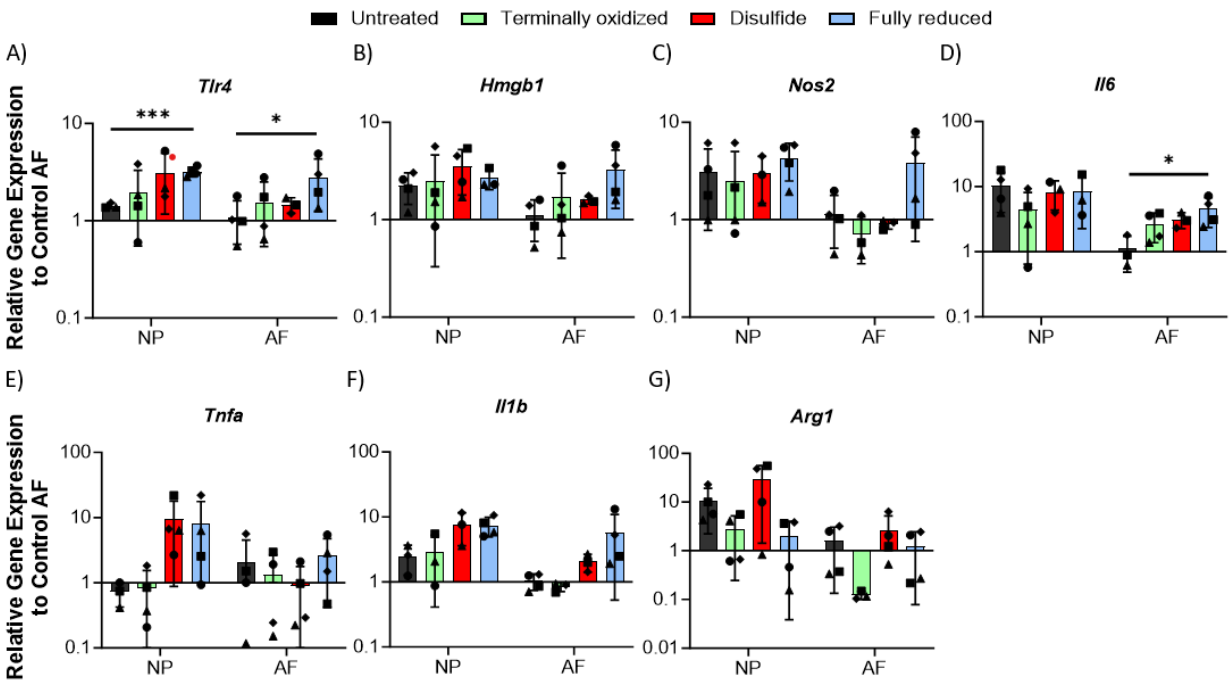

Figure A.2: 6-day gene expression results of separated NP and AF regions treated with HMGB1 isoforms using an *ex vivo* IVD motion segment model.

Gene expression of **A)** *Tlr4* **B)** *Hmgb1*, **C)** *Nos2*, **D)** *Il6*, **E)** *Tnfa*, **F)** *Il1b* and **G)** *Arg1* in separated NP and AF treated with terminally oxidized, disulfide, and fully reduced HMGB1 isoforms. (N=3-4) *p<0.05

A.4 Discussion

This appendix chapter examined the effect of exogenous HMGB1 treatment on IVD motion segments for a period of 6 days in an attempt to elucidate how different HMGB1 isoforms can affect the TLR4/HMGB1 signaling process in the IVD. Using the *ex vivo* IVD culture model described in Chapters 3-5, motion segments were co-cultured with exogenous HMGB1 isoforms in the media for 6 days. Supernatants were collected to analyze pro-inflammatory cytokine release (ex. NO, IL-1β, and TNFα), and gene expression of separated NP and AF was analyzed to observe TLR4 or HMGB1 signaling changes.

Treatment of the IVD using exogenous terminally oxidized, disulfide, and fully reduced isoforms does not seem to affect the inflammatory or structural response of the IVD. There was no significant difference in NO, GAG, TNFα, or IL-1β release into the media across time points and treatment. There was, however, an increase in LDH release for disulfide and fully reduced IVD motion segments compared to untreated IVDs, suggestive of cell death or metabolic activity.

PCR analysis shows an increase in *Tlr4* gene expression in the fully reduced isoform group, suggestive of increased *Tlr4* activation in both the NP and AF regions of the disc. There is also a significant increase in pro-inflammatory *Il6* gene expression in the fully reduced AF. While the disulfide HMGB1 isoform is often considered to be the most pro-inflammatory, our results show otherwise. Both disulfide and fully reduced HMGB1 isoform treatment led to an increased release of LDH into the media, which is usually indicative of cell death. Additionally, the fully reduced treated IVD exhibited higher *Tlr4* activation compared to the untreated IVD, whereas disulfide did not have the same effect. These results may be due to a low dose of 1 µg/mL used in the study. Literature has recently shown that it can require as much as 9 µg/mL of the HMGB1 isoform in order to see a significant effect on cells [239]. Salo *et al*. showed that using at least a 5 µg/mL

concentration, disulfide HMGB1 exogenous culture on murine macrophages induced IL-6, TNFα, IL-10 secretion but not NO production [239]. Additionally, contrary to our gene expression results, they saw that fully reduced HMGB1 did not result in any detectable cytokine or NO production compared to disulfide HMGB1 stimulation [239]. Their study also showed a time-dependent response where HMGB1 isoform treatment did not have a significant inflammatory response by 24 hours of treatment, peaking at 7-9 hours.

Thus, much is still unknown about how these exogenous HMGB1 isoforms can impact IVD inflammatory response, as well as structure and function. Future directions include conducting an *ex vivo* dose- and time-dependent HMGB1 isoform study, mechanical testing of HMGB1-treated discs, and repeating the aforementioned study using an *in vivo* rat model.